

# **Investigating the effects of diet-induced obesity on acute Doxorubicin-induced cardiotoxicity in a tumour-bearing model**

by

Bianca Annina Bock



*Thesis presented in partial fulfilment for the degree of Master of Science  
(Physiological Sciences) in the Faculty of Science at Stellenbosch University*

Supervisor: Dr. BJN Sishi

Co-Supervisor: Prof. AM Engelbrecht

April 2019

## **DECLARATION OF ORIGINALITY**

By submitting this thesis, I declare that the entirety of the work contained therein is my own, original work, that I am the sole author thereof (save to the extent explicitly otherwise stated), that reproduction and publication thereof by Stellenbosch University will not infringe any third party rights and that I have not previously in its entirety or in part submitted it for obtaining any qualification.

**April 2019**

## ABSTRACT

**Introduction:** Obesity is a well-known global pandemic that is fundamentally caused by an energy imbalance between calories consumed and calories expended. A major consequence to obesity are metabolic perturbations that are accompanied by insulin insensitivity and central obesity. Not only, but also are these factors associated with metabolic syndrome, they increase the risk of developing cardiovascular disease. Recently, obesity has been linked to the development of cancer, particularly breast and prostate cancer. While numerous mechanisms have been proposed, by far the biological mechanisms that has received much attention include insulin, insulin-like growth factor-1 (IGF-1), sex hormones and adipokines. While research on the mechanisms underlying obesity and its relationship with cancer are still in the early stages, understanding the processes of carcinogenesis in obesity-related cancers may lead to the development of treatments and better preventative strategies. Interestingly, the use of doxorubicin (DOX), a potent chemotherapeutic agent, is limited by its cumulative, dose- dependent toxicity that can lead to the development and progression of congestive heart failure. Considering that these inflammatory diseases have mainly been studied in isolation, there are very few, if any studies that have investigated cancer and cardiotoxicity in the context of obesity, to better understand the complex relationship that these diseases have with one another and how cardiovascular function is adversely affected in this scenario. Therefore, this study hypothesized that cancer in an obese environment increases the risk of developing early-stage DOX-induced cardiotoxicity.

**Methods:** Three-week-old female C57BL6 mice were acclimatized and randomly placed on either a high (H) fat diet or standard (S) diet for eight weeks to induce obesity. After eight weeks on the diet, these groups were further divided into two more groups were half of the mice in S and in H groups were inoculated with EO771 breast cancer cells and the others were not (non-tumour control group). Once tumours were palpable, animals were divided into more groups were some received DOX treatment. Each animal on treatment received three intraperitoneal injections of 4 mg/kg DOX resulting in a cumulative dose of 12 mg/kg. Animals remained on their respective diets for the duration of the study and were monitored daily. Four days after the last injection, animals were weighted, euthanized and their hearts excised. The blood collected was used to analyse circulating cytokines, adipokines and other markers of cardiovascular damage, while heart tissue was preserved in formalin for histological staining, or snap frozen for biochemical analyses including oxidative stress and apoptosis.

**Results:** Animals exposed to the high fat diet gained significantly more weight by the end of the study ( $29.24 \pm 1.99$  g,  $p < 0.0001$ ) versus those on the standard diet ( $19.72 \pm 0.52$  g). Not only did these animals display increased gonadal adiposity, circulating levels of glucose and leptin were also elevated. Furthermore, this group of animals showed a decreased heart-to-body weight ratio and fibrosis when compared to their control counter parts. In the presence of a tumour (T), there was a considerable decline in body weight in both diet groups (S+T and H+T) when compared to the diet groups (S and H) alone. This study also observed a decrease in body weight when group S+T was compared to group H+T. Interleukin-6 (IL-6) levels were significantly augmented in group H+T ( $64.95 \pm 11.62$  pg/ml,  $p < 0.01$ ) versus group H ( $24.17 \pm 5.59$  pg/ml). While no major histological changes were observed in the high fat diet fed animals (H and H+T), interstitial congestion within the heart tissue and reduced fibrosis was evident in the standard fed group with a tumour ( $1.23 \pm 0.20\%$ ,  $p < 0.001$ ) when compared to the standard diet fed animals alone ( $2.40 \pm 0.23\%$ ). When DOX (D) treatment was introduced to animals that received either diet, the body weight of animals fed the high fat diet (H+D) ( $25.02 \pm 0.84$  g,  $p < 0.001$ ) remained significantly higher than the animals fed the standard diet in the presence of DOX (S+D) ( $19.05 \pm 0.23$  g). Moreover, body weight loss was also observed when the high fat diet alone group (H) ( $29.24 \pm 1.99$  g) was compared to the high fat diet animals with tumours and treated with DOX (H+T+D) ( $21.30 \pm 1.25$  g,  $p < 0.0001$ ). This group of animals (H+T+D) also displayed significantly decreased adiposity and leptin levels, however the IL-6 concentration was elevated ( $126.90 \pm 34.92$  pg/ml,  $p < 0.05$ ) when compared to group H alone ( $24.17 \pm 5.59$  pg/ml). There was no evidence of cardiovascular damage or apoptotic cell death.

**Discussion and Conclusion:** It is clear from the results above that a diet high in fat contributes to the development of obesity and the dysregulation of adipokines inducing an inflammatory state. However, this inflammatory response did not have a major impact on cardiovascular health. When the complication of cancer arises in the context of obesity, the inflammatory state is aggravated due the rise in the pro-inflammatory cytokine IL-6. Although cancer is known to result in significant weight loss, in this context, the loss of weight, particularly fat mass may be initially viewed as beneficial. However if this loss of weight is sustained over an extended period of time, detrimental effects become evident. When DOX therapy was administered in this co-morbid state, it too contributed to the decrease in body weight, adiposity and leptin concentrations, while IL-6 levels remained elevated. It is therefore possible that the weight loss observed in this study may be attributed to the stimulation of degradation pathways as these pathways are known to be triggered by inflammation and also DOX. While this study did not demonstrate considerable alterations

in myocardial tissue, possibly due to the model not being severe enough to induce such changes in a short period of time, this study is the first to our knowledge to develop a co-morbid model of obesity and cancer with chemotherapy.

## OPSOMMING

**Inleiding:** Vetsug is 'n welbekende globale pandemie wat fundamenteel veroorsaak word deur 'n energie wanbalans tussen kalorieë wat ingeneem en verbruik word. 'n Hoofnagevolg van vetsug is metaboliese wysigings wat met insulienweerstandigheid en sentrale vetsugtigheid gepaard gaan. Nie alleen is hierdie faktore verwant aan die metaboliese sindroom nie maar dit verhoog ook die risiko vir die ontwikkeling van kardiovaskulêre siekte. Vetsugtigheid is onlangs verbind met die ontwikkeling van kanker, en meer spesifiek bors en prostaatkanker. Terwyl verskeie meganismes voorgestel is, is die mees bekende insulien, insulienagtige groeifaktor 1 (IGF-1), geslagshormone en adipokiene. Hoewel navorsing nog in 'n vroeë stadium is om die meganismes wat onderliggend vetsug met kanker te verbind, is dit noodsaaklik om die prosesse van karsinogenese in vetsug verwante kankers te verstaan om sodoende behandelingsopsies asook voorkomende strategieë te ontwikkel. Die gebruik van doksorubisien (DOX), 'n kragtige chemoterapeutiese middel, word beperk deur die kumulatiewe dosis-afhanklike toksisiteit wat aanleiding kan gee tot kongestiewe hartversaking. Meeste van hierdie inflammatoriese siektes is in isolasie bestudeer en daar is weinig, indien enige studies wat kanker en kardiotoksiteit in die konteks van vetsugtigheid bestudeer het, om sodoende die komplekse verband wat hierdie siektes met mekaar deel, en hoe kardiovaskulêre funksie negatief hierdeur geaffekteer word te verstaan. Hierdie studie hipotetiseer dat kanker in 'n vetsugtige omgewing die risiko vir die ontwikkeling van vroeë stadium DOX-geïnduseerde kardiotoksiteit verhoog.

**Metodes:** Drie-week oue vroulike C57BL6 muise is geklimatiseer en ewekansig verdeel in hoë vetdieet (H) of standaarddieet (S) groepe vir agtweke om sodoende vetsugtigheid te induseer. Hierdie groepe is verder in twee verdeel waar een groep met E0771 borskankerselle geïnokuleer is en die ander groep as kontrole gedien het. Die diere was verder verdeel in twee groepe die oomblik toe die gewasse voelbaar was met een groep wat daarna DOX ontvang het. Elke dier op behandeling het drie intraperitoneale inspuitings van 4 mg/kg DOX ontvang in 'n kumulatiewe dosis van 12 mg/kg. Die diere is op die groepdieete gehou en daaglik gemonitor oor die verloop van die studie. Vier dae na die finale inspuiting is die diere geweeg gevolg deur genade dood waarna die harte gedisekteer is. Die bloed is versamel om sirkulerende sitokiene, adipokiene en merkers van kardiovaskulêre skade te ondersoek, terwyl die hart in formalien gepreserveer is vir histologiese kleuring of geklampvries vir biochemiese analise insluitend oksidatiewe stres en apoptose.

**Resulte:** Die diere wat blootgestel is aan die hoë vetdieet het betekenisvolle gewigstoename teen die einde van die studie ( $29.24 \pm 1.99$  g,  $p < 0.0001$ ) vergeleke met die standaarddieet ( $19.72 \pm 0.52$  g) getoon. Nie net het die diere ook verhoogde gonodale adipositeit gelewer nie, maar sirkulerende glukose en leptien is ook verhoog gewees. Verder het hierdie groep diere verlaagde hart-tot-liggaamsgewigverhouding en fibrose vertoon teenoor die kontrole groep. In die teenwoordigheid van die tumor (T) was daar 'n besondere afname in liggaamsgewig in beide die dieetgroepe (S+T and H+T) teenoor die standaardgroepe alleen (S and H). Hierdie studie het 'n afname in liggaamsgewig tussen groep S+T teenoor groep H+T waargeneem. Interleukien-6 (IL-6) vlakke het betekensivol verskil in groep H+T ( $64.95 \pm 11.62$  pg/ml,  $p < 0.01$ ) teenoor groep H ( $24.17 \pm 5.59$  pg/ml). Terwyl geen histologiese veranderinge waargeneem is in die hoë vetdieet diere nie (H en H+T), is interstisiële kongestie en verlaagde fibrose in die standaarddieet groep met die tumor waargeneem ( $1.23 \pm 0.20\%$ ,  $p < 0.001$ ), vergeleke met die standaarddieet groep diere ( $2.40 \pm 0.23\%$ ). Tydens die aanvang van DOX (D) behandeling is daar in beide dieetgroepe op die hoë vetdieet (H+D) ( $25.02 \pm 0.84$  g,  $p < 0.001$ ) 'n betekenisvolle verhoging waargeneem vergeleke met die standaarddieet groep in die teenwoordigheid van DOX (S+D) ( $19.05 \pm 0.23$  g). Liggaamsgewig verlies is waargeneem in die hoë vetdieet alleen groep (H) ( $29.24 \pm 1.99$  g) teenoor die hoë vetdieet groep diere met die tumor en wat met DOX behandel is (H+T+D) ( $21.30 \pm 1.25$  g,  $p < 0.0001$ ). Hierdie groep diere (H+T+D) het ook betekensivol verlaagde adipositeit en leptienvlakke vertoon hoewel die IL-6 konsentrasie verhoog was ( $126.90 \pm 34.92$  pg/ml,  $p < 0.05$ ) vergeleke met die H groep alleenlik ( $24.17 \pm 5.59$  pg/ml). Daar is geen bewyse vir kardiovaskulêre skade of apoptiese seldood nie.

**Bespreking en gevolgtrekking:** Dit is duidelik uit hierdie resultate dat 'n hoë vetdieet bydra tot the ontwikkeling van vetsug en die disregulering van adipokiene en die inflammatoriese toestand. Hierdie inflammatoriese respons het nie 'n groot impak op kardiovaskulêre gesondheid gehad nie. Wanneer kanker in 'n vetsugtige konteks ondersoek word, het die inflammatoriese toestand vererger as gevolg van die toename in die pro-inflammatoriese sitokien IL-6. Hoewel kanker gewoonlik met gewigsverlies geassosieer word, kan die gewigsverlies wat in hierdie konteks waargeneem is, veral vetmassa, aanvanklik voordelig wees. Indien hierdie gewigsverlies oor 'n langer tydperk gehandhaaf word kan dit as nadelig en gevaarlik beskou word. Wanneer DOX terapie toegedien word in die ko-morbiede stadium het dit self bygedra tot die verlies aan liggaamsgewig, adipositeit en leptienkonsentrasies, terwyl IL-6 vlakke verhoog was. Dit is dus moontlik dat die gewigsverlies wat in hierdie studie waargeneem is bydraend tot die stimulering van degraderingspadweë, en dat hierdie weë ook deur inflammasie en DOX gestimuleer is. Alhoewel hierdie studie nie merkbare

veranderinge in die miokardiale weefsel kon demonstreer nie, omrede die model in 'n relatief kort periode nie die skade kan veroorsaak nie, het die studie wel daarin geslaag om 'n nuwe ko-morbiede model van vetsug, kanker en chemoterapie te beskryf.

## ACKNOWLEDGEMENTS

First and foremost I would like to thank **God** for all the opportunities He sent my way.

I would like to thank everyone who supported and encourage me. Without your support I would not have been able to complete this task; I would specifically like to thank the following person(s):

To my parents, **Evelyn** and **Andrew Bock** and together with **my siblings**. Thank you for giving me the chance to educate myself, for your financial support, a shoulder to cry on in the difficult times, the encouragement throughout my studies and the spiritual support which has helped me every step of the way. Thank you for walking this journey with me and for believing in me, I am forever grateful.

To my Supervisor **Dr Balindiwe Sishi**, thank you for devoting your time and patience in assisting me throughout my studies. You have moulded my understanding in the physiological field and challenged my thinking. Thank you for allowing me to complete my studies with you.

To my co-supervisor **Prof Engelbrecht**, thank you for allowing me to firstly do my internship with you and for allowing me to stay on and do my Masters. Thank you for friendliness and generosity when I had queries throughout my studies.

To **Dr Nell** thank you for the Afrikaans translation of my abstract and for your guidance in understanding physiology better.

To **Curtley**, I do not know how to repay you for the tremendous amount of support you have given me. Physiology is not your speciality but you done your utmost best to assist me in all avenues of my studies and my personal well-being.

To my **extended family and friends** for the words of encouragement, prayers and unfailing care about my well-being, thank you.

To the Late **Des Mcleod** and the **ECHO** family thanks for all you have invested in me as a student.

To **Devereux** and **Sameera** thank you for the amazing friendship and for showing your support and assisting me whilst finishing your own studies.

To **Claudia** and **Carmelita** who have not only been my departmental friends but have grown to be my support system and friends, thank you. I will treasure all the memories we have together and thanks for assisting me in my studies when needed.

To my project partner, **Zaakiyah**, thank you for teaching me and showing me the ropes of our project. Through all our trials and tribulation, I am so grateful I could get to know you better and learn from you.

To **Ilze**, thank you for helping me sort out the samples, helping with the plasma analysis and giving me a better understanding of statistical analysis.

To **Yigael** thank you for being my lift to campus and thanks for the good music and answering all my random questions to and from campus.

To past and present **CORG** members and special thanks to **Muneeb** and **Tope** for catching up, checking in, words of encouragement and assisting me when needed.

To the **Stellenbosch University Animal Unit** for providing me with the animals to complete my study. To **Noel** for showing me good animal care and **Judy Faro** for your assistance during harvesting and for keeping a clean working unit.

To Mr **Reggie Williams** thanks for showing me the ropes of doing histology and going beyond measure to assist me, working in your lab was pleasant and I enjoyed the experience.

To Mr **Fani Rautenbacht** thank you for patience and humbleness in showing and teaching me to do oxidative stress analysis.

To the Division of Molecular Biology and Human Genetics, Stellenbosch University Medical Campus for doing the Luninex assay.

To **Jonnifer**, thank for always assisting where you can and always checking in with me and for being my driver to and from Tygerberg.

To **Dr Krgysman, Dr Lacerda, Dr Josephs** and the **cleaning staff** for keeping a clean department and workable lab environment to operate efficiently.

To **Dr Isaacs** for always going beyond the call of duty in assisting with microscope problems and any technical queries within the department.

To **Dr Tania Davis** thank you for your patient and kind heart that always helped and gave me advice during my studies.

To all the fellow students and the humble post docs, that I could ask for assistance and advise when required thank you.

To **Grazelda** for making sure the orders were in to complete the project and **academic staff** members; thank you for allowing me to do my internship and continuing my studies at the department. Thank you for having an open door for advice and I hope the department will grow from strength to strength.

To **NRF** for providing me with funding for my studies.

## LIST OF FIGURES

<b>Figure 1.1:</b> Causes of childhood and adulthood obesity.....	3
<b>Figure 1.2:</b> The anatomical structure of the heart showing the ventricles and atriums..	5
<b>Figure 1.3:</b> Mechanisms by which obesity causes the dysfunction of adipokines and how it causes carcinogenesis.....	15
<b>Figure 1.4:</b> Different anthracycline classes used in the treatment of various cancers..	16
<b>Figure 1.5:</b> Classification of DOX-induced cardiotoxicity .....	20
<b>Figure 1.6:</b> Risk factors associated with the development of DOX-induced cardiotoxicity...	21
<b>Figure 2.1:</b> Study Design.....	26
<b>Figure 2.2:</b> Transfer stack preparation layout .....	30
<b>Figure 3.1:</b> Percent body weight gain overtime of mice fed a standard diet (S) or high fat diet (H) for $\pm 12$ weeks. ....	36
<b>Figure 3.2:</b> Biometric parameters of mice fed a standard (S) or high fat diet for $\pm 12$ weeks.	37
<b>Figure 3.3:</b> Weekly food consumption in mice fed a standard (S) or high fat diet (H) for $\pm 12$ weeks.....	38
<b>Figure 3.4:</b> Weekly water consumption in mice fed a standard (S) or high fat diet (H) for $\pm 12$ weeks.....	38
<b>Figure 3.5:</b> Fasting blood parameters of mice fed a standard (S) or high fat diet (H) for $\pm 12$ weeks .....	40
<b>Figure 3.6:</b> Cardiac hypertrophy index of mice fed a standard (S) or high fat diet (H) for $\pm 12$ weeks.....	42
<b>Figure 3.7:</b> H&E histological stains of heart tissue sections from mice fed a standard (S) or high fat diet (H) for $\pm 12$ weeks.....	43

<b>Figure 3.8:</b> Picrosirius red histological stain of heart tissue sections from mice fed a standard (S) or high fat diet (H) for $\pm 12$ weeks.....	43
<b>Figure 3.9:</b> Percentage fibrosis in the myocardium of mice fed a standard (S) or high fat diet (H) for $\pm 12$ weeks.....	44
<b>Figure 3.10:</b> Relative apoptotic protein expression of mice fed a standard (S) or high fat diet (H) for $\pm 12$ weeks.....	45
<b>Figure 3.11:</b> Oxidative stress parameters from mice fed a standard (S) or high fat diet (H) for $\pm 12$ weeks. ....	46
<b>Figure 3.12:</b> Percent (%) body weight gain overtime of mice fed a standard diet (S) or high fat diet for $\pm 12$ weeks, and/or inoculated with cancer cells from eight weeks. ....	48
<b>Figure 3.13:</b> Biometric parameters of mice fed standard (S) or high fat diet (H) for $\pm 12$ weeks, and/or inoculated with cancer cells from eight weeks. ....	49
<b>Figure 3.14:</b> Weekly food consumption in mice fed a standard (S) or high fat diet (H) for $\pm 12$ weeks, and/or inoculated with cancer cells from eight weeks. ....	50
<b>Figure 3.15:</b> Weekly water consumption in mice fed a standard (S) or high fat diet (H) for $\pm 12$ weeks, and/or inoculated with cancer cells from eight weeks.. ....	51
<b>Figure 3.16:</b> Fasting blood parameters of mice fed a standard (S) or high fat diet (H) for $\pm 12$ weeks, and/or inoculated with cancer cells from eight weeks. ....	52
<b>Figure 3.17:</b> Cardiac hypertrophy index of mice fed a standard (S) or High fat diet (H) for $\pm 12$ weeks, and/or inoculated with cancer cells from eight weeks. ....	53
<b>Figure 3.18:</b> H&E histological stains of heart tissue sections from mice fed a standard (S) or high fat diet (H) for $\pm 12$ weeks, and/or inoculated with cancer cells from eight weeks.. ....	54
<b>Figure 3.19:</b> Picrosirius red histological stain of heart tissue sections from mice fed a standard (S) or high fat diet (H) for $\pm 12$ weeks, and/or inoculated with cancer cells from eight weeks .....	55

<b>Figure 3.20:</b> Percentage fibrosis in the myocardium of mice fed a standard (S) or high fat diet (H) for $\pm 12$ weeks, and/or inoculated with cancer cells from eight weeks..	55
<b>Figure 3.21:</b> Relative apoptotic protein expression of mice fed a standard (S) or high fat diet (H) for $\pm 12$ weeks, and/or inoculated with cancer cells from eight weeks.	56
<b>Figure 3.22:</b> Oxidative stress parameters from mice fed a standard (S) or high fat diet (H) for $\pm 12$ weeks, and/or inoculated with cancer cells from eight weeks..	57
<b>Figure 3.23:</b> Percent body weight gain overtime of mice fed a standard diet (S) or high fat diet (H) for $\pm 12$ weeks, and/or inoculated with cancer cells from eight weeks, and /or treated with DOX.	58
<b>Figure 3.24:</b> Biometric parameters of mice fed a standard (S) or high fat diet (H) for $\pm 12$ weeks, and/or inoculated with cancer cells from eight weeks, and/or treated with DOX..	59
<b>Figure 3.25:</b> Weekly food consumption in mice fed a standard (S) or high fat diet (H) for $\pm 12$ weeks, and/or inoculated with cancer cells from eight weeks, and/or treated with DOX.	60
<b>Figure 3.26:</b> Weekly water consumption in mice fed a standard (S) or high fat diet (H) for 12 weeks, and/or inoculated with cancer cells from eight weeks, and/or treated with DOX.	61
<b>Figure 3.27:</b> Fasting blood parameters of mice fed a standard (S) or high fat diet (H) for $\pm 12$ weeks, and/or inoculated with cancer cells from eight weeks, and/or treated with DOX.	62
<b>Figure 3.28:</b> Cardiac hypertrophy index of mice fed a standard (S) or high fat diet (H) for $\pm 12$ weeks, and/or inoculated with cancer cells from eight weeks, and/or treated with DOX.	63
<b>Figure 3.29:</b> H&E histological stains of heart tissue sections from mice fed a standard (S) or high fat diet (H) for $\pm 12$ weeks, and/or inoculated with cancer cells from eight weeks, and/or treated with DOX..	65
<b>Figure 3.30:</b> Picrosirius red histological stain of heart tissue sections from mice fed a standard (S) or high fat diet (H) for $\pm 12$ weeks, and/or inoculated with cancer cells from eight weeks, and/or treated with DOX.	66

<b>Figure 3.31:</b> Percentage fibrosis in the myocardium of mice fed a standard (S) or high fat diet (H) for $\pm 12$ weeks, and/or inoculated with cancer cell from eight weeks, and/or treated with DOX.....	67
<b>Figure 3.32:</b> Relative apoptotic protein expression of mice fed a standard (S) or high fat diet (H) for $\pm 12$ weeks, and/or inoculated with cancer cells from eight weeks, and/or treated with DOX.....	68
<b>Figure 3.33:</b> Oxidative stress parameters from mice fed a standard (S) or high fat diet (H) for $\pm 12$ weeks, and/or inoculated with cancer cells from eight weeks, and/or treated with DOX.	69
<b>Figure 3.34:</b> Summary of the main findings from the study:.....	79

## LIST OF TABLES

<b>Table 1.1:</b> Different substrates utilized by the heart under various conditions.....	5
<b>Table 1.2:</b> Mechanisms by which DOX mediates its anti-cancer actions.....	18
<b>Table 1.3:</b> Different mechanisms by which DOX induces cardiotoxicity.....	19
<b>Table 2.1:</b> Dietary components of the standard and high fat diets.....	24
<b>Table 2.2:</b> Primary and secondary antibodies used for western blot analysis.....	31
<b>Table 2.3:</b> H&E staining procedure.....	33
<b>Table 2.4:</b> Procedure of Picrosirius Red staining.....	34

## LIST OF ABBREVIATIONS

<b>Akt</b>	Protein kinase B
<b>AMPK</b>	AMP-activated protein kinase
<b>ANOVA</b>	Analysis of Variance
<b>ATP</b>	Adenine Triphosphate
<b>AU</b>	Arbitrary units
<b>BHT</b>	Butylated hydroxytoluene
<b>BMI</b>	Body Mass Index
<b>BSA</b>	Bovine serum albumin
<b>CD (CDs)</b>	Conjugated dienes
<b>CHF</b>	Congestive heart failure
<b>CNS</b>	Central nervous system
<b>CVD</b>	Cardiovascular Disease
<b>DAG</b>	Diacylglycerol
<b>DIO</b>	Diet induced obesity
<b>DNA</b>	Deoxyribonucleic acid
<b>DOX</b>	Doxorubicin
<b>ECL</b>	Enhanced chemiluminescence
<b>EDTA</b>	Ethylenediaminetetraacetic acid
<b>FFA</b>	Free Fatty Acids
<b>GLU</b>	Glucose
<b>GLUT-4</b>	Glucose transporter type 4
<b>HBSS</b>	Hank's balanced salt solution
<b>HCL</b>	Hydrochloric acid
<b>H+D</b>	High fat diet + Doxorubicin group
<b>H &amp; E</b>	Hematoxylin and eosin
<b>HF</b>	Heart Failure
<b>HFD</b>	High Fat Diet
<b>HOMA</b>	Homeostatic model assessment
<b>H+T+D</b>	High fat diet + Tumour + Doxorubicin group
<b>H+T+V</b>	High fat diet + Tumour + Vehicle Control group
<b>H+V</b>	High fat diet + Vehicle Control group

<b>HW</b>	Heart weight
<b>HW-to-FBW</b>	Heart weight-to-Final Body weight
<b>IGF-1</b>	Insulin-like growth factor 1
<b>IGFBP</b>	Insulin-like growth factor-binding protein
<b>IGFBP-3</b>	Insulin-like growth factor-binding protein 3
<b>IL-6</b>	Interleukin-6
<b>i.p</b>	Intraperitoneal
<b>IR</b>	Insulin resistance
<b>IRS-1</b>	Insulin receptor substrate
<b>JAK</b>	Janus kinase
<b>Kilocal</b>	Kilocalories
<b>LAC</b>	Lactate
<b>MAPK</b>	Mitogen-activated protein kinase
<b>MDA</b>	Malondialdehyde
<b>mPTP</b>	Mitochondrial permeability transition pore
<b>NaCl</b>	Sodium chloride
<b>NaF</b>	Sodium fluoride
<b>NEFA</b>	non-esterified fatty acids
<b>NFκB</b>	Nuclear factor kappa light chain enhancer of activated B cells
<b>PARP</b>	Poly (ADP-ribose) polymerase
<b>PI3K</b>	Phosphoinositide-dependent protein kinase 1
<b>PKB</b>	Protein kinase B
<b>PKC</b>	Protein kinase C
<b>PMSF</b>	Phenylmethylsulfonyl fluoride
<b>PTFE</b>	Polytetrafluoroethylene
<b>PVDF</b>	Polyvinylidene fluoride
<b>RAS</b>	Renin-Angiotensin System
<b>RAF</b>	Rapidly Accelerated Fibrosarcoma
<b>RIPA</b>	Radioimmunoprecipitation assay
<b>RISK</b>	Reperfusion injury salvage kinase
<b>ROS</b>	Reactive Oxygen Species
<b>SD</b>	Standard Diet
<b>S+D</b>	Standard diet + Doxorubicin group

<b>SEM</b>	Standard error of mean
<b>SDS</b>	Sodium dodecyl sulfate
<b>SDS-PAGE</b>	Sodium dodecyl sulfate- polyacrylamide gel electrophoresis
<b>STAT</b>	Signal transducer and activator of transcription proteins
<b>S+T+D</b>	Standard diet + Tumour + Doxorubicin group
<b>S+T+V</b>	Standard diet + Tumour + Vehicle control group
<b>S+V</b>	Standard diet + Vehicle control group
<b>T2DM</b>	Type 2 Diabetes Mellitus
<b>TBA</b>	Thiobarbituric acid
<b>TBARS</b>	Thiobarbituric Acid Reactive Substances
<b>TBS-T</b>	Tris-buffer saline Tween 20
<b>TG</b>	Triglyceride
<b>TNF-<math>\alpha</math></b>	Tumour necrosis factor alpha
<b>WAT</b>	White adipose tissue

## UNITS

<b>µg :</b>	microgram
<b>mg :</b>	milligram
<b>g</b>	gram
<b>kg :</b>	kilogram
<b>nM:</b>	nanomolar
<b>µM :</b>	micromolar
<b>mM:</b>	millimolar
<b>M:</b>	molar
<b>nm :</b>	nanometer
<b>µm:</b>	micrometer
<b>mm</b>	millimeter
<b>mm<sup>2</sup></b>	millimeters squared
<b>mm<sup>3</sup></b>	millimeters cubic
<b>µL</b>	Microliter
<b>mL</b>	milliliter
<b>L</b>	litre
<b>pg/ml</b>	Pictogram per milliliter
<b>ng/mL</b>	nanogram per milliliter
<b>mg/mL</b>	milligram per milliliter
<b>g/mL</b>	gram per milliliter
<b>mmol/L</b>	millimole per liter
<b>µmol/gram</b>	micromole per gram
<b>mg/m<sup>2</sup></b>	milligram per meter squared
<b>µg/kg</b>	microgram per kilogram
<b>mg/kg</b>	milligrams per kilogram
<b>kg/m<sup>2</sup></b>	kilogram per meter squared
<b>v/v%</b>	volume in volume percent
<b>Amps</b>	Ampere
<b>AU</b>	Arbitrary Units
<b>°C</b>	degrees Celsius
<b>V</b>	Volt

<b>%</b>	percentage
<b>kcal</b>	Kilocalorie
<b>kDa</b>	Kilo Dalton
<b>mA</b>	Milli-ampere
<b>Hrs</b>	hours
<b>Mins</b>	minutes
<b>Secs</b>	seconds
<b>rmp</b>	Rate per minute
<b>1°</b>	Primary
<b>2°</b>	Secondary

## TABLE OF CONTENT

DECLARATION OF ORIGINALITY .....	i
ABSTRACT.....	ii
OPSOMMING .....	v
ACKNOWLEDGEMENTS .....	viii
LIST OF FIGURES .....	x
LIST OF TABLES.....	xiii
LIST OF ABBREVIATIONS.....	xiv
UNITS.....	xvii
TABLE OF CONTENT .....	xix
1. LITERATURE REVIEW .....	1
1.1 Obesity in context .....	1
1.1.1 Obesity defined.....	1
1.1.2 Epidemiology of obesity .....	2
1.1.3 Consequences of obesity on health status .....	3
1.2 The heart .....	4
1.2.1 Myocardial metabolism.....	4
1.2.2 Myocardial adaption and maladaptation during obesity .....	6
1.3 Mechanisms that link obesity to cardiovascular damage.....	6
1.3.1 Cardiac remodelling of the heart .....	6

1.3.2 Stages of heart failure.....	8
1.4 Lipid accumulation and the development of insulin resistance .....	8
1.4.1 Oxidative stress and mitochondrial dysfunction in context .....	9
1.4.2 Adipokines and the heart.....	10
1.4.3 Pro-inflammatory cytokines (other adipokines).....	12
1.5 Mechanisms underlying the obesity-cancer link .....	13
1.5.1 Insulin, IGF-1 and IGFBPs .....	13
1.5.2 Hormone dependent cancers .....	13
1.5.3 Adipokine dysregulation .....	14
1.6 Anthracycline chemotherapeutic treatment .....	15
1.6.1 Doxorubicin-induced cardiotoxicity.....	18
1.6.2 Cardiotoxicity classification.....	19
1.6.3 Risk factors associated with the development of cardiotoxicity .....	20
2. MATERIALS AND METHODS.....	23
2.1 Ethical considerations .....	23
2.2 Study design.....	23
2.2.1 Obesity Induction and Diet Composition.....	23
2.2.2 Cancer cell inoculation and tumour growth .....	24
2.2.3 Doxorubicin preparation and administration.....	25
2.2.4 Humane endpoints .....	25

2.3 Blood analysis.....	26
2.3.1 Luminex multiplex assay.....	26
2.4 Oxidative stress analysis.....	27
2.4.1 Measurement of early stage lipid peroxidation (Conjugated Dienes assay) .....	27
2.4.2 Measurement of late stage lipid peroxidation (TBARS assay) .....	28
2.5 Western blot analysis.....	28
2.5.1 Tissue lysate preparation.....	28
2.5.2 Protein determination.....	29
2.5.3 Preparation of tissue lysates, protein separation and transfer .....	29
2.5.4 Visualisation.....	31
2.5.5 Total protein standardizing.....	31
2.6 Histological analysis.....	31
2.6.1 Tissue processing.....	31
2.7 Histological staining.....	32
2.7.1 Haematoxylin and Eosin staining.....	32
2.7.2 Sirius Red stain for collagen.....	33
2.8 Statistical analysis.....	34
3. RESULTS.....	35
3.1 Establishing diet-induced obesity.....	35
3.1.1 Body weight.....	35

3.1.2 Food consumption and fluid intake .....	37
3.1.3 Fasting blood parameters.....	39
3.2 Effect of obesity on the heart.....	41
3.2.1 The impact of diet-induced obesity on the cardiac hypertrophy index .....	41
3.2.2 The effect of a high fat diet on myocardial ultrastructure and collagen deposition.....	42
3.2.3 The effect of a high fat diet on apoptotic protein expression.....	44
3.2.4 The effect of a high fat diet on oxidative stress parameters.....	45
3.3 Establishing a state of co-morbidity .....	47
3.3.1 Body weight .....	47
3.3.2 Food consumption and water intake.....	49
3.3.3 Fasting blood parameters.....	51
3.4 Effect of obesity and cancer on the heart.....	53
3.4.1 The impact of diet-induced obesity and cancer on the cardiac hypertrophy index .....	53
3.4.2 The effect of a high fat diet and cancer on myocardial ultrastructure and collagen deposition .....	53
3.4.3 The effect of a high fat diet and cancer on apoptotic protein expression.....	56
3.4.4 The effect of a high fat diet and cancer on oxidative stress parameters.....	56
3.5 Establishing a condition of obesity, cancer and acute cardiotoxicity .....	57
3.5.1 Body weight .....	57
3.5.2 Food consumption and water intake.....	59

3.5.3 Fasting blood parameters.....	61
3.6 Effect of obesity, cancer and doxorubicin therapy on the heart .....	63
3.6.1 The impact of diet-induced obesity, cancer and doxorubicin therapy on the cardiac hypertrophy index .....	63
3.6.2 The effect of a high fat diet, cancer and doxorubicin therapy on myocardial ultrastructure and collagen deposition.....	64
3.6.3 The effect of a high fat diet, cancer and doxorubicin therapy on apoptotic protein expression .....	67
3.6.4 The effect of a high fat diet, cancer and doxorubicin therapy on oxidative stress parameters	68
4. DISCUSSION .....	70
4.1 Increased fat in the diet induced obesity.....	71
4.2 Effect of obesity on the heart .....	72
4.3 Cancer in an obese state induces body weight loss and increased inflammation .....	74
4.4 DOX treatment and tumour presence decrease body weight.....	76
4.5 Effect of chemotherapeutic treatment during cancer in an obese context .....	77
5. Limitations and future directions .....	80
6. REFERENCE LIST .....	81
7. APPENDICES .....	98
7.1 Appendix A: Supplementary Results.....	98
7.2 Appendix B: Detailed Protocols .....	102
7.3 Appendix C-Reagents and solutions preparation.....	125

7.4 Appendix D: Equipment and Reagents list.....	131
7.5 Appendix E: Grime scale.....	136
7.6 Appendix F: Ethics Letter.....	137

## 1. LITERATURE REVIEW

### 1.1 Obesity in context

#### 1.1.1 Obesity defined

While being overweight or obese has previously been considered a serious health problem, it is now considered a global pandemic. The worldwide prevalence of obesity was almost doubled in the 1980s and tripled by 2016 in adults and children respectively (Segal *et al.*, 2017). In the same year, approximately 13% of the world's adult population (11% of men and 15% of women) were obese, whereas an estimated 41 million children under the age of five years were deemed obese or overweight. It was previously thought that this condition occurred in high-income countries, however it is now prevalent in low- to middle-income countries as well, particularly in the urban and peri-urban regions. In Africa, the number of overweight children under the age of five has risen by nearly 50% since 1990s (WHO, 2017).

Being overweight or obese is defined as an excessive accumulation of fat that may impair overall health. This excessive accumulation fat, known as adiposity, is due to increased food intake which is then stored in adipose tissue (Lin *et al.*, 2000). Clinically, obesity is measured by the determination of the body mass index (BMI), a simple index of weight-to-height measure in kilograms/meter squared ( $\text{kg/m}^2$ ). An individual is considered overweight if their BMI is equal to or greater than  $25 \text{ kg/m}^2$ , whereas an obese individual has a BMI of equal to or greater than  $30 \text{ kg/m}^2$  (Ford *et al.*, 2011). Although BMI provides the most useful population measure of being overweight or obese as it is the same for both males and females, it should be considered as a guide because it may not correspond to the same degree of 'fatness' in different individuals especially in the context of gender.

Other useful measures of determining whether an individual is overweight or obese include the waist to hip ratio and waist circumference, which are often used alongside BMI for a more holistic indication of where excessive fat is stored within the body. More sophisticated techniques such as underwater weighting, x-ray absorptiometry have also been established, however they require specialised equipment resulting in these techniques being expensive and thus traditional measurements are often adhered to (Deurenberg, 1999; Leopoldo *et al.*, 2016). Apart from establishing ways to diagnose obesity it is also important to understand the risk factors that are associated with this disease state.

### 1.1.2 Epidemiology of obesity

There are numerous causes for the development of obesity, however the fundamental cause is an energy imbalance between calories consumed and calories expended (Mraz & Haluzik, 2014). Simply put, if one consume more calories than one expend, one gains weight, and if more calories is used than consume then weight is lost. It should be bared in mind that this does not take into account the types of calories individuals ingest which is important in terms of the balance between carbohydrates, proteins and fats. Globally, there has been an increased intake of energy-dense foods that are high in unsaturated fats mainly due to affordability, followed by a decrease in physical activity (Finkelstein *et al.*, 2005). This may be due to various factors namely:

- (i) Environment: the sedentary nature of many forms of work, changing modes of transportation, and the rise in urbanization,
- (ii) Behaviour: increased physical inactivity, the selection of economically cheaper and palatable food and socio-cultural behaviour and,
- (iii) Physiology: the energy imbalance due to lifestyle choices of the individual, as well as genetic predisposition (Swinburn *et al.*, 2011, Hruby & Hu, 2015).

Although the above mentioned factors play an important role in this context, the genetic contribution to this state cannot be ignored (Albuquerque *et al.*, 2015). More often than not, it has been documented that obesity appears to occur more in families where some family members are already obese, or are born from parents who were or are currently obese. In support of this theory, Reilly *et al.*, (2005) demonstrated that the odds in children being obese increased to 2.93%, 4.66% and 11.75% if the father, mother or both parents respectively were obese, thus signifying a dominant influence of parental obesity. Moreover, parental obesity is deemed better to predict obesity during adulthood than the child's own weight status (Fuemmeler *et al.*, 2013). Interestingly, in an obesity-conducive environment, genetic factors influence the propensity of a child to becoming obese. Leptin deficiency, hypothyroidism, growth hormone deficiency or side effects associated with drugs such as steroids, have all been shown to contribute to childhood obesity (Güngör, 2014). Some of the common antenatal and postnatal factors thought to influence childhood and adulthood obesity include gestational diabetes mellitus, maternal weight gain during pregnancy, intra-uterine growth retardation, babies that are either too small or too large for gestational age, early bottle feeding, infant over nutrition

and early adiposity. It should be mentioned however that the above conditions do not influence childhood or adult obesity more than personal lifestyle choices as well as environmental and behavioural factors. Figure 1.1 below illustrates the factors already discussed that have an established role in obesity and other factors that will not be discussed as part of this literature review.

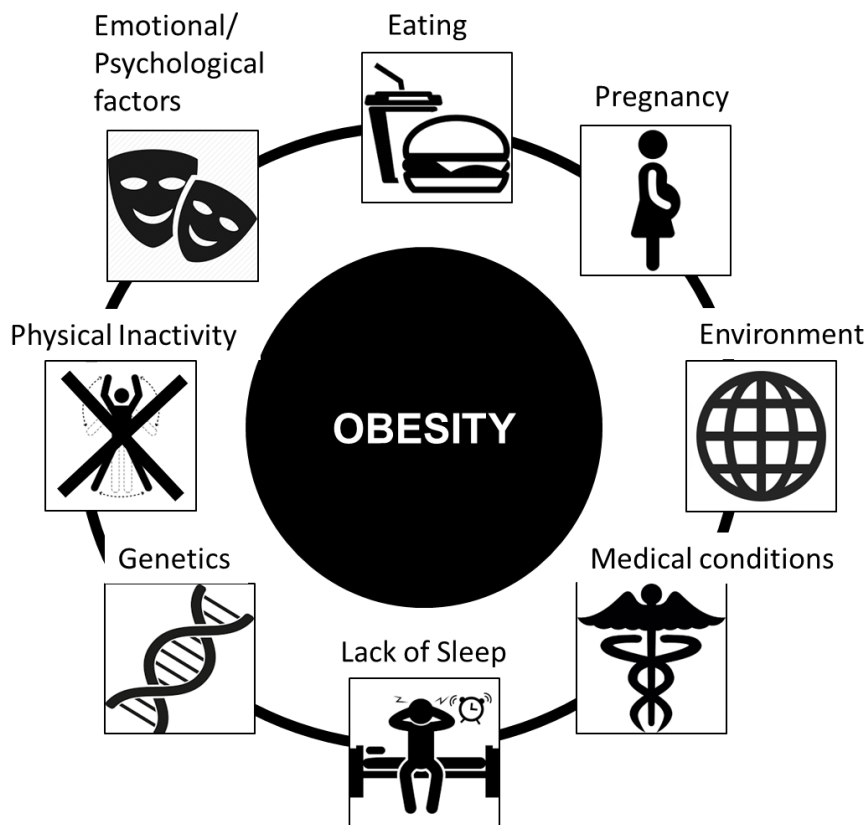


**Figure 1.1: Causes of childhood and adulthood obesity.** Obesity is a multifactorial disease and usually consists of many factors that interact and contribute to the condition based on genetic predisposition, lifestyle choice, environmental and behavioural factors.

### 1.1.3 Consequences of obesity on health status

A major consequence to obesity as defined by the National Heart, Lung, and Blood Institute, are metabolic perturbations accompanied by insulin insensitivity (which makes it difficult to utilise blood glucose), and central obesity (excess fat around the abdominal and stomach area

of the body). These factors are often associated with metabolic syndrome, a condition defined as abnormalities in three or more of the following: waist circumference, fasting blood triglycerides, cholesterol levels, blood pressure and fasting glucose levels (Aggoun, 2007). Together, these factors have a long-term risk of cardiovascular disease (CVD) and type 2 diabetes mellitus (T2DM) (Kahn & Flier, 2000; O'Neill & O'Driscoll, 2015) and ultimately impacts on the quality of life as health is compromised.

## 1.2 The heart

### 1.2.1 Myocardial metabolism

The heart is a four chambered organ (two ventricles and two atriums) and together with the lungs are responsible for the replenishment of oxygen rich blood to various organs in the body (Figure 1.2). As this organ plays a critical role in maintaining blood circulation, it requires a high demand of energy (ATP) output provided by the abundant mitochondria present (Marieb & Hoehn, 2013). The heart's metabolic machinery consists of three components: (i) substrate utilization, (ii) the breakdown of substrates by mitochondria to produce energy and, (iii) the transfer of the energy and utilization thereof in maintaining myocardial function (Scolletta & Biagioli, 2010). Under normal conditions the main substrate utilized by mitochondria are fatty acids and followed by pyruvate (Stanley & Chandler, 2002; Kolwicz *et al.*, 2013). The heart has a wide scope and flexibility in using other substrates including carbohydrates, amino acids and ketone bodies to allow for its 24/7 contractile function (Kolwicz *et al.*, 2013). The importance of a switch in substrate utilization is demonstrated through different scenarios that require the heart to work harder (e.g. exercise) or, during times of nutrient stress (e.g. fasting) or, when the myocardium becomes damaged because of disease. Depending on the type, severity and duration of the stress, the shift in substrate utilization can be temporary (adaptation) or long-term (maladaptation). Table 1.1 depicts the different substrates utilized under various conditions and shows how the heart switches from one substrate to another.

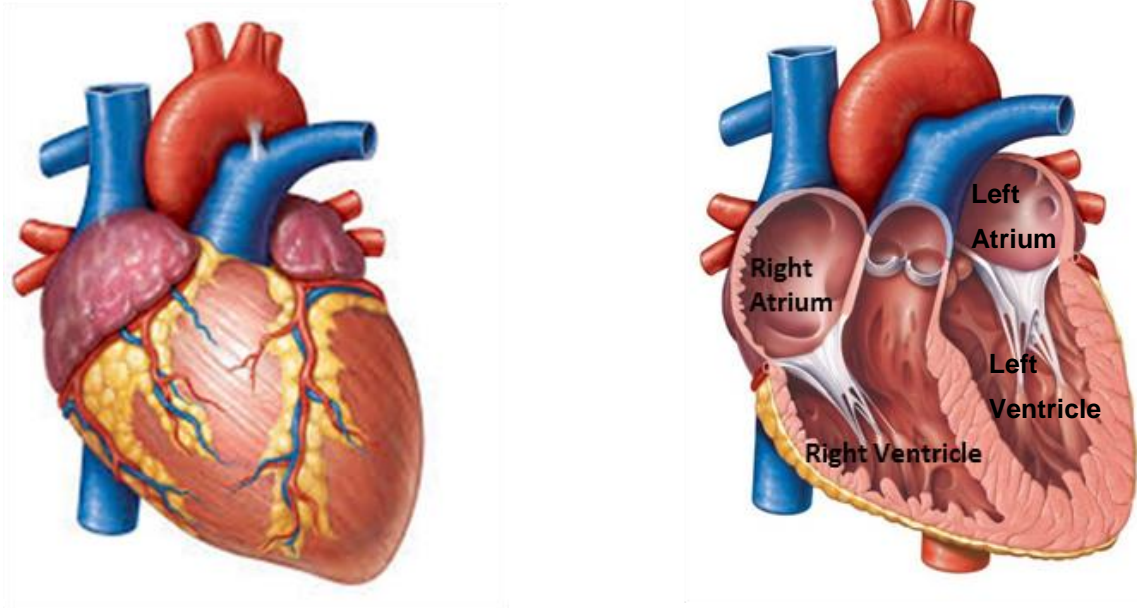


**Figure 1.2: The anatomical structure of the heart showing the ventricles and atriums.** The structural display of the hearts anatomical layout four chambered heart, two ventricles (left and right) and two atriums( left and right),obtained from Marieb & Hoehn, 2013.

**Table 1.1: Different substrates utilized by the heart under various conditions**

(Adapted from Stanley & Chandler, 2002; Harmancey *et al.*, 2008; Kolwicz *et al.*, 2013; Ritterhoff & Tian, 2017)

Condition	Short Explanation	Main Substrate
Foetus Heart	- Normal contractile function and cardiac output in developing heart under low oxygen environment	Glucose Lactate
Normal Adult heart	- Normal contractile function and cardiac output	Free Fatty Acids Glucose
Exercise	- Increased energy, blood flow and oxygen to skeletal muscles	Lactate
Fasting/Starvation	- Low glucose presence and glycogen stores are used up	Ketone Bodies Amino Acids
Ischemia	- Area in heart that no longer functions	Glucose Ketone bodies
Diabetes/Obesity	- Decrease in oxidative metabolism resulting in increased oxidative stress, insulin resistance, lipid accumulation and energy depletion	Glucose

### 1.2.2 Myocardial adaption and maladaptation during obesity

As mentioned previously, under normal conditions, the heart utilizes fatty acids as the main substrate for energy production, but during heart failure for example, glucose and lactate are used (Stanley & Chandler, 2002). During this state, the adult heart is said to mimic the foetus heart, and although not completely understood, it is believed that since fatty acid metabolism utilizes more energy than glucose metabolism, the anaerobic glycolysis that takes place is a more energy efficient mechanism for generating energy to maintain cardiovascular function (Schulze, 2009).

While fat in the body is often associated with negative connotations, it is an essential substrate particularly with reference to white adipose tissue (WAT). Not only is it responsible for the management and storage of excess lipid triglycerides (Vázquez-Vela *et al.*, 2008), it functions as a paracrine and endocrine organ that has an interactive role in the secretion of adipokines. Even though adipokines are circulating hormones that communicate with other organs to maintain energy balance (adiponectin) and food intake (leptin) (Lau *et al.*, 2005), their dysregulation has been implicated in inflammatory conditions that have been shown to induce peripheral insulin tissue resistance and CVD (Kwon & Pessin, 2013). In obese individuals and rodent models, the expression of pro- to anti-inflammatory adipokines is at least in part augmented to induce insulin resistance. Collectively, these findings suggest that not only is there malfunction in the paracrine and endocrine secretions of WAT, obesity-related insulin resistance may result from an imbalance between the expressions of pro- and anti-inflammatory adipokines. Together with the increase in adipose tissue, a state of hypoxia is induced which results in a switch of WAT from a storage organ to an actively secreting organ. This dysregulation is thus believed to be one of the causes of obesity-induced T2DM, dyslipidaemia, CVD and cancer (Fernández-Sánchez *et al.*, 2011).

## 1.3 Mechanisms that link obesity to cardiovascular damage

### 1.3.1 Cardiac remodelling of the heart

Under obese conditions, there is an increase in body fat which augments cardiac output and blood volume (Marieb & Hoehn, 2013). To compensate for this change, the heart requires a bigger output rate supplied by the change in the hearts preload. Although this change may initially be an adaptive mechanism, over time this adaptation can be maladaptive as left

ventricular remodelling with enlargement of the ventricle occurs (Harmancey *et al.*, 2008). The increased tension that arises in the left ventricular wall eventually culminates in left ventricular hypertrophy. Considering that obesity leads to other disorders, further damage to the heart is almost inevitable.

Cardiomyocytes are the most abundant cells contained in the heart and have a low regenerative capacity (Sawyer *et al.*, 2010; Kikuchi & Poss, 2012). When irreversible damage occurs, activated fibroblasts in the heart deposit collagen to replace the dead or dying cells. This deposition of collagen is known as fibrosis (Mahajan *et al.*, 2015). The consequence of this results in a decrease in the number of cardiomyocytes and thickening of the ventricular wall. Furthermore, since fibroblasts lack the flexibility of cardiomyocytes, myocardial contractility is reduced due to the stiffness of the myocardium. The above changes demonstrate a phenomenon known as cardiac remodelling which has been established in many preclinical research models (Abel *et al.*, 2008, Calligaris *et al.*, 2013; Russo & Frangogiannis, 2016). Leopoldo and colleagues (2016) illustrated insulin resistance, hyperleptinemia, collagen deposition and ultrastructural changes of the myocardium in rats fed a high fat diet over a period of 15 weeks. It is therefore clear to see how the state of obesity induced by diet over time negatively impacts on normal cardiovascular function.

Other mechanism by which obesity can contribute to cardiac remodeling is the high blood glucose occurs. The toxic effect of the overabundance of fasted blood glucose term glucotoxicity has been linked to the symptom associated with the development of heart failure (Chess & Stanley, 2008). The over-expression of glucose becomes toxic to the heart and activates various pathways and downstream mechanisms. Hyperglycemia induces ROS production and this causes mitochondrial dysfunction and fragmentation. Since there is a shift in substrate utilization, AMP-activated protein kinase (AMPK) mediates metabolic adaptation under stress conditions by inhibiting energy-consuming pathways. It stimulates both FA oxidation and glycolysis to produce ATP whilst reducing ATP consuming processes (anabolic pathways). AMPK forms part of the mechanism to preserve energy under stressful conditions. The depletion of ATP or the ability to produce sufficient ATP eventually lead to the downstream activation of pathways are directly associated with signaling mechanisms associated with mitochondrial dysfunction and ROS production and thus cause damage within the heart. Hyperglycemia is able to promote the fibrogenic phenotype and the activation of the

inflammatory state (Russo & Frangogiannis, 2016). All these known pathways can contribute to how obesity causes damage to the heart.

### 1.3.2 Stages of heart failure

Heart failure (HF) is defined as the inability of the heart to function effectively and affects the pumping ability of the heart; it is strongly associated with chronic shift in substrate utilization often associated with metabolic disease. The heart is an insulin-responsive organ and therefore insulin insensitivity associated with diabetes can lead to glucotoxicity and shift in the metabolic state of the heart which is how diabetes cardiomyopathy can occur (Riehle & Abel, 2016). Clinically HF is classified by four different stages according to the (NYHA, 2019). Clinicians classify patients due to the severity of symptoms and signs of heart disease as follows. Stage 1: showing risk factors of heart failure development but no heart disease and symptoms, Stage 2: Heart disease and no structural changes or symptoms, Stage 3: structural heart disease and mild symptoms and Stage 4: advanced heart disease with heart failure symptoms and patients' require therapy and treatment. Although various symptoms and causes can affect the heart the end-point stage 4 when heart failure occurs becomes life threatening as the heart has lost most of its functionality.

### 1.4 Lipid accumulation and the development of insulin resistance

A distinct feature of obesity is the excessive accumulation of circulating free fatty acids (FFAs) in the blood. These FFAs are thought to bring about the onset of insulin resistance (IR) which is a feature of obesity and other metabolic diseases associated with obesity (Boden, 2011). Under normal conditions insulin signaling is involved in the regulation of blood glucose transport and storage, as well as the maintenance of lipolysis; however when insulin is down-regulated, IR ensues (Boden, 2011). As such, a few theories have been proposed that link fat accumulation due to diet-induced obesity (DIO) to the development of IR. Firstly, when there is an increase in free FFAs in a cell, these generate reactive oxygen species (ROS) and diacylglycerol (DAG) which go on to stimulate the serine/threonine protein kinase C (PKC) cascade. This cascade is responsible for the phosphorylation and activation of the insulin receptor substrate (IRS-1) at its threonine residue. However, under these conditions, it is the serine residue that gets phosphorylated which inhibits the activity of the PI3K/Akt (PKB)

pathway responsible for the translocation of glucose receptors (e.g.: GLUT 4) onto the cell membrane (Petersen & Shulman, 2006). Secondly, obesity is an inflammatory condition and is therefore associated with an elevated concentration of pro-inflammatory cytokines. These include tumour necrosis factor-alpha (TNF- $\alpha$ ) and interleukin-6 (IL-6), both of which are known to inhibit the action of insulin. Not only are these cytokines upregulated with chronic inflammation and conditions of muscle wasting, their stimulation of immune and inflammatory responses occurs through nuclear factor kappa light chain enhancer of activated B cells (NF $\kappa$ B) (Riehle & Abel, 2016b). Which will induce the transcription of genes involved in cell death and protein degradation (Sishi *et al.*, 2013). Thirdly, the failure of packaging excess lipids into lipid droplets can be toxic to non-adipose tissue. The deleterious effects of lipid accumulation in non-adipose tissue is known as lipotoxicity (Wende & Abel, 2011). Interestingly, triglycerides can also serve as a storage facility for long chain non-esterified fatty acids (NEFAs) as well as their products including ceramide and DAG. Therefore, within the scope of lipotoxicity, it can be concluded that excess saturated fatty acids, DAG and ceramide in obesity can induce chronic adipose tissue inflammation, IR and mitochondrial dysfunction, all of which have a harmful effect on multiple organs and systems in the body.

#### 1.4.1 Oxidative stress and mitochondrial dysfunction in context

As mentioned previously, myocardial tissue is particularly vulnerable to oxidative damage more than any other tissue due to its high oxidative environment and limited antioxidant defenses. Moreover, one third of the hearts weight is comprised of mitochondria (Kolwicz *et al.*, 2013; Octavia *et al.*, 2012). ROS is an unavoidable consequence to ATP production and when a state of oxidative stress occurs, the antioxidant systems in the heart become overwhelmed by the free radicals that are produced. If the stress is moderate, senescence or cell cycle inhibition takes place; however if the stress is severe, apoptosis and/or necrosis can be initiated (Carvalho *et al.*, 2013). The onset of apoptosis results from lipid peroxidation of mitochondrial membrane phospholipids which causes a collapse in the mitochondrial membrane potential, the opening of the mitochondrial membrane permeability transition pore (mPTP), cytochrome c leakage and downstream caspase-3 activation (Webster, 2012; Kubli, & Gustafsson, 2012). The end result for the heart is a reduced capacity to generate energy and in the long term, the heart will fail.

The most prominent role for mitochondria is to supply energy in the form of ATP during

oxidative phosphorylation. Furthermore, mitochondria are involved in a vast array of anabolic and catabolic processes, and are required for the assembly of iron-sulphur clusters, which are essential cofactors of many enzymes (Stehling & Lill, 2013). In addition to their role in different biochemical pathways, mitochondria regulate apoptosis and participate in the process of development and ageing (Gustafsson & Gottlieb, 2006). Therefore, mitochondrial integrity is vital for cardiomyocyte function and two opposing processes collectively termed as mitochondrial dynamics maintain this integrity (Hom & Sheu, 2009). Mitochondria constantly fluctuate between fusion (fuse) and fission (divide) events which regulate the length of these organelles as well as their degree of interconnectivity. The rate at which these events happen is influenced by metabolic and pathological stimuli within mitochondria and the surrounding cellular environment (Westermann, 2010). The antagonistic and balanced actions of the fusion and fission machinery shapes mitochondria and through the dynamic nature of these organelles, allows cells to respond to the ever-changing physiological hues. On the one hand, a shift towards fusion promotes the generation of interconnected mitochondria which is beneficial in metabolically active cells, however on the other hand, a shift towards fission favors mitochondrial fragmentation which is considered detrimental (Westermann, 2010). Not only are fusion and fission events important for growth, mitochondrial redistribution and maintenance of a healthy mitochondrial pool, they play a critical role in disease-related processes such as apoptosis and mitophagy (mitochondrial specific degradation *via* autophagy) (Kubli & Gustafsson, 2012). Autophagy is defined as cellular process involved in self-cannibalization and involves the promotion of both cell survival and cell death activation (Rabinowitz & White, 2010)

#### 1.4.2 Adipokines and the heart

Adipokine secretion plays a role in insulin sensitivity, the regulation of food intake and energy homeostasis of the body under normal conditions (Guerre-Millo, 2008). During obesity, adipokines are considerably elevated and in this manner are considered dysregulated (Lau *et al.*, 2005). Their increased levels have been linked to the stimulation of pathways involved in oxidative stress and inflammation by endocrine, paracrine and autocrine systems. The longer the inflammation continues, the higher the risk of damage. Generally, two stages of inflammation exist: acute and chronic. Acute inflammation constitutes the initial stage of inflammation and is regulated through the activation of the innate immune system. This type of

inflammation is short-lived (temporary) and is usually beneficial to the host. If inflammation persists, the second stage of inflammation, or chronic inflammation is initiated, and this predisposes the host to various chronic illnesses (Lawrence & Gilroy, 2007). During this event, inflammatory cells such as mast cells and leucocytes are deployed to the site of injury, which leads to a 'respiratory burst' due to the increased consumption of oxygen, and therefore an increased release and accumulation of ROS is expected (Saeidnia & Abdollahi, 2013). It is for this reason that inflammation and oxidative stress cannot be easily separated.

Leptin, an adipokine encoded by *ob* gene and secreted by adipose tissue, is involved in the regulation of body weight on the bases that it modulates food intake and energy expenditure through the stimulation of neurotransmitters in the hypothalamus (Lau *et al.*, 2005; Schäffler & Schölmerich, 2010). In pathological conditions such as obesity, the balance of leptin actions may shift to stimulate inflammation, oxidative stress, and smooth muscle hypertrophy. These actions may contribute to the pathogenesis of hypertension, atherosclerosis, left ventricular hypertrophy, and T2DM (Deswal, 2011). Under these conditions, elevated levels of leptin are observed due to the disruption of the leptin signalling cascade within the central nervous system (CNS). Therefore, the maintenance of energy balance is impaired which results in the body becoming insensitive to leptin, or otherwise leptin resistant. This resistance allows for leptin levels to rise in blood circulation and correlates with an individual's BMI (Maskari & Alnaqdy, 2006). While numerous investigation have been conducted to understand the importance of leptin in obesity-related CVD, hyperleptinaemia has been confirmed to be a predictor of acute cardiovascular events (Hou & Luo, 2011).

In contrast, adiponectin, the most abundant adipokine secreted by adipocytes appears to have an opposing effect to the above mentioned adipokine in obesity. Not only is it also responsible for energy homeostasis, it possesses anti-inflammatory effects and improves insulin sensitivity (Fernández-Sánchez *et al.*, 2011). Although its cardioprotective role has been well studied, clinical investigations have identified adiponectin deficiency (hypoadiponectinaemia), or the down-regulation thereof, as seen during obesity or related pathologies, as an independent risk factor for CVD (Singla *et al.*, 2010). The up-regulation of adiponectin both genetically or pharmacologically, has been illustrated to improve obesity-induced endothelial cell dysfunction and hypertension, and also prevents atherosclerosis, myocardial infarction and diabetic cardiomyopathy (Ouchi *et al.*, 2006; Shibata *et al.*, 2009; Hui *et al.*, 2012). While the exact

mechanisms are yet to be fully elucidated, it is speculated that adiponectin protects cardiovascular health through its vasodilatory, anti-apoptotic, anti-inflammatory and anti-oxidative properties in both cardiac and vascular cells (Hopkins *et al.*, 2007; Shibata *et al.*, 2009; Hui *et al.*, 2012). Based on the above literature, it is clear to see the importance of adipokines in maintaining cardiovascular health.

#### 1.4.3 Pro-inflammatory cytokines (other adipokines)

Some adipokines are also classified as cytokines since they are secreted by not only adipocytes but also other cell types. These include interleukin-6 (IL-6) and tumour necrosis factor-alpha (TNF- $\alpha$ ). TNF- $\alpha$  plays a major role in a broad range of diverse actions which include growth and differentiation (Kirillova *et al.*, 1999), inflammation (Schutz *et al.*, 1992), apoptosis and necrosis (Basu *et al.*, 2002). IL-6 is produced in response to host infections and tissue injury by contributing to the stimulation of acute phase responses, haematopoiesis and immune reactions (Tanaka *et al.*, 2014). Although these cytokines function pleiotropically (anti- and pro-inflammatory), their expressions are transcriptionally and post translational controlled, and their dysregulated synthesis plays a pathological role in chronic inflammation and autoimmunity (Ishihara & Hirano, 2002). Over the past decades, it has become evident that excess adipose tissue gives rise to chronic, low grade inflammation, which plays a significant role in the development of obesity and associated disorders such as insulin resistance, T2DM, metabolic syndrome and CVD (Lau *et al.*, 2005; Singla, 2010; Boden, 2011; Hsieh, 2011). Under these conditions, WAT secretes increased levels of TNF- $\alpha$  and IL-6 which may not only have local effects on WAT, but also systemic effects on other organs (Ronti *et al.*, 2006; Vázquez-Vela *et al.*, 2008). While TNF- $\alpha$  in adipose tissue plays a central role in lipid metabolism and insulin regulation, IRS-1 activity is prohibited during obesity. Additionally in this context, IL-6 is implicated to play a central role between obesity and inflammation as it promotes the accumulation of FFAs (Fernández-Sánchez *et al.*, 2011; Wueest *et al.*, 2014).

There is a growing concern that this prolonged pro-inflammatory state and the dysregulation of adipokines within obese individuals, serves as the ideal micro-environment for the cancer cells to thrive. For a normal cell to evolve into a cancerous one, it requires specialized events for the transition to take place. Each cell is equipped with controlling genes responsible for surveillance and to suppress the initiation and progression of pro-neoplastic cells (Hanahan & Weinberg, 2000). Since the metabolic state of the body is used as a source of survival for cancer cells,

obesity provides a “scape goat” for these cells to surpass these check points because of its effect on metabolic regulation. Recent research has found that as BMI increases by 5 kg/m<sup>2</sup>, the incidence of cancer increases by 10% (Basen-Engquist & Chang, 2011). The link between obesity and cancer has been demonstrated in numerous cohort studies (Basen-Engquist & Chang, 2011; Matthews & Thompson, 2016) and the percentages of cancer attributed to obesity were 11% for colon cancer, 9% for post-menopausal breast cancer, 39% for endometrial cancer, 25% for kidney cancer and 37% for oesophageal cancer (Basen-Engquist & Chang, 2011). In an effort to understand the link between obesity and cancer risk, current studies are focused on the mechanisms involved. However, due to the complex nature of obesity and the numerous mechanisms involved, which may differ across cancer sites, various pathophysiological mechanisms have been proposed and will be discussed in the next section.

### 1.5 Mechanisms underlying the obesity-cancer link

While numerous mechanisms have been proposed, a comprehensive summary of all possible systems is beyond the scope of this review, and thus only the most relevant and emerging processes linking obesity to carcinogenesis will be highlighted.

#### 1.5.1 Insulin, IGF-1 and IGFbps

By far the biological mechanisms that have received much attention include insulin, insulin-like growth factor-1 (IGF-1), sex hormones and adipokines. It is well known that during obesity, a state of hyperinsulinemia occurs and works by preventing apoptosis and promotes cell proliferation. The augmented levels of insulin in this scenario reduces IGF binding proteins (IGFBPs) which then leads to increased IGF-1 levels, a change in the cellular environment and ultimately tumour growth (Calle & Kaaks, 2004). Coincidentally, insulin also regulates growth hormone which in turn contributes to the production of IGF-1 and IGFBP-3 (Nam *et al.*, 1997). Even though studies measuring IGFBP-3 have been inconsistent, elevated levels of IGF-1 have been associated with an increased risk of pre- and post-menopausal breast cancer and prostate cancer (Shanmugalingam *et al.*, 2016).

#### 1.5.2 Hormone dependent cancers

There is growing evidence to support the role of the effect of sex hormones and their link between these two inflammatory conditions, particularly those that are considered to be

hormone dependent (e.g.: breast, ovarian uterine and prostate) (Folkerd & Dowsett, 2010). Sex hormones are mainly produced by steroidogenic organs and constitute estrogens, androgens and progestogens. The binding of estrogen to its receptor (ER) triggers intracellular signalling pathways that initiate cell division and tumour progression (Brown & Simpson, 2014). Moreover, excess aromatase secreted from adipose tissue leads to elevated levels of estradiol not being bound which damages DNA. Interestingly, adipose tissue can also act as reservoir for carcinogens and xenochemicals where the release thereof can contribute to carcinogenesis (Hsieh, 2011).

### 1.5.3 Adipokine dysregulation

As has been previously established, leptin during obesity is up-regulated whilst adiponectin is down-regulated. The abnormal secretion of these adipokines, as well as the pro-inflammatory state that is induced (Figure 1.3), has been associated with the proliferation and survival of cancer cells through the activation of the RAS/RAF-MAPK signalling pathway and the suppression of anti-inflammatory events respectively (Hsieh, 2011). In addition, IL-6 which is increased during obesity, promotes cell survival *via* the JAK/STAT signalling pathway (Bromberg & Wang, 2008). While colon, prostate and breast cancers have been linked with elevated leptin levels, adiponectin has been negatively associated with these cancers (Nalabolu, Palasamudram & Jamil, 2014).

Other mechanisms linking obesity to cancer that deserve mentioning but will not be elaborated on, include: obesity-related hypoxia, genetic susceptibility, adipose stromal cell migration, inflammation and oxidative stress (Van Kruijsdijk *et al.*, 2009; Bilić, 2014; National Cancer Institute, 2017). These factors point toward the relationship between adipose tissue hypoxia, and the development of insulin resistance that stimulates reduced adiponectin and exaggerated leptin gene expressions. While research on the biological mechanisms underlying obesity and its relationship with cancer are still in the early stages, understanding the processes of carcinogenesis in obesity-related cancers may lead to the development of treatments and better preventative strategies.

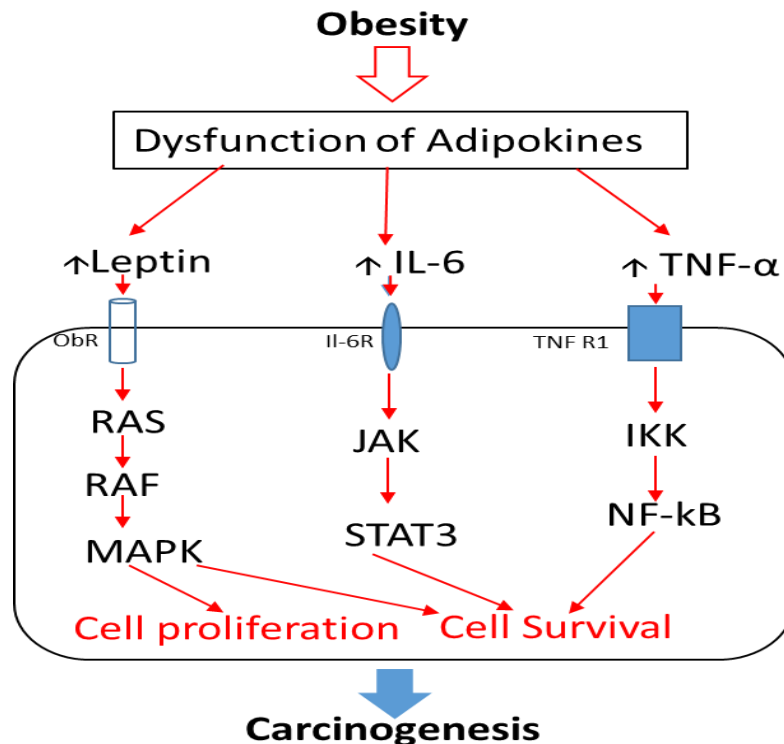


**Figure 1.3: Mechanisms by which obesity causes the dysfunction of adipokines and how it causes carcinogenesis.** Process takes place *via* the activation of cell proliferative and survival pathways induced by irregular adipokine secretion and pro-inflammatory cytokines (adopted from Hsieh, 2011).

### 1.6 Anthracycline chemotherapeutic treatment

Anthracyclines (ANTs) are a class of anti-neoplastic antibiotics extracted from *Streptomyces* bacterium (Malhotra & Perry, 2003) and are used for the treatment of various cancers including lymphomas and leukaemias, breast, ovarian, prostate, stomach, uterine, bladder and paediatric cancers (Šimůnek *et al.*, 2009). These chemotherapeutic agents are thus among the most potent anti-cancer treatment regimens ever developed, and are effective against more cancer types than any other chemotherapeutic agent (Šimůnek *et al.*, 2009). Although the advances in cancer treatment has brought hope to patients against a disease that was previously thought to be incurable, their life threatening side effects cannot be ignored. As indicated in Figure 1.4, Doxorubicin (DOX), Daunorubicin, Epirubicin and Idarubicin are the four different anti-cancer agents belonging to the class of ANTs. Structurally, these drugs look similar in that they contain a tetracyclic ring which makes up the aglyconic moiety, and a sugar moiety known as

daunosamine. However, what differentiates these ANTs from one another are the modifications in the side groups attached to the tetracyclic ring (McGowan *et al.*, 2017). These minor differences are said to be responsible for their different levels of potency.

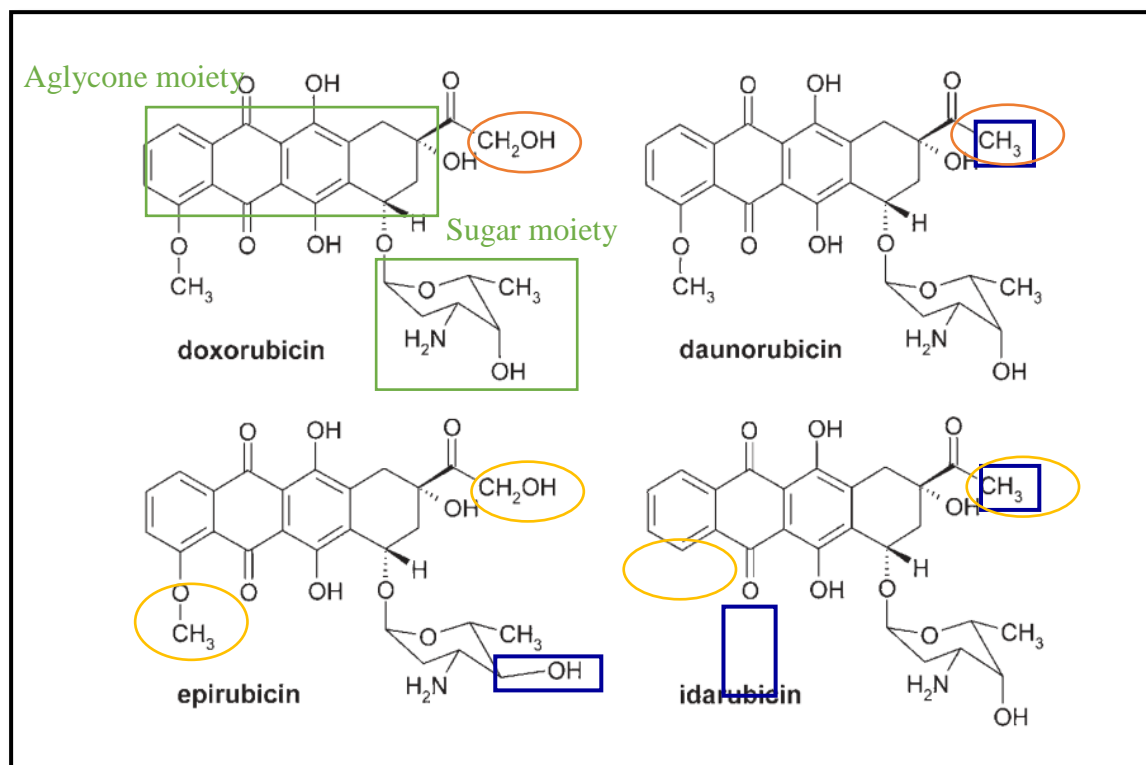


**Figure 1.4: Different anthracycline classes used in the treatment of various cancers.** Structurally, they all contain a tetracyclic ring which makes up the aglyconic moiety and a sugar moiety. The variation in the side chains of the aglyconic moiety differentiates them from one another. Orange circles distinguish between doxorubicin and daunorubicin, while yellow circles distinguishes between epirubicin and idarubicin (obtained from Šimůnek *et al.*, 2009).

DOX, isolated in the 1960s, forms part of the first line chemotherapeutic treatment regimens for many cancers and is marketed as Adriamycin® or Rubex® among other names (Takemura & Fujiwara, 2007; Puma *et al.*, 2008; Zhu *et al.*, 2010; Octavia *et al.*, 2012). DOX affects cancer cell proliferation through DNA intercalation because of its binding affinity to Topoisomerase II. Topoisomerase II induces single and double stranded DNA breaks during DNA replication and once the process is complete, these breaks can be resealed again. DOX exploits this function by stabilizing topoisomerase II in a specific conformation when DNA is cut. This causes DOX-DNA crosslinks which prevents DNA from being resealed, the repair process is thus halted and consequently cell death is induced. Another known mechanism by which this anti-cancer agent kills actively replicating cells is oxidative stress which causes oxidative damage to DNA,

proteins and lipids (Table 1.2). Once DOX enters the cell it undergoes a one electron reduction leading to the formation of an unstable DOX metabolite which is in turn converted back to DOX. This continuous redox cycling results in the production of oxygen derived free radicals (Thorn *et al.*, 2012). The ROS generated contributes to DNA alkylation, protein oxidation and lipid peroxidation, all of which can trigger different cell death modalities (Carvalho, 2013; Sawyer *et al.*, 2010).

Unfortunately, DOX's potent anti-tumour effects are overshadowed by its adverse influence on other organs especially the myocardium. This condition is termed cardiotoxicity and is a major setback to the considerable progress made in the field of oncology (Minotti *et al.*, 2004; Schimmel *et al.*, 2004). The toxic effects exhibited are attributed to DOX's cumulative and dose-dependent damage that leads to irreversible changes in the heart that manifests as left ventricular dysfunction and congestive heart failure (Chen *et al.*, 2007; Montaigne *et al.*, 2012). In the hopes of reducing and preventing these detrimental consequences, a number of initiatives have been tried and tested. These include: liposomal DOX formulations (Sawyer *et al.*, 2010), anti-oxidant therapy (Schimmel *et al.*, 2004), reduced treatment dosages as well as life time cumulative doses (Gianni *et al.*, 2008), to name but a few. However despite these efforts, cardiotoxicity still remains clinically relevant and some of these interventions risk treatment efficacy and chemotherapy resistance (Housman *et al.*, 2014).

**Table 1.2: Mechanisms by which DOX mediates its anti-cancer actions**  
(adopted from Carvalho *et al.*, 2013)

Anti-cancer mechanism	Pathway effected	Outcomes
DNA intercalation, cross-linking, and alkylation	- Topoisomerase (I and II) and helicase inhibition	- Inhibition of protein and DNA synthesis - Interference with DNA unwinding and separation - Onset of cell dysfunction or death
ROS production	- Quinone-semi-quinone recycling - DOX-iron recycling	- DNA damage - Lipid peroxidation - Increased DNA alkylation - cell death induction <i>via</i> caspases
Damage to cell membranes	- Plasma protein binding	- Production of free radicals and disruption of lipid bilayer

### 1.6.1 Doxorubicin-induced cardiotoxicity

Cardiotoxicity, as defined by the National Cancer Institute (2017), is toxicity that affects the ability of the heart to do fulfil its function. This term however is rather ambiguous considering that numerous drugs and other chemotherapeutics adversely affect the heart and its vasculature. DOX-induced cardiotoxicity is hypothesized to arise from multiple pathways including oxidative stress (Octavia *et al.*, 2012), apoptosis (Arola *et al.*, 2000), disruption of iron (Gammella *et al.*, 2014) and calcium homeostasis (Chen *et al.*, 2007). As well as mitochondrial dysfunction (Zhang *et al.*, 2009), inhibition of nucleic acid and protein (Takemura & Fujiwara, 2007), and changes in the adrenergic function (Ferreira *et al.*, 2008; Carvalho, 2013) as demonstrated in Table 1.3. Since the degree of myocardial damage induced by DOX therapy varies depending on dose, duration and DOX formulation, cardiotoxicity that induces myocardial dysfunction is known as acute, while cardiotoxicity associated with myocardial cell death is classified as chronic.

**Table 1.3: Different mechanisms by which DOX induces cardiotoxicity**  
(adopted from Carvalho *et al.*, 2013; Damiani *et al.*, 2016)

Cardiotoxic Mechanisms	Pathways effected	Outcomes
ROS generation	- Enzymatically <i>via</i> the mitochondrial respiratory chain, or non-enzymatically <i>via</i> DOX-iron complexes	- Increased free radical production, iron accumulation and oxidative damage
Mitochondrial dysfunction	- Disruption of mitochondrial dynamics (fusion and fission)	- Cell death, oxidative stress and calcium dysregulation
Topoismerase and helicase inhibition	- DOX binds to DNA and to enzymes involved in DNA healing	- Inhibits DNA replication, leading to activation cell death pathways
Damage membrane phospholipids (e.g.: cardiolipin)	- Drug-lipid complex formation	- Disruption of oxidative phosphorylation
Cell death induction	- Caspase dependent and independent pathways of apoptosis	- Death of cardiomyocytes

### 1.6.2 Cardiotoxicity classification

Acute or early-onset cardiotoxicity occurs either during or shortly after treatment. Although this is clinically manageable, it results in mild to moderate irregularities in heart beat functionality (Carvalho *et al.*, 2013; Zhang *et al.*, 2012). Also included in this classification is sub-acute cardiotoxicity which can occur a few weeks after treatment. It is characterized by the oedema and inflammation of the pericardial and myocardial walls (pericarditis–myocarditis syndrome) (Barrett-Lee *et al.*, 2009; Thorn, *et al.*, 2012). In contrast to acute toxicity, chronic cardiotoxicity occurs weeks, months (early-onset), years and even decades (late-onset) following chemotherapy (Figure 1.5). Not only is this type of cardiotoxicity the most detrimental due to its dose-dependent effects, it is associated with numerous risk factors and has no cure. Clinically it is characterized by a decline in blood pressure and ejection fraction, along an increased heart rate with failure (Barrett-Lee *et al.*, 2009; Zhang *et al.*, 2012; Thorn *et al.*, 2012). While these long term effects may have been mainly attributed to oxidative stress and consequently apoptosis downstream, clinical data obtained from anti-oxidant therapy has produced disappointing results (Vincent *et al.*, 2013). As mitochondria are responsible for ROS production in a cell and they are also a target of DOX damage, attention has since shifted from oxidative stress to mitochondrial dysfunction as a major contributor to cardiotoxicity (Cove-

Smith *et al.*, 2014). Mitochondrial dysfunction has been discussed in this review (sub-section 1.1.3) albeit in the context of obesity, however this phenomenon has been implicated to play an important role in this scenario as these organelles are the earliest and most prominent histomorphological features of DOX-induced cardiomyopathy (Minotti *et al.*, 1999). It is has been demonstrated that DOX has a high affinity for cardiolipin, a phospholipid enriched in the inner mitochondrial membrane, which results in the accumulation of DOX within mitochondria. This accumulation drives the sustained free radical production and oxidative damage (Li *et al.*, 2010) The end result of these events is mitochondrial dysfunction due to an imbalance in the fusion and fission processes. Even though the relationship between acute and chronic cardiotoxicity has not been well illustrated to establish whether the two conditions are directly, partially or independently connected, they are currently seen as two unique conditions despite sharing similar risk factors.

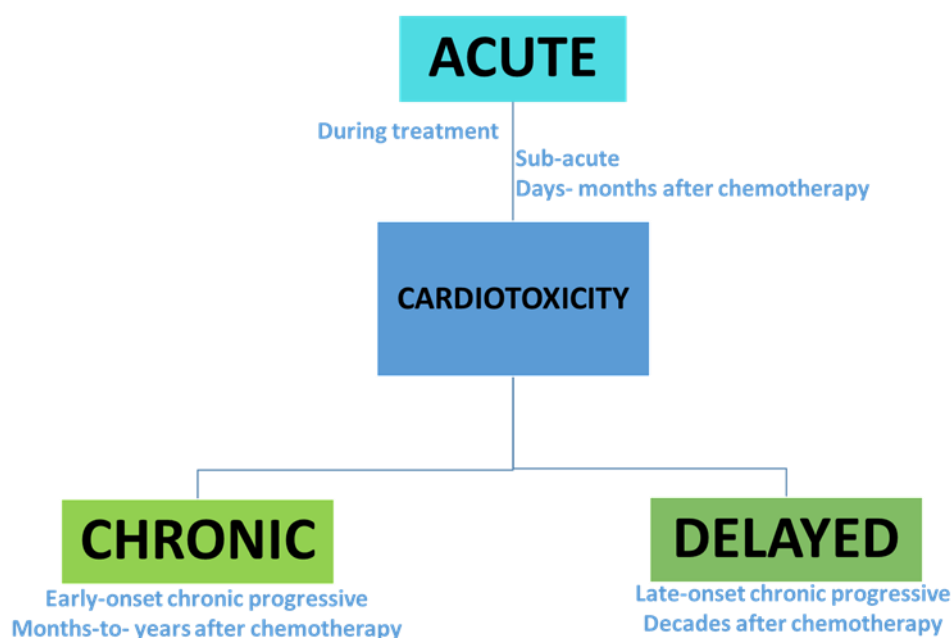


**Figure 1.5: Classification of DOX-induced cardiotoxicity**

### 1.6.3 Risk factors associated with the development of cardiotoxicity

There are various risk factors that contribute to an individual developing DOX-induced cardiotoxicity as illustrated in Figure 1.6. These include age, gender, previous chemotherapy use, cumulative DOX dose, an underlying heart condition and any other inflammatory condition that endangers the heart such as obesity and insulin resistance (Pai & Nahata, 2000). As obesity

is the most critical risk factor associated with CVD (section 1.3), cancer (section 1.4) and now DOX-induced cardiotoxicity, there are clear overlaps in mechanisms and signalling pathways involved, all of which have already been elaborated on previously in this review. Work published by Barrett-Lee and colleagues (2009) demonstrated an increased risk of heart failure with an increase in DOX cumulative dose. Furthermore, young people below the age of 15 and the older generation (older than 60 years) were found to be at most risk. In fact, similar work published in the 1970s showed a 3% risk of cardiotoxicity at cumulative DOX doses of 400 mg/m<sup>2</sup>, 7% at 550 mg/m<sup>2</sup> and 18% at 700 mg/m<sup>2</sup> (Vonn Hoff *et al.*, 1979). Through this work and the work of many others, DOX cumulative doses are now limited to 400 mg/m<sup>2</sup>. It is well known that women are at less risk of CVD or maintain a better cardiac function than men at least before menopause, due to their hormonal status (Regitz-Zagrosek *et al.*, 2006). However, in this context, sexual dimorphism has been understudied. From what is known from pre-clinical models, DOX-induced toxicity in males is associated with severe weight loss, reduced survival rates, changes in myocardial function and mitochondrial respiration, a down-regulation in signalling pathways responsible for energy production and decreased mitochondrial biogenesis, cardiolipin content and mitochondrial DNA (Moulin *et al.*, 2015). While the exact mechanisms mediating these sexual differences in unknown, further research aimed at exploring the role of sex hormones is necessary.

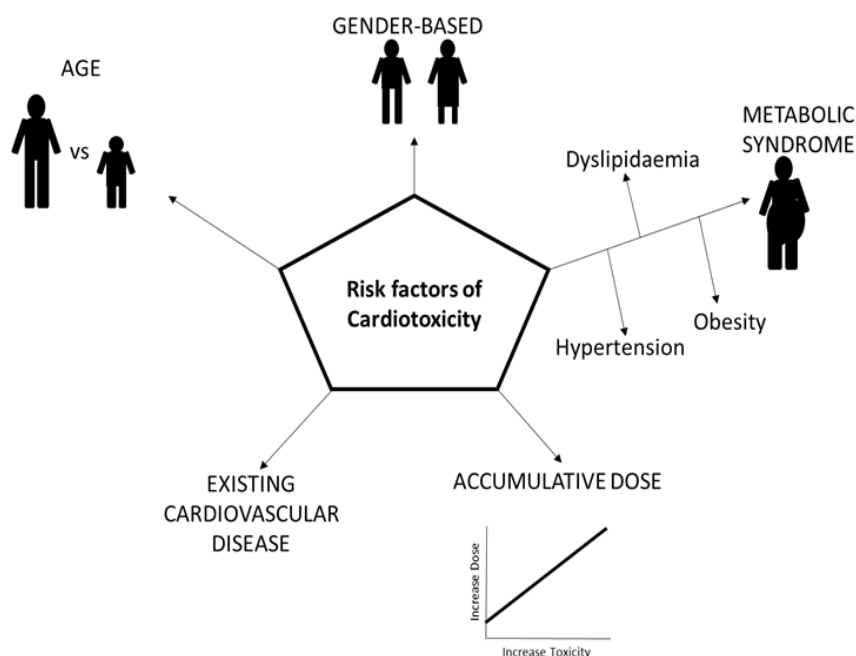


**Figure 1.6: Risk factors associated with the development of DOX-induced cardiotoxicity**

In conclusion, this review has attempted to provide a brief synopsis of the complications that arise during obesity. Not only does this disease risk myocardial health and performance, is it a risk factor for other inflammatory associated diseases that also place the heart at risk. Considering that these diseases have mainly been studied in isolation, there are very few, if any studies that have investigated cancer and cardiotoxicity in the context of obesity, to better understand the complex relationship that these diseases have with one another and how cardiovascular function is adversely affected in this co-morbid state. Therefore, this study hypothesizes that cancer in an obese environment increases the risk of developing early-stage DOX-induced cardiotoxicity. We aim to establish a relatable diet-induced obese mouse model that will be inoculated with breast cancer cells to induce tumours, and then further treated with DOX. To evaluate the effects of obesity, cancer and DOX treatment on the heart, markers of inflammation, oxidative stress, cell death, fibrosis and adipokines concentrations will thus be analysed.

## 2. MATERIALS AND METHODS

### 2.1 Ethical considerations

All *in vivo* experiments were ethically approved (ethics no# **SU-ACUM13-00015**) and performed under conditions that complied with the guidelines for the care and use of laboratory animals implemented at Stellenbosch University. Experiments conform to the accepted standards for the use of animals in research and teaching as reflected in the South African National Standards 10386: 2008 (Appendix F).

### 2.2 Study design

The *in vivo* study employed the use of female C57BL6 mice, which were weaned at 3 weeks of age and allowed to acclimatize for one week before the study commenced. Mice were housed in groups of five in static micro-isolation cages following a 12-hour dark/light cycle in a pathogen-free environment. Room temperature was maintained at  $\pm 22$  °C. Standard mice chow and water was available *ad libitum*, and the general welfare of the animals was monitored daily.

This study investigated DOX induced cardiotoxicity in an obese tumour bearing mice model. In brief, the mice were divided into two groups where one group was fed a high fed diet to induce obesity and the other a standard diet. Following obesity, the two groups were divided and half of the obese and standard mice were inoculated with tumours. The four remaining groups were further divided into eight experimental groups where half were subjected to DOX treatment. Figure 2.1 details the different experimental groups. A detailed discussion of the study design follows below.

#### 2.2.1 Obesity Induction and Diet Composition

Following the acclimatization period, mice were randomly divided into two experimental groups and were fed either a standard diet (D12450J, Research diet Inc., New Jersey, USA) or a high fat diet (D12492 Research diet Inc., New Jersey, USA) as outlined in **Table 2.1**. The high fat diet was used to induce obesity, and is specially designed such that the standard diet matches the sucrose components of the high fat diet. In addition, the standard diet was employed instead of the standard laboratory chow diet to prevent the potential effects of phytoestrogens,

which have previously been shown to produce variation in standard chow weight gain (Ulman, 2011). The animals remained on their respective diets throughout the duration of the study.

**Table 2.1: Dietary components of the standard and high fat diets**

(Adopted from Ulman, 2011)

Diet component	Standard diet (D12450J)		High fat diet (D12492)	
	gram %	kcal%	gram %	kcal%
Protein	19.2	20	26.2	20
Carbohydrates	67.3	70	26.3	20
Fat	4.3	10	34.9	60
Total		100		100
Kcal/gram	3.85		5.24	
<b>Ingredients</b>	<b>gram</b>	<b>Kcal</b>	<b>gram</b>	<b>Kcal</b>
Casein, 30 Mesh 200	200	800	200	800
L-Cystine	3	12	3	12
Corn Starch	506.2	2024.8	0	0
Maltodextrin 10	125	500	125	500
Sucrose	68.8	275.2	68.8	275.2
Cellulose BW200	50	0	50	0
Soybean Oil	25	225	25	225
Lard*	20	180	245	2205
Mineral Mix S10026	10	0	10	0
Dicalcium Phosphate	13	0	13	0
Calcium Carbonate	5.5	0	5.5	0
Potassium Citrate, 1 H <sub>2</sub> O	6.5	0	6.5	0
Vitamin Mix V10001	10	40	10	40
Choline Bitartrate	2	0	2	0
FD&C Yellow Dye #5	0.04	0	-	-
FD&C Blue Dye #1	0.01	0	0.05	0
<b>Total</b>	<b>1055.05</b>	<b>4057</b>	<b>773.85</b>	<b>4057</b>
Cholesterol (mg)/4057 kcal		54.4		216.4
Cholesterol (mg)/kg		51.6		279.6

### 2.2.2 Cancer cell inoculation and tumour growth

After eight weeks on the different diets, animals were further divided into two more groups, where half of the animals on the standard and high fat diet were inoculated with cancer cells. E0771 cells were grown and maintained as described in Appendix B. The cells were prepared for each mouse and mice were restrained and anaesthetized under 3% (v/v) isoflurane (Isofor, Safeline Pharmaceuticals, Florida, South Africa) in an anaesthetic chamber. The fourth

mammary pad was then subcutaneously inoculated with  $\sim 1.2 \times 10^5$  E0771 breast cancer cells. The tumour size was monitored using digital callipers by taking three measurements: perpendicular, horizontal and diagonal to the mouse's body. The volume of the tumours was calculated as follows: from the three readings taken, the largest volume served as the length (longitudinal/perpendicular) and the smallest volume served as the width (transverse/horizontal). The following formula was used:

$$\text{Tumour volume (mm}^3\text{)} = 0.5 \times (\text{length} \times \text{width}^2)$$

Once tumours reached a volume of  $\pm 200\text{-}300 \text{ mm}^3$ , chemotherapeutic drug treatment commenced.

### 2.2.3 Doxorubicin preparation and administration

DOX (D5794, LKT® laboratories, Minnesota, USA) stock solution was prepared as described in Appendix C. Mice were weighed prior to drug administration in order to determine the volume of drug. Following this, the above four groups were again randomly divided to create eight experimental groups. Where half of the animals on the standard diet, standard diet with tumour, high fat diet and the high fat diet with tumours received DOX treatment. DOX was administered via intraperitoneal injection every fourth day at a concentration of 4 mg/kg, resulting in a cumulative dose of 12 mg/kg. The vehicle control group received three intraperitoneal injections of Hank's balanced salt solution –HBSS (H8264, Sigma-Aldrich, Missouri, USA). Four days after the last injection, mice were euthanized following complete sedation with 3% (v/v) isoflurane (Isofor, Safeline Pharmaceuticals, Florida, South Africa) and cervical dislocation was performed to confirm death. Subsequently, blood was collected and hearts were rapidly excised where half of the tissue was frozen in liquid nitrogen for molecular analysis and the other preserved in formalin for histology. Additional gonadal adipose tissue (located in the third and fourth quadrant of mouse) was weighted and used to calculate gonadal adiposity as percentage of final body weight. A summary of the study design and experimental groups is demonstrated in Figure 2.1 below.

### 2.2.4 Humane endpoints

As this study involves the inoculation of tumour cells, as well as chemotherapy administration, the following humane endpoints were established:

- When tumour growth restricted mobility of the mice or influenced general welfare
- When the mice began to bite tumours
- When the mice exhibited changes in posture and facial expression, as determined using the grimace scale (see Appendix E)

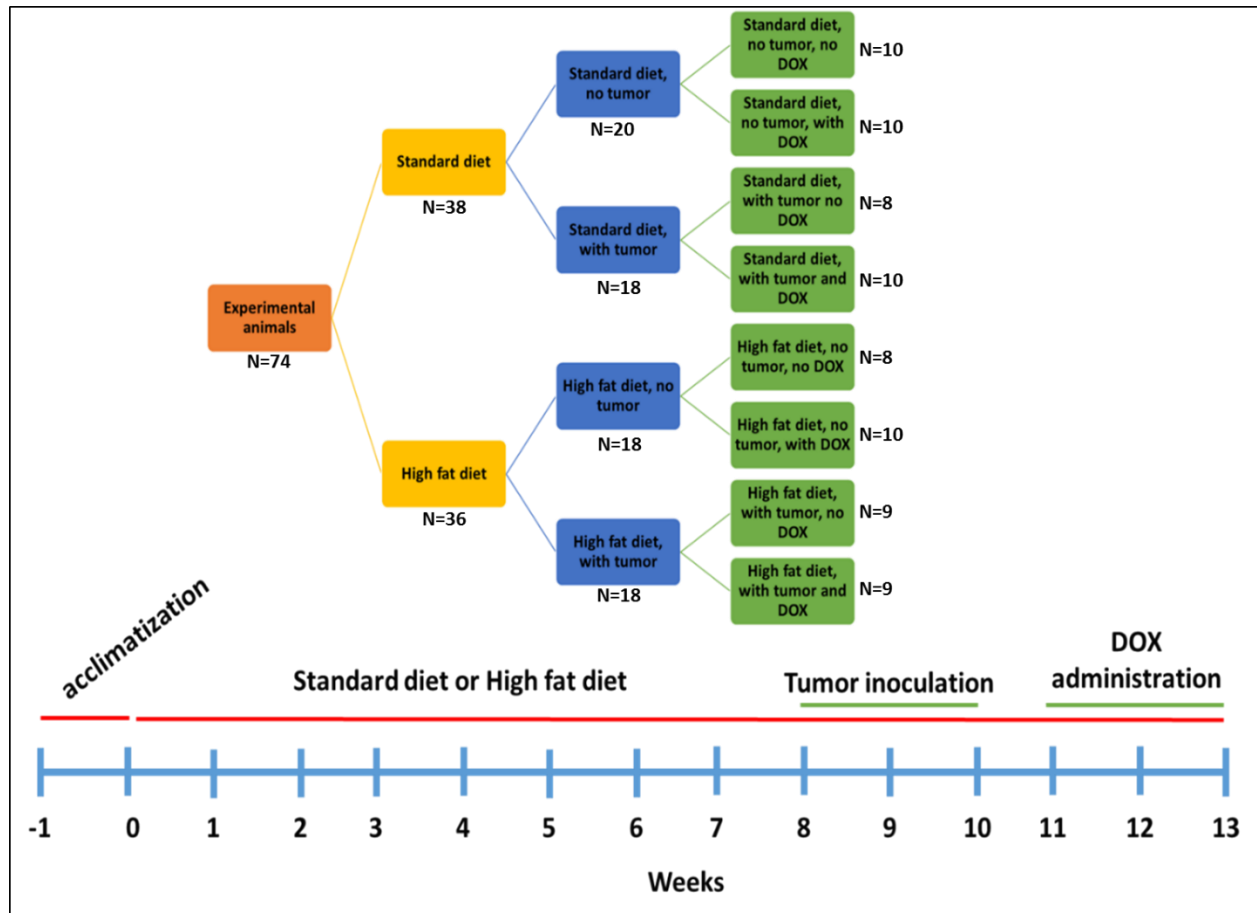


**Figure 2.1: Study Design**

### 2.3 Blood analysis

The following experimental analysis was performed with the assistance of a specialized technician from the LUMINEX PLATFORM at the Division of Molecular Biology and Human Genetics, Stellenbosch University Medical Campus.

#### 2.3.1 Luminex multiplex assay

After blood was collected it was separated into plasma using EDTA tubes (VGRV450474R, Lasec, Cape Town, South Africa). The plasma was used to test for various analytes using the ProcartaPlex Mix & Match Mouse 4-plex Luminex kit (PPX-04-MXCE327, Biocom-

Invitrogen, Massachusetts, USA) custom panel. The following four analytes were measured simultaneously using the Bio-Plex® MAGPIX™ Multiplex reader (MAGPIX13046704, Bio-Rad Laboratories, Inc., California, USA): TNF- $\alpha$  (EX01-20607-901), IL-6 (EX01A-20603-901), IL-10 (EPX01A-20614-901) and Leptin (EX01A-12039-901). The assay utilises fluorescent dyes and magnetic bead-based Luminex XMAP® technology. Each analysis was assigned different microspheres (beads) that are internally colour coded with fluorescent dyes and coated with a capture antibody specific for the analyte. The plasma was pooled together with the capture beads and incubated for one hour. The biotinylated detection antibody was added and incubated for 30 minutes to form an immune complex and then washed. Quantification was performed by the detection of the reporter molecule Streptavidin-Phycoerythrin conjugate, which was added to bind to the detection antibody as each analyte fluoresces at a different signal. Data obtained was expressed in pg/ml for each analyte.

In addition, fasting blood glucose, triglyceride and lactate levels were taken using the tail prick method where 5  $\mu$ l of blood was collected on test strips using the Accu-Chek® Performa Nano (Roche Diagnostics, Mannheim, Germany) and Accutrend Plus® (Roche Diagnostics, Mannheim, Germany) respectively.

## 2.4 Oxidative stress analysis

The following experimental analysis were performed at the Oxidative Stress Centre at Cape Peninsula University of Technology (CPUT).

### 2.4.1 Measurement of early stage lipid peroxidation (Conjugated Dienes assay)

Conjugated dienes (CDs) are polyunsaturated free fatty acids and serves as an early marker of lipid peroxidation. This assay makes use of UV light using a Multiskan™ Spectrophotometer (51119200, Thermo Electron Corporation, Massachusetts, USA). A volume of  $\pm$  50  $\mu$ l of tissue lysate was prepared in phosphate buffer and added to a centrifuge tube in a 1:5 ratio with 250  $\mu$ l chloroform-methanol buffer (see Appendix C). The Eppendorf tubes were centrifuged at 14 000 rpm for 1 minute, where after two layers were formed and 200  $\mu$ l of the bottom chloroform layer was transferred to a new tube. Tubes were left overnight in 4°C with the lids open to allow for evaporation under a flow of nitrogen. The following day, 1 ml cyclohexane (102822, Merck, Massachusetts, USA) was added to each tube, which was then vortexed for  $\pm$  20 seconds. A

volume of 300  $\mu$ l of the blank (cyclohexane) and tissue lysate samples were loaded in triplicate into clear UV 96 wells plates. The plate was read at a wavelength of 220-320 nm to determine absorbance at 234 nm. The content of CDs was then expressed as  $Abs_{234}$ /gram wet weight of the myocardial tissue.

#### 2.4.2 Measurement of late stage lipid peroxidation (TBARS assay)

Malondialdehyde (MDA) is a by-product of lipid peroxidation and a late marker for oxidative stress. The thiobarbituric acid reactive substance (TBARS) assay was used to measure the concentration of MDA's within the tissue lysate. MDA interacts with thiobarbituric acid (TBA) to form a single MDA-TBA adduct, which can be measured colourimetrically as it produces a pink colour (Noeman *et al.*, 2011). This reaction is used proportionally to quantitatively measure the by-products produced (Devasagayam *et al.*, 2004). Tissue samples were prepared in a phosphate buffer (see Appendix B & C) in 1:10 ratio and homogenised using POLYTRON® PT 2100 Homogenizer (Thermo Fisher Scientific, Massachusetts, USA). The supernatant was collected and a volume of 50  $\mu$ l supernatant was added to 6.25  $\mu$ l TBA reagent to create an acidic environment and then incubated for 45 minutes in a 90 °C water bath. After cooling, the supernatant was then transferred to a 96-well flat bottom plate and the absorbance was measured at 532 nm using a Multiskan <sup>TM</sup>Spectrophotometer (Thermo Electron Corporation, 51119200, Massachusetts, USA). The absorbance reading obtained is directly proportional to amount of MDA present in the tissue lysate. The concentration of MDA per sample was determined using the MDA (820756, Merck, Massachusetts, USA) equivalence standard and expressed as  $\mu$ mol/gram of MDA.

### 2.5 Western blot analysis

#### 2.5.1 Tissue lysate preparation

To extract and isolate protein,  $\pm$  20 mg of heart tissue was incubated in 200  $\mu$ l (1:10 ratio) of Radio-immunoprecipitation buffer (RIPA) (see Appendix C). The tissues were homogenized on ice using POLYTRON® PT 2100 Homogenizer (Thermo Fisher Scientific, Massachusetts, USA) and then sonicated using an Ultrasonic Liquid processor (630-0427, Sonics & Material Inc., Newton, USA) for 15 seconds at 10 Amps. Once the foam had settled the lysates were centrifuged at 12 000 rpm for 15 seconds at 4 °C. The pellet was discarded, and the supernatant was transferred to a pre-chilled Eppendorf tube.

### 2.5.2 Protein determination

Protein concentration was determined using the Direct Detect™ Infrared Spectrometer (DDHW00010, Merck, Massachusetts, USA), which uses infrared rays (IR) to detect peptide bonds which make up the protein chain. Briefly, a 2 µl of each tissue lysate sample was placed on the hydrophilic polytetrafluoroethylene (PTFE) transparent membrane and then air-dried prior to the quantification of protein in mg/ml. In accordance with the manufactures instructions, RIPA buffer was used as a blank.

### 2.5.3 Preparation of tissue lysates, protein separation and transfer

Samples containing ~40 mg protein content were prepared on ice for western blotting. A volume of 15 µl of Laemmli's buffer was added and then boiled for 5 minutes at 95 °C. Samples were centrifuged at 10 000 rpm for 1 minute at room temperature before separation by electrophoresis. See Appendix C for detailed buffer protocols.

Using the Mini- PROTEAN® II electrophoresis cell (165-2940, Bio-Rad, California, USA) proteins were separated by sodium dodecyl sulphate-polyacrylamide gel electrophoresis (SDS-PAGE). The samples were loaded into the gel with a commercial molecular weight marker, BluEye Prestained ladder (PM007-0500, Biocom Biotech, Centurion, SA) Proteins were separated by electrophoresis on a 12% TGX stain free™ FastCast™ acrylamide gel (1610185, Bio-Rad Laboratories, Inc. California, USA) at a constant voltage of 100 V and current of 300 mA for approximately 60-90 minutes (see Appendix B). Once the proteins had separated, the gel was removed and then activated using the ChemiDoc™ XRS + System (170-8265, Bio-Rad Laboratories, Inc., California, USA). After gel activation, the resolved proteins were transferred to polyvinylidene fluoride (PVDF) membranes using the Trans-Blot® Turbo™ RTA Mini PVDF Transfer Kit (1704270, Bio-Rad Laboratories, Inc., California, USA). Transfer stacks were activated in transfer buffer for 3 minutes. The PVDF membrane was activated in 100% methanol (1.06007, Merck, Massachusetts, USA) until translucent and then placed in transfer buffer for 3 minutes. The transfer stack was assembled as depicted in Figure 2.2.

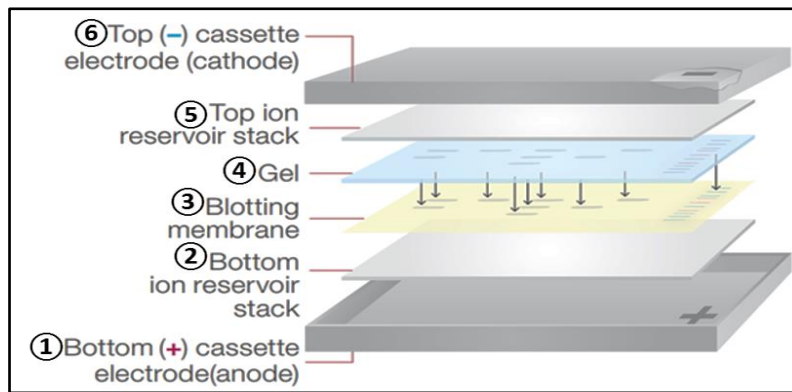


**Figure 2.2: Transfer stack preparation layout**

The ‘sandwich’ was prepared as follows: ①Cassette → ②blotting paper → ③PVDF membrane → ④Gel → ⑤blotting paper → ⑥Cassette (Image from protocol of Bio-Rad Laboratories, Inc., California, USA)

The proteins from the gel were transferred to the membrane for 30 minutes at 25 V, 1.0 A using the Trans-Blot® Turbo™ transfer system (1704270, Bio-Rad Laboratories, Inc., California, USA). After transfer, membranes were soaked for 30 seconds in 100% methanol (1.06007, Merck, Massachusetts, USA), and protein transfer was confirmed using the ChemiDoc™ XRS+ System. The membranes were washed in 1x Tris-buffer saline-TWEEN 20 (TBS-T, see Appendix C) and incubated in blocking buffer containing 5% (v/v) fat free milk in 1x TBS-T for two hours at room temperature to prevent non-specific binding. After blocking, the membranes were washed in 1x TBS-T (3x for 5 minutes) and then placed in 5 ml TBS-T containing specific primary antibody overnight or 48 hours at 4°C shown in Table 2.2. The membranes were washed in 1x TBS-T (3x for 5 minutes) and incubated in horseradish peroxidase-conjugated secondary antibody for one hour at room temperature.

**Table 2.2: Primary and secondary antibodies used for western blot analysis**

Primary Antibody	Molecular weight (kDa)	Secondary Antibody	Dilution factor	Company and Catalogue #
Caspase-3	Total: 35 kDa Cleaved: 17& 19 kDa	Anti-Rabbit	1:1000	Cell Signalling Technology #9662S
PARP1	Total:116 kDa Cleaved: 89 kDa	Anti-Rabbit	1:1000	Cell Signalling Technology #9532S
<b>Secondary Antibody</b>				
Anti-Rabbit Secondary HRP-Linked			1:10000	Cell Signalling Technology #7074S

#### 2.5.4 Visualisation

After removing membranes from the secondary antibody, membranes were washed in 1x TBS-T (3x for 5 minutes) and then covered with Clarity™ ECL Western Blotting Substrate (1705061, Bio-Rad Laboratories Inc., California, USA) and exposed to UV light using the ChemiDoc™ XRS+ System to quantify the expression of the specific protein bands.

#### 2.5.5 Total protein standardizing

A modern method using Image Lab™ Software (Bio-Rad Laboratories Inc., California, USA), and the total protein image of the membrane was used to standardize protein expression to account for equal protein loading.

### 2.6 Histological analysis

#### 2.6.1 Tissue processing

For histological analysis, the 10% neutral formalin-fixed heart tissue was placed in a pre-labelled embedding cassette. The tissue was then processed using the Shandon Elliot Suplex processor (SCE 0540, Biotech laboratories, UK) using a 20-hour processing protocol outlined as follows: **1)** dehydration in different concentrations of alcohol, **2)** clearing tissue with xylene, and **3)** impregnation of tissue with Paraplast® wax (327204, Sigma Aldrich, Missouri, USA), (See Appendix B, for full procedure). Upon completion, the tissue was embedded into a block in Paraplast® wax at 60°C using the Leica Modular Tissue Embedder (EG1160, Leica

Biosystems, Wetzlar, Germany) and then sectioned into 5 µm sections with a Leica microtome (RM2125 RTS, Leica Biosystems, Wetzlar, Germany). The ribbons of tissue were placed onto a warm water bath to stretch out the tissue before mounting it onto a glass slide; the slides were then placed in a 70°C oven prior to specific histological staining.

## 2.7 Histological staining

The following experimental analysis was performed under the supervision and assistance of histological technician, at the Stellenbosch University medical campus, histological lab.

### 2.7.1 Haematoxylin and Eosin staining

The standard Haematoxylin and Eosin (H&E) staining method allows for the visualization of general morphology. H&E are two different dyes: haematoxylin being basic, stains acidic components of a cell, while eosin is acidic, and stains basic cellular components. The nucleus of the cell is stained blue by haematoxylin and the cytoplasm is stained pink by eosin. Prior to staining, the slides were placed in an incubator for the wax to melt off the tissue. Heart tissue sections, as outlined in section 2.6.1, were stained with H&E using the Leica AutoStainer XL (ST5010, Leica Biosystems, Wetzlar, Germany) following the procedure in Table 2.3. The haematoxylin solution (SAAR28001LC, Merck, Massachusetts, USA) and eosin solution (3801600E, Leica Biosystems, Wetzlar, Germany) was filtered before the run. Once staining was complete, the tissue was covered with a glass cover slip and DPX mounting medium (06522, Sigma-Aldrich, Missouri, USA) was used to cover the heart tissue sections and left to dry for 48 hours.

Slides were analysed by 40x objective lens on the Nikon Eclipse E400 microscope (Nikon instruments, Tokyo, Japan) with a SPOT RT Color Digital camera (Diagnostics Instruments, Inc., Michigan, USA) with NIS Elements software. Images were analysed by using scoring system to quantify damage based on study by Selçuk and colleagues (2015).

**Table 2.3: H&E staining procedure**

Step	Solution	Time	Repetitions
1	Oven (60°C)	2 minutes	X1
2	Xylene	5 minutes	X2
3	Ethanol (99%)	2 minutes	X2
4	Ethanol (96%)	2 minutes	X1
5	Ethanol (70%)	2 minutes	X1
6	Tap water	2 minutes	X1
7	Haematoxylin	8 minutes	X1
8	Running water	5 minutes	X1
9	Eosin	4 minutes	X1
10	Running water	1 minutes	X1
11	Ethanol (70%)	30 seconds	X1
12	Ethanol (96%)	30 seconds	X1
13	Ethanol (99%)	30 seconds	X1
14	Xylene	1 minutes	X1

### 2.7.2 Sirius Red stain for collagen

Sirius red stain is specific application to colourimetrically stain collagen (Horobin *et al.*, 2002). Prior to staining slides are placed in an incubator for the wax to melt off the tissue. The haematoxylin (SAAR28001LC, Merck, Massachusetts, USA) and Picosirius red solutions was filtered before use (see appendix C for full protocol). Table 2.4 describes the staining procedure of Picosirius red staining procedure that was followed. Once staining was complete, tissue was covered with a glass cover slip, DPX mounting medium and left to dry for 48 hours.

Slides were analysed using the same microscope settings as mention in section 2.7.1. Images were analysed by using Image J software by colour threshold method which is explained in detail in Appendix A.

**Table 2.4: Procedure of Picrosirius Red staining**

Step	Solution	Time	Repetitions
1	Oven (60°C)	2 minutes	X1
2	Xylene	5 minutes	X2
3	Ethanol (99%)	2 minutes	X2
4	Ethanol (96%)	2 minutes	X1
5	Ethanol (70%)	2 minutes	X1
6	Tap water	1 minutes	X1
7	Haematoxylin	8 minutes	X1
8	Running water	10 minutes	X1
9	Picrosirius red	1 hour	X1
10	Acidified water	30 seconds	X2
11	Physically remove water from sides by vigorously shaking to air-dry water.		
12	Ethanol (70%)	30-seconds	X1
13	Ethanol (96%)	30 seconds	X2
14	Ethanol (99%)	30 seconds	X1
15	Xylene	1 minute	X1

## 2.8 Statistical analysis

MS Excel was used to capture the data and data analysis software system, Graph Pad Software version 7 (San Diego California, USA) was used to do statistical analysis and to generate graphs. To compare two groups, an unpaired t-test was performed. For more than two groups, a one-way ANOVA or were applicable a two-way repeat measurement ANOVA with a Bonferroni post hoc test for both test was performed. Statistical significance was defined by  $p < 0.05$ .

### 3. RESULTS

#### 3.1 Establishing diet-induced obesity

A basic criteria used for both animals and humans to assess the development of obesity is to evaluate overall body weight gain as well as the increase fat content in the body (Hariri & Thibault, 2010). Although in humans BMI is used as a method to define and classify obesity, the increased body weight of rodents is confirmed by significantly higher body weight percentages. This study utilized a high fat diet (HFD) to induce obesity and this was matched calorie wise with a standard diet (SD) which served as the control group.

##### 3.1.1 Body weight

No differences in initial body weight was observed before the introduction of the respective diets (Figures 3.1 & 3.2A). After five weeks however, mice fed the HFD showed a significant increase in body weight when compared to mice fed the SD. At the end of the treatment protocol, the final body weight for the HFD group was  $29.24 \pm 1.99$  g, ( $p < 0.0001$ ) when compared to the SD group ( $19.72 \pm 0.52$  g) (Figures 3.1 & 3.2B). This equates to a more than two-fold increase in percentage body weight change between the groups (HFD:  $90.72 \pm 11.08\%$ ,  $p < 0.001$  versus SD:  $34.69 \pm 7.13\%$ ) (Figure 3.2C). To further confirm obesity, adiposity was considerably elevated in the HFD group ( $4.68 \pm 0.70\%$ ,  $p < 0.001$ ) than the SD group ( $1.37 \pm 0.16\%$ ) (Figure 3.2D). According to these results, it is clear that the chosen high fat diet used in this study was sufficient to induce obesity.

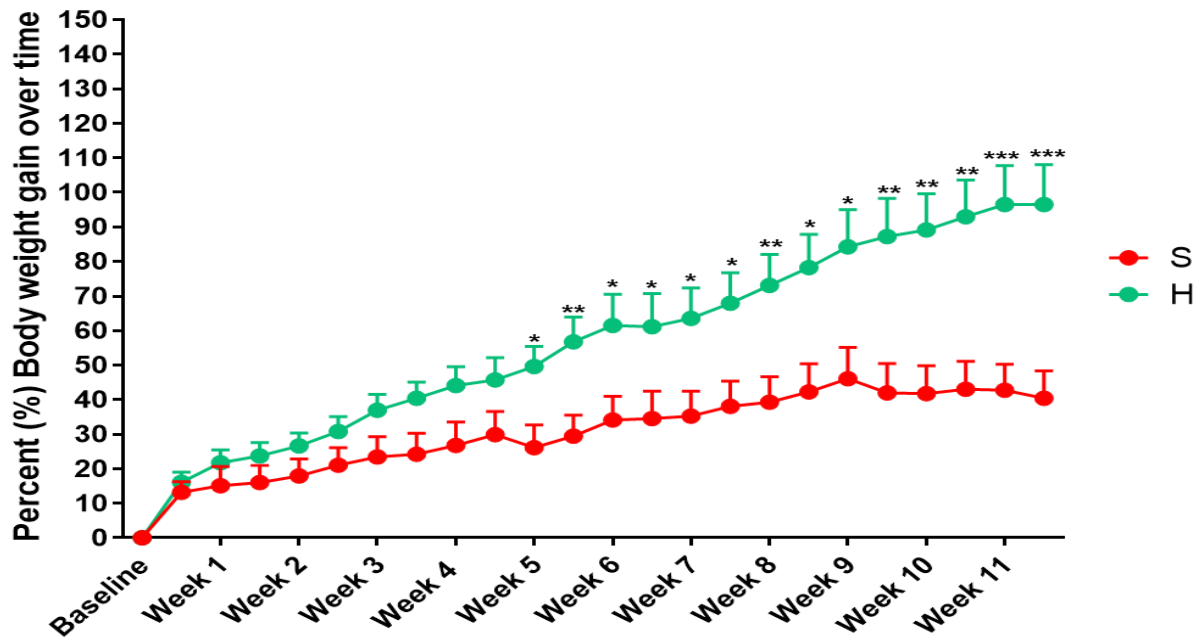


**Figure 3.1: Percent body weight gain overtime of mice fed a standard diet (S) or high fat diet (H) for ±12 weeks.** Body weight data was recorded twice a week from the start of the respective diets until the end of the treatment protocol. Data is represented as mean + SEM (n=8-10). \*p<0.05, \*\*p<0.01, \*\*\*p<0.001 versus S.

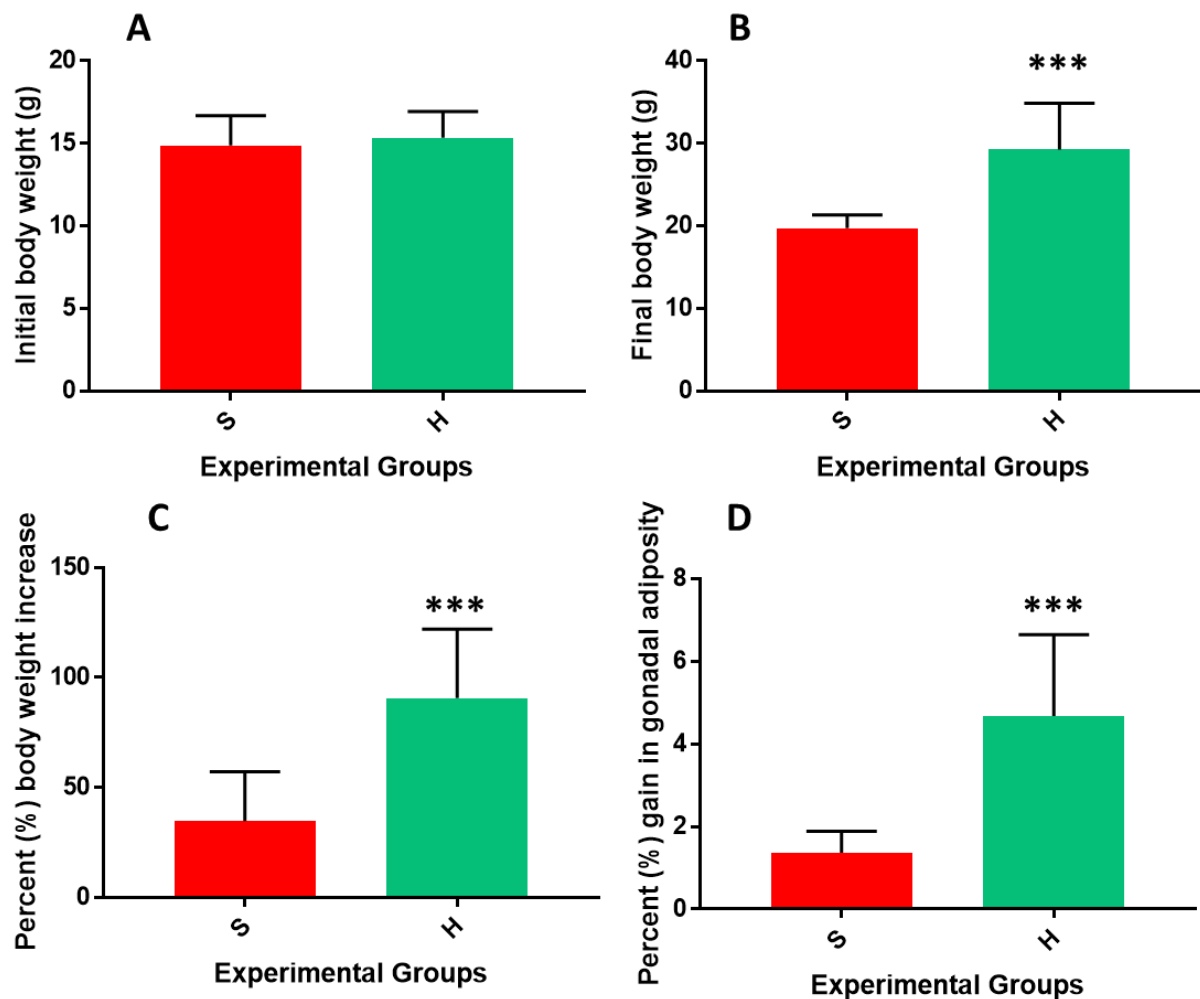


**Figure 3.2: Biometric parameters of mice fed a standard (S) or high fat diet for ±12 weeks.** (A) Initial body weight, (B) final body weight before euthanasia, (C) percentage (%) body weight gain and (D) percentage (%) gonadal adiposity of experimental groups. Data is represented as mean ± SEM (n=8-10). \*\*\*p<0.001 versus S. Abbreviations: g – grams

### 3.1.2 Food consumption and fluid intake

To complement the body weight data above, the total amount of food (Figure 3.3) and water (Figure 3.4) consumed was determined for each group on a weekly basis. As expected, mice fed the high fat diet consumed more rat chow than those on the standard diet. Significance was mainly observed after weeks 1, 4, 10 and 12. Additionally, these animals also consumed more water although statistically these results were not significant.

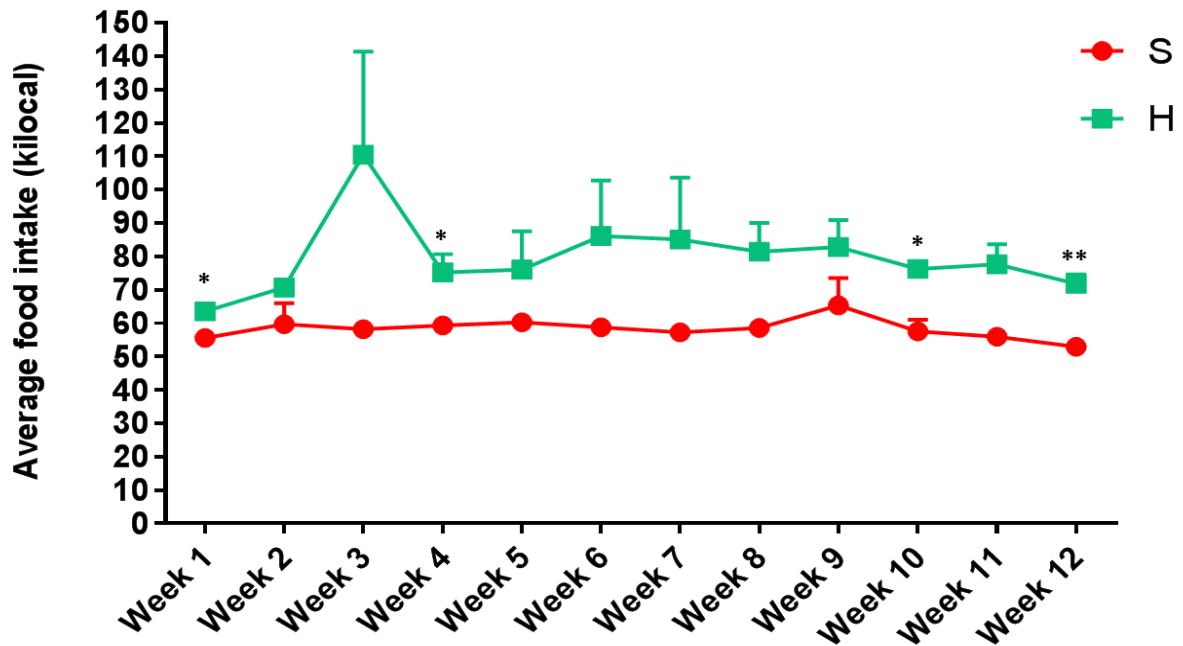


**Figure 3.3: Weekly food consumption in mice fed a standard (S) or high fat diet (H) for  $\pm 12$  weeks.** Food intake was measured weekly for each group to determine the average kilocalories (kcal) consumed. Data is represented as mean + SEM (n=8-10). \* $p < 0.05$ , \*\* $p < 0.01$  versus SD. Abbreviations: kilocal – kilocalories.

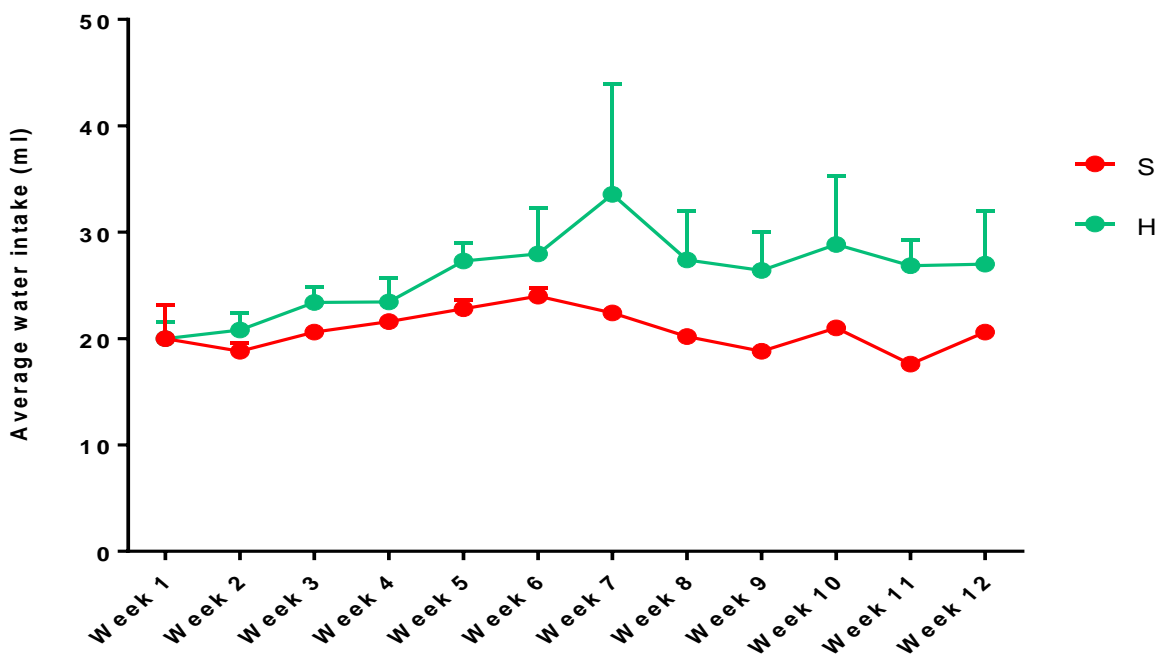


**Figure 3.4: Weekly water consumption in mice fed a standard (S) or high fat diet (H) for  $\pm 12$  weeks.** Water intake was measured daily but evaluated weekly for each group to determine the average amount of water consumed. Data is represented as mean + SEM (n=8-10). Abbreviations: ml – millilitres.

### 3.1.3 Fasting blood parameters

Prior to euthanasia, mice were fasted for 12 hours where fasting blood glucose (Figure 3.5A), triglycerides (Figure 3.5B) and lactate (Figure 3.5C) levels could be determined. Moreover, adipokines such as TNF- $\alpha$  (Figure 3.5D), IL-6 (Figure 3.5E) and leptin (Figure 3.5F) were also evaluated. While no noteworthy changes were observed for triglycerides, lactate, TNF- $\alpha$  and IL-6 levels, fasting blood glucose and leptin levels were significantly up-regulated in the HFD group (glucose:  $8.50 \pm 0.40$  mmol/L,  $p < 0.01$ ; leptin:  $11671.00 \pm 4538.00$  pg/ml,  $p < 0.05$ ) versus the SD group (glucose:  $6.00 \pm 0.50$  mmol/L; leptin:  $1072.00 \pm 403.40$  pg/ml). Although insulin levels were not measured in this study so that the homeostatic model assessment of insulin resistance (HOMA-IR) could also be determined, the elevated fasting glucose levels in this group is possibly indicative of insulin resistance. The increased leptin levels observed further confirm the state of obesity.

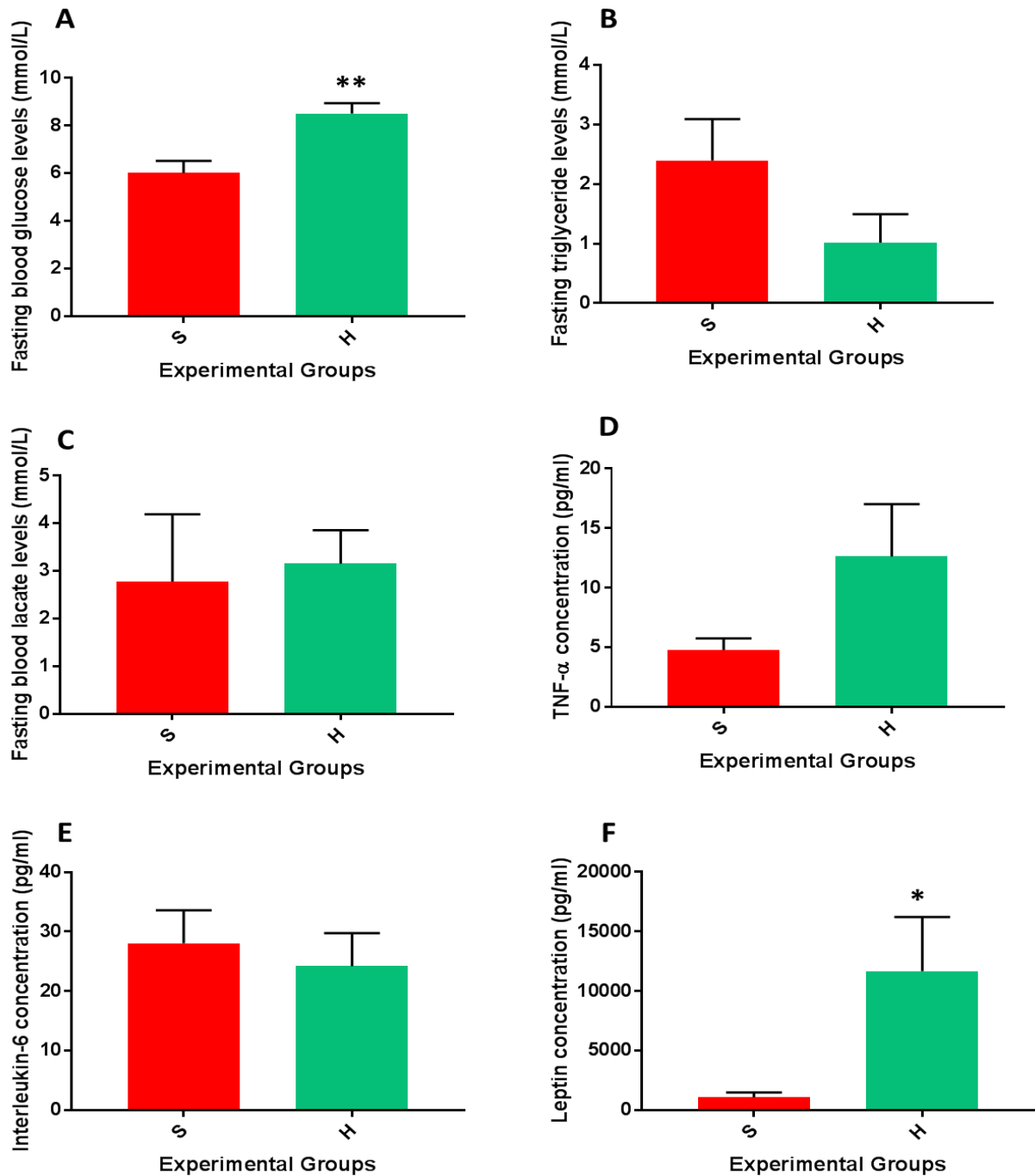


**Figure 3.5: Fasting blood parameters of mice fed a standard (S) or high fat diet (H) for  $\pm 12$  weeks.** Mice were starved for 12 hours prior to euthanasia to determine (A) glucose, (B) triglycerides, (C) lactate, (D) TNF- $\alpha$ , (E) interleukin-6 and (F) leptin levels. Data is represented as mean  $\pm$  SEM (n=5-6). \*\*p<0.01, \*p<0.05 versus S.

## 3.2 Effect of obesity on the heart

The mechanisms by which obesity affects the heart is complex due to the various changes that take place. Our next objective was then to evaluate the impact of diet-induced obesity on myocardial health.

### 3.2.1 The impact of diet-induced obesity on the cardiac hypertrophy index

Cardiac hypertrophy is known as the increased growth of the heart associated with thickening of the ventricular walls. On the one hand, physiological cardiac hypertrophy is associated with the increased size of the heart to compensate for increased functionality during activities such as exercise. ‘Athletes heart’ as it is commonly known, results in hyperplasia to increase the output rate of blood supply, however the cardiac morphology remains the same. On the other hand, pathological cardiac hypertrophy, increases the size of the heart as a result of disease. Often when cardiomyocytes die, fibroblasts invade cardiac tissue to deposit collagen to replace dead cardiomyocytes, resulting in fibrosis (Kavazis, 2015). For this study, the heart to final body weight ratio was used to examine hypertrophy as a result of the HFD. We have already established that the HFD increased body weight (Figure 3.2B); however, no changes were observed in overall final heart weight (Figure 3.6A). Interestingly, the heart-to-body weight ratio revealed a surprising result. Mice on the HFD demonstrated a significantly reduced ratio ( $0.004 \pm 0.0002$ ,  $p < 0.001$ ) than those in the SD group ( $0.006 \pm 0.0002$ ) (Figure 3.6B). While this result does not definitively demonstrate pathological cardiac hypertrophy, it may indicate that by the time this study was terminated, it was too early for hypertrophy to be evident, therefore this is indicative that hypertrophy did not occur within the HFD group.

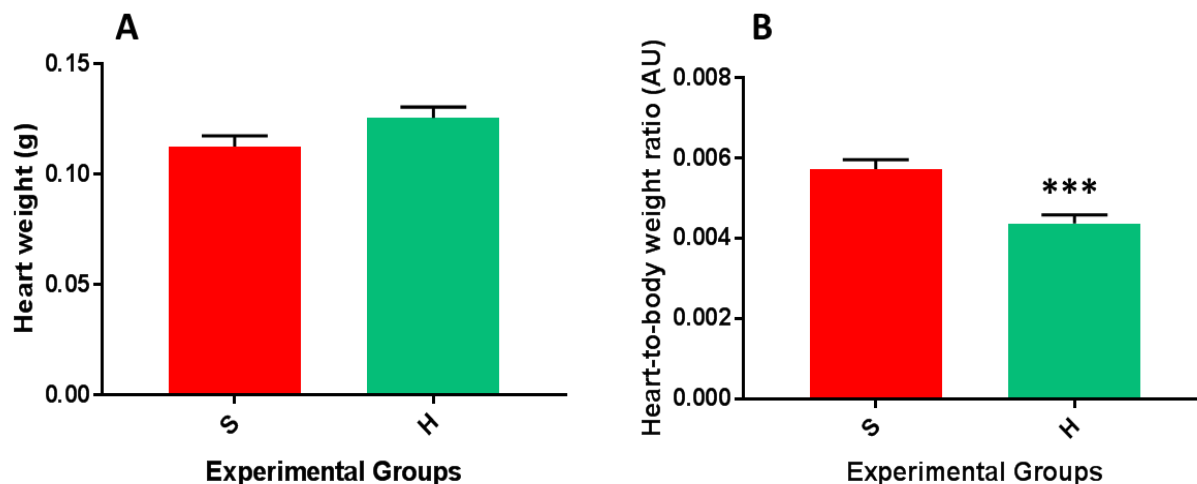


**Figure 3.6: Cardiac hypertrophy index of mice fed a standard (S) or high fat diet (H) for  $\pm 12$  weeks.** (A) Heart weight and (B) heart-to-body weight ratio of experimental groups. Data is represented as mean  $\pm$  SEM (n=8-10). \*\*\*p<0.001 versus S. Abbreviations: g – grams, AU-arbitrary units.

### 3.2.2 The effect of a high fat diet on myocardial ultrastructure and collagen deposition

To further evaluate potential changes in myocardial structure and the presence of fibrosis (Figure 3.7), H&E and Picrosiruis red stains (Figure 3.8) were performed respectively. A scoring system based on previously published data (Selçuk *et al.*, 2015) was used to semi-qualitatively assess heart tissue sections for various factors indicative of structural damage. According to the three parameters evaluated which included (i) eosinophilic cytoplasm and pyknotic nuclei indicating nuclear condensation, (ii) intra-cytoplasmic vacuoles and (iii) inflammatory cell infiltration and congestion, no significant changes were observed for any of these parameters between the two groups. Using Image J analysis software, percentage fibrosis was determined. Although blood vessels contain connective tissue, they were specifically excluded when these sections were quantified. As shown in Figure 3.9, the percentage fibrosis in the HFD group was substantially reduced ( $1.17 \pm 1.11\%$ ,  $p < 0.001$ ) when compared to the SD group ( $2.06 \pm 1.65\%$ ).

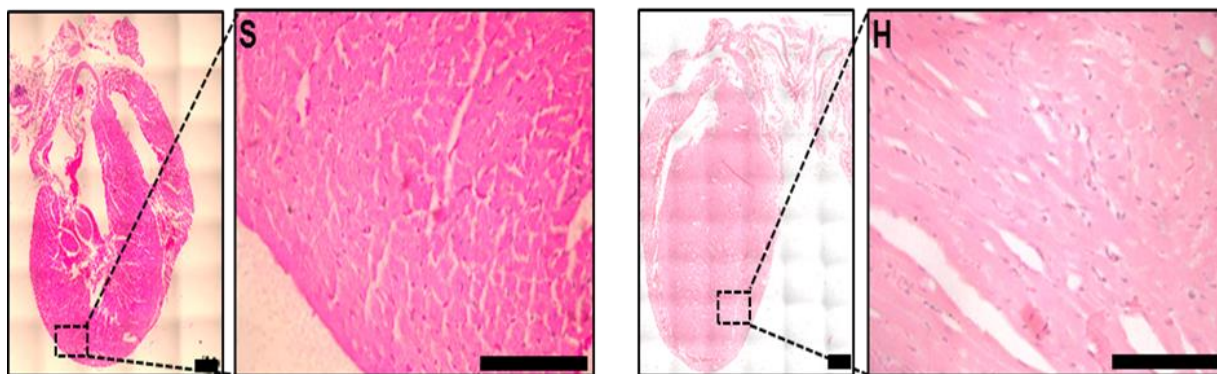


**Figure 3.7: H&E histological stains of heart tissue sections from mice fed a standard (S) or high fat diet (H) for  $\pm 12$  weeks.** Representative images of 5  $\mu\text{m}$  thick heart sections picked at random and stained for structural defects. 4-5 images from three different mice per group were assessed. Magnification and scale bar: 10x and 100  $\mu\text{m}$  (entire section) and 40x and 500  $\mu\text{m}$  (enlargement). Purple colour- nucleus and pink colour – cytoplasm.

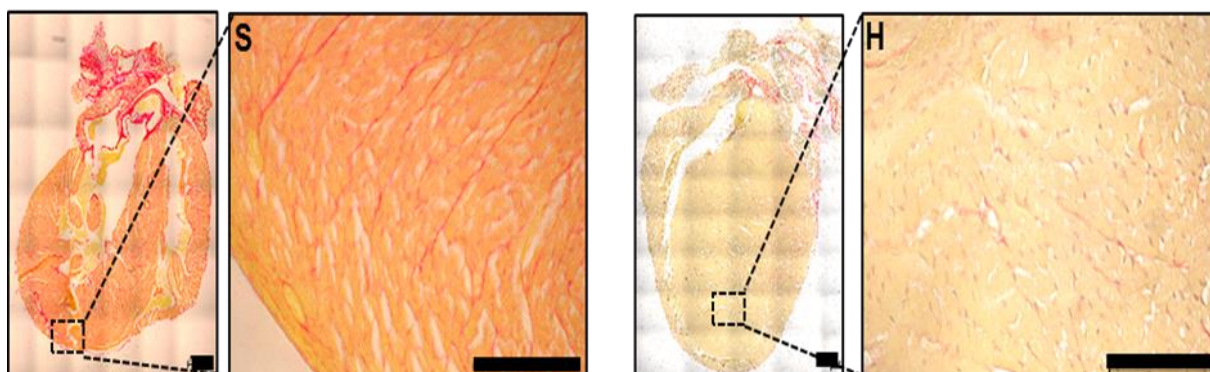


**Figure 3.8: Picrosirius red histological stain of heart tissue sections from mice fed a standard (S) or high fat diet (H) for  $\pm 12$  weeks.** Representative images of 5  $\mu\text{m}$  thick heart sections picked at random and stained for collagen deposition (fibrosis). 4-5 images from three different mice per group were assessed. Magnification and scale bar: 10x and 100  $\mu\text{m}$  (entire section) and 40x and 500  $\mu\text{m}$  (enlargement) Red colour – fibrosis (collagen I and II), yellow colour - cytoplasm, brown, grey or black colour- nucleus.

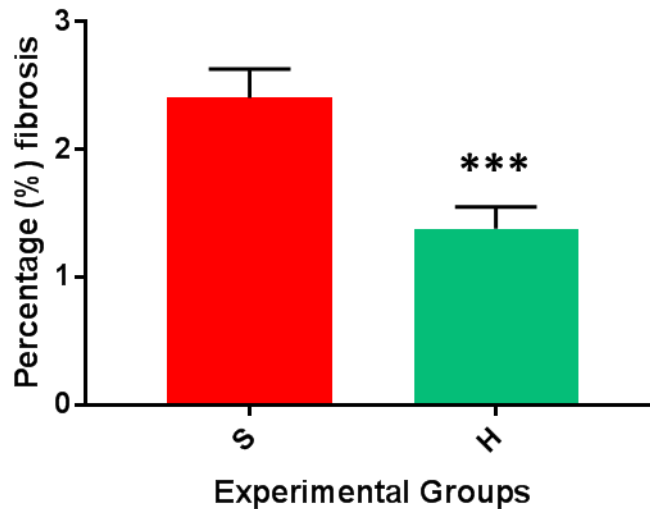


**Figure 3.9: Percentage fibrosis in the myocardium of mice fed a standard (S) or high fat diet (H) for ±12 weeks.** 4-5 images from three different mice per group were quantified for fibrosis using the colour threshold of Image J analysis software. Data is represented as mean ± SEM (n=3). \*\*\*p<0.001 versus S.

### 3.2.3 The effect of a high fat diet on apoptotic protein expression

Caspase-3 is a 35 kDa protein that forms part of downstream processes responsible for cell death and contributes to the proteolytic cleavage of other proteins such as Poly (ADP-ribose) polymerase (PARP). The cleavage of both proteins is indicative of their activity status and the onset of apoptosis. However, the cleavage of PARP may not always be dependent on caspase-3 activity. As shown in Figure 3.10 below, no statistically significant results were obtained between the two groups for the full length proteins detected. While this study also tried to detect the presence of the active forms of these proteins, we were unsuccessful. This could either imply that apoptosis is not taking place or that the cleaved products are degraded as soon as they are produced.

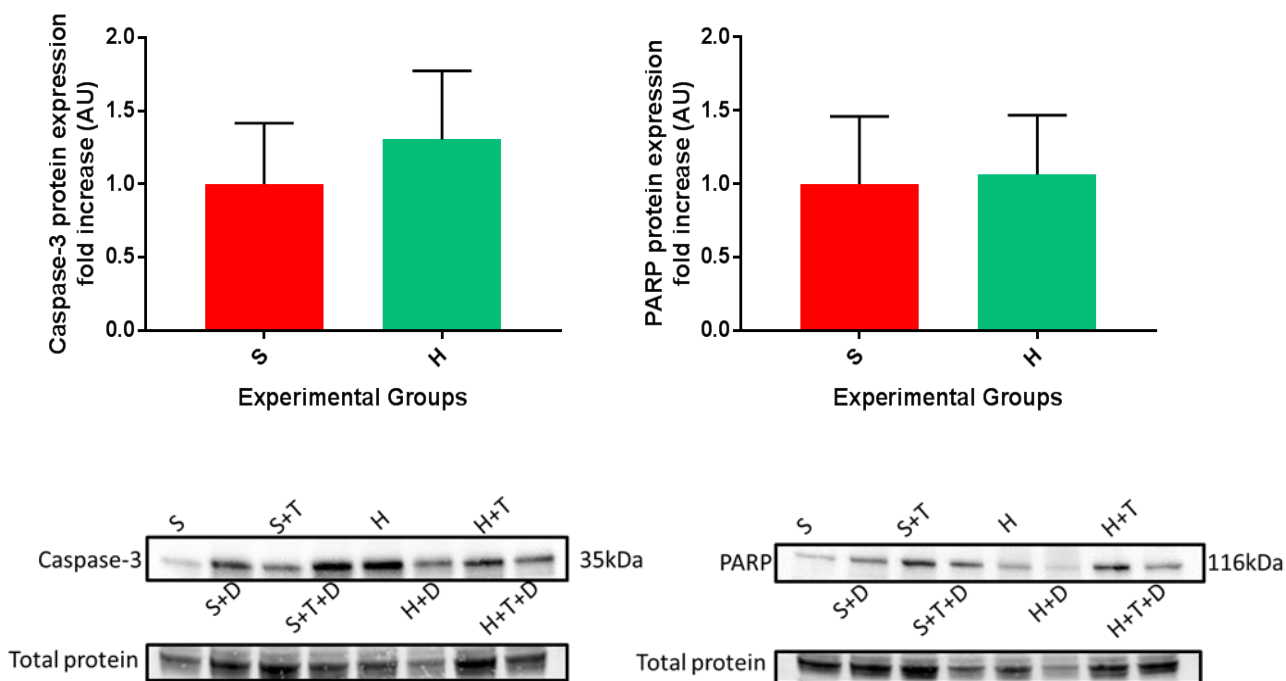


**Figure 3.10: Relative apoptotic protein expression of mice fed a standard (S) or high fat diet (H) for  $\pm 12$  weeks.** Representative graphs and western blot images of full length caspase-3 and PARP are illustrated. Protein expression was normalized to total protein and presented as a fold change relative to control (S). All values are presented as mean  $\pm$  SEM (n=4). Abbreviations: AU - arbitrary units.

### 3.2.4 The effect of a high fat diet on oxidative stress parameters

It is widely accepted that oxidative stress is part and parcel of obesity, and is linked to other inflammatory conditions. Lipid peroxidation is oxidative stress damage to membrane phospholipids and thus forms part of the oxidative stress cascade. Conjugated diene (CD) production is an early biochemical event of lipid peroxidation, while malondialdehyde (MDA) is produced towards the end of the process. This study found a modest increase ( $0.177 \pm 0.011 \mu\text{mol/g}$ ) and a modest decrease ( $0.003 \pm 0.001 \mu\text{mol/g}$ ) in CD and MDA levels respectively in the HFD group relative to the SD group, but these changes were insignificant (Figure 3.11). This lack of oxidative stress damage may also explain why no apoptotic activity was evident.

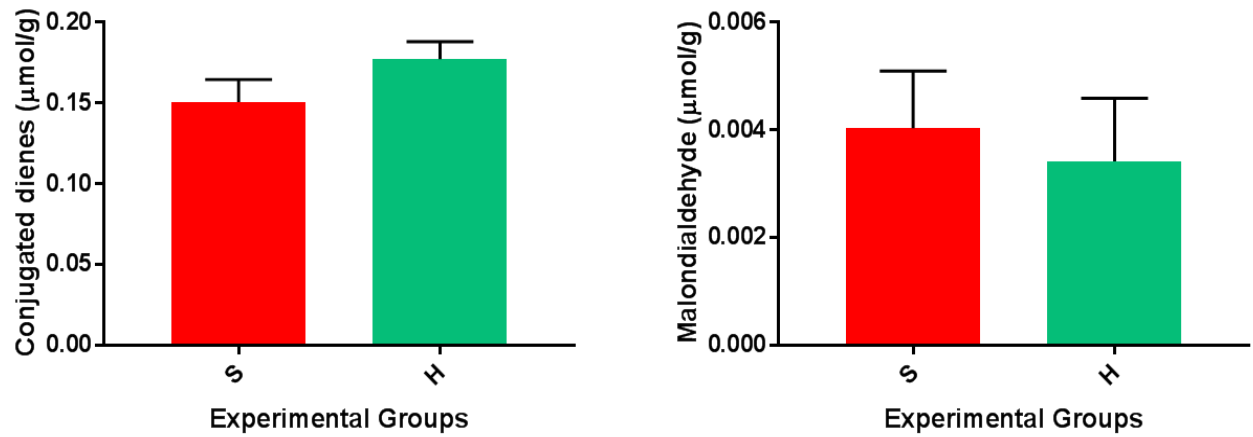


**Figure 3.11: Oxidative stress parameters from mice fed a standard (S) or high fat diet (H) for ±12 weeks.** Heart tissue lysates were used to evaluate the expression of early (conjugate dienes) and late (malondialdehydes) markers of lipid peroxidation. Data is represented as mean ± SEM (n=4-5).

### 3.3 Establishing a state of co-morbidity

In order to establish a model of co-morbidity, this study randomly sub-divided the two main diet groups into a further two groups, where some groups were inoculated with cancer cells to induce tumors while others were not. By doing this, this study was simulating a condition of diet-induced obesity and cancer to create a co-morbid state, and how these inflammatory conditions affect cardiovascular health.

#### 3.3.1 Body weight

Following the inoculation of cancerous cells at week eight, significant differences were observed between the groups fed a HFD (H) alone and a HFD plus tumour (H+T); as well as the SD plus tumour (S+T) and H+T groups (Figure 3.12). Considering that the HFD group lost weight and gonadal adiposity in the presence of a tumour (Figure 3.13B, C & D) when compared to the HFD group alone, these differences indicate that having cancer not only negatively influences body weight mass, the amount of fat accumulated in the body also decreases. However, being overweight or obese in this scenario appears to be protective, considering that the SD group lost considerable weight in the presence of a tumour by week nine. While losing weight as a result of obesity is beneficial, the loss of weight due to a disease in this context may prove to be detrimental.

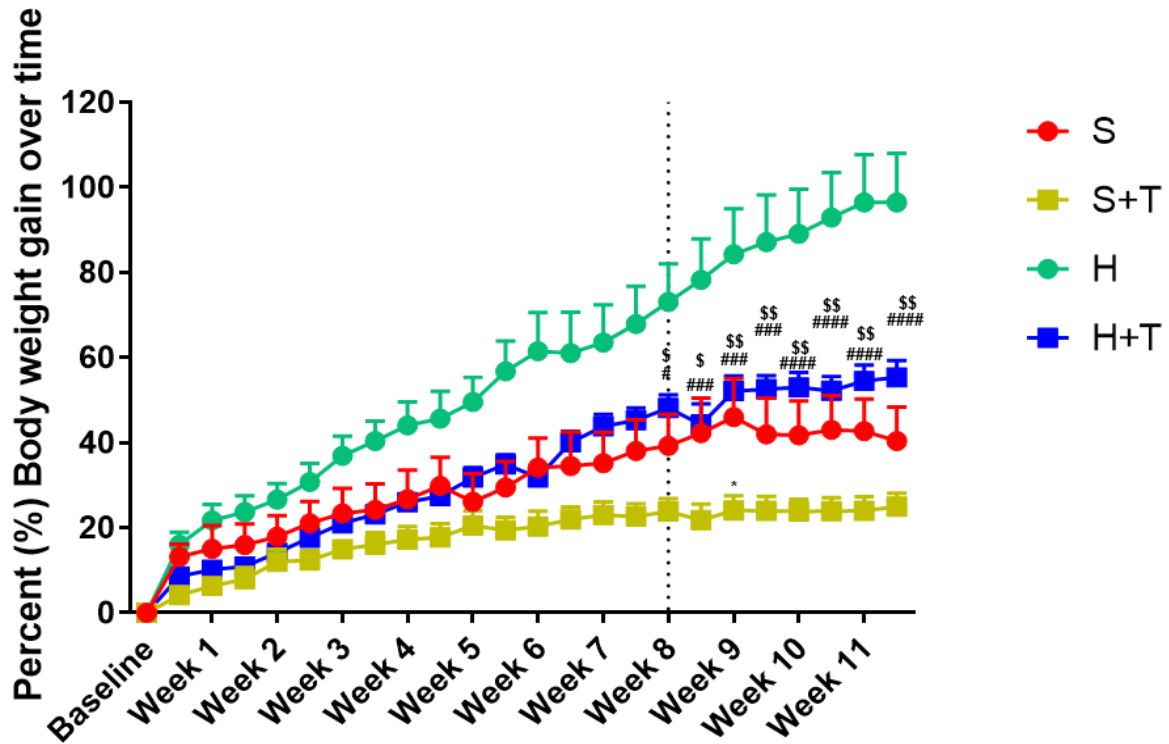


**Figure 3.12: Percent (%) body weight gain overtime of mice fed a standard diet (S) or high fat diet for  $\pm 12$  weeks, and/or inoculated with cancer cells from eight weeks (represented by the vertical dotted line). Body weight data was recorded twice a week from the start of the respective diets and the inoculation of tumours until the end of the treatment protocol. Data is represented as mean  $\pm$  SEM (n=8-10). \* $p < 0.05$  (S versus S+T), ### $p < 0.001$ , ##### $p < 0.0001$  (versus H), \$ $p < 0.05$ , \$\$ $p < 0.01$  (versus S+T).**

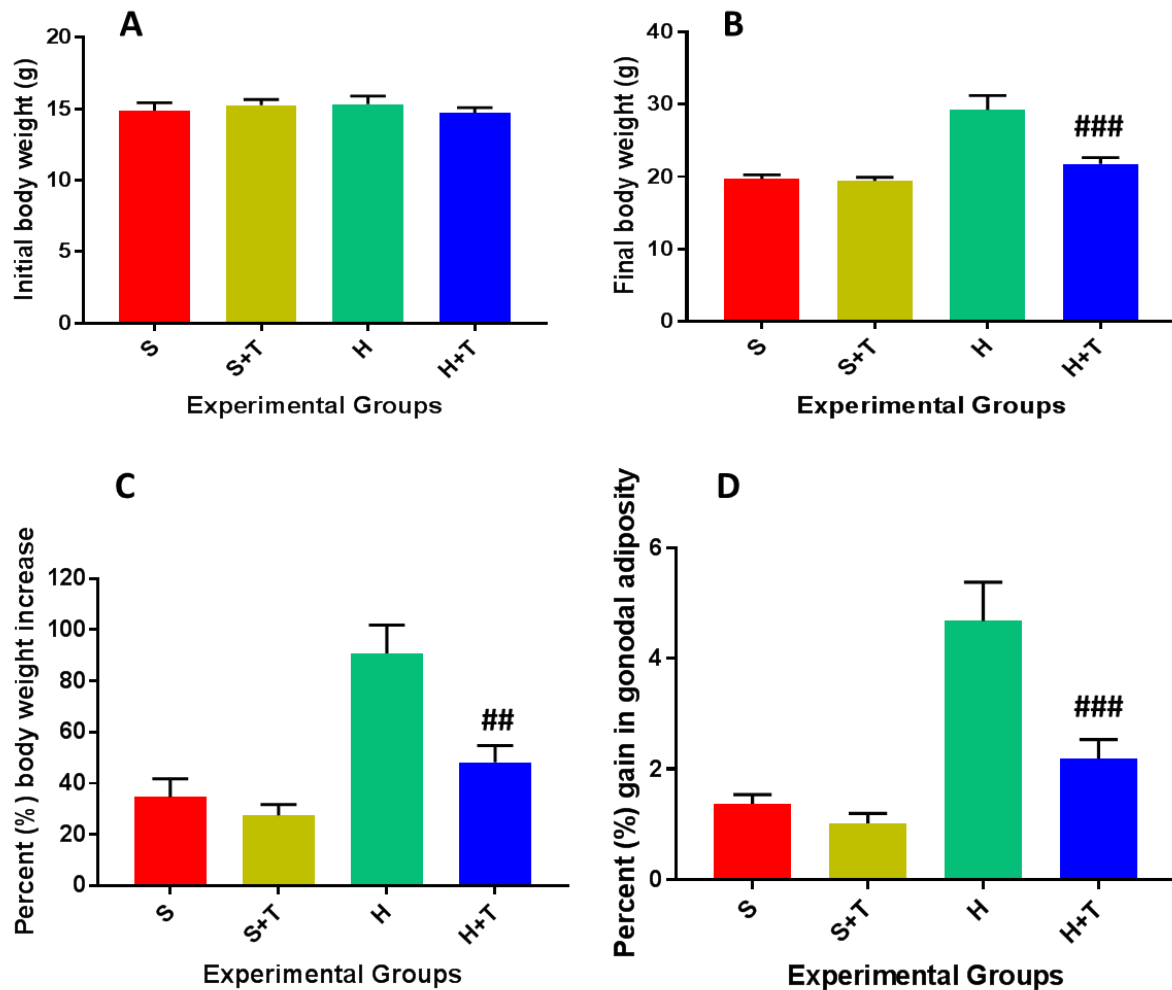


**Figure 3.13: Biometric parameters of mice fed standard (S) or high fat diet (H) for  $\pm 12$  weeks, and/or inoculated with cancer cells from eight weeks. (A) Initial body weight, (B) final body weight before euthanasia, (C) percentage (%) body weight gain and (D) percentage (%) gonadal adiposity of experimental groups. Data is represented as mean  $\pm$  SEM (n=8-10). ##p<0.01, ###p<0.001 (versus H). Abbreviations: g – grams.**

### 3.3.2 Food consumption and water intake

To complement the body weight data above, the total amount of food (Figure 3.14) and water (Figure 3.15) consumed was determined for each group on a weekly basis. As illustrated in the figures below, considerable differences were observed between groups S+T and H+T at weeks 8, 9 and 10, however this significance was lost by the time the study was completed. Interestingly, animals fed the SD in the presence of a tumour drank significantly more water than those animals fed the SD alone.

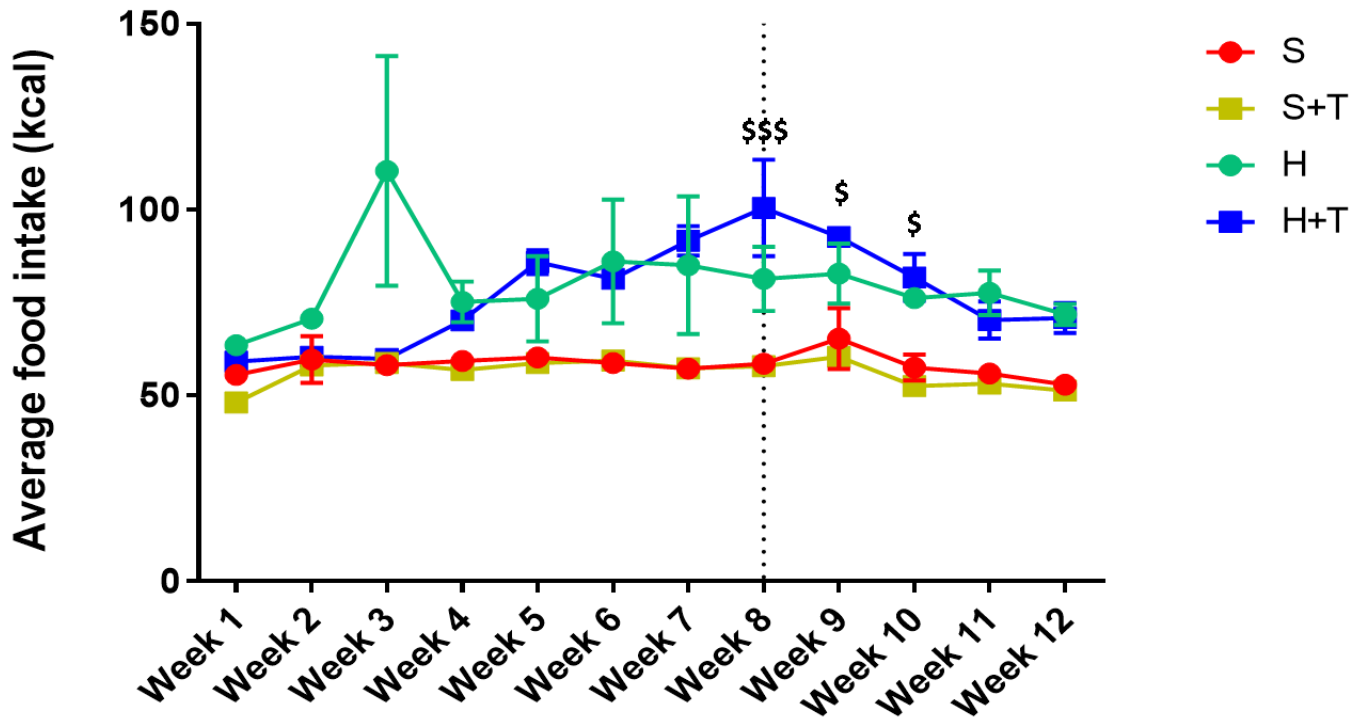


**Figure 3.14: Weekly food consumption in mice fed a standard (S) or high fat diet (H) for  $\pm 12$  weeks, and/or inoculated with cancer cells from eight weeks (represented by the vertical dotted line). Food intake was measured weekly for each group to determine the average kilocalories (kcal) consumed. Data is represented as mean + SEM (n=8-10).  $^{\$}p < 0.05$ ,  $^{\$ \$ \$}p < 0.001$  (versus S+T). Abbreviations: kcal – kilocalories.**

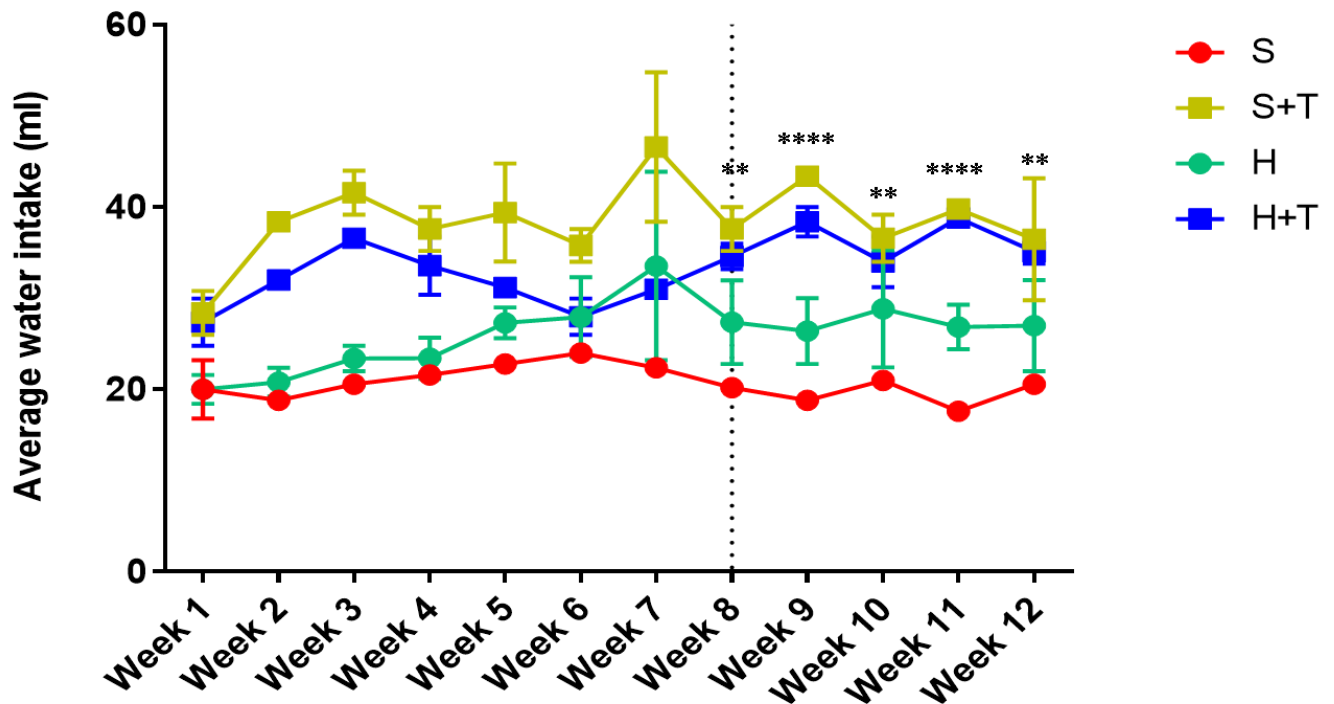


**Figure 3.15: Weekly water consumption in mice fed a standard (S) or high fat diet (H) for  $\pm 12$  weeks, and/or inoculated with cancer cells from eight weeks (represented by the vertical dotted line). Water intake was measured daily but evaluated weekly for each group to determine the average amount of water consumed. Data is represented as mean + SEM (n=8-10). \*\*p<0.01, \*\*\*\*p<0.0001 (versus S). Abbreviations: ml – millilitres.**

### 3.3.3 Fasting blood parameters

In an effort to determine whether the presence of a tumour induces a change in fasting blood parameters in experimental animals fed either a SD or HFD, glucose (Figure 3.16A), triglycerides (Figure 3.16B), lactate (Figure 3.16C), TNF- $\alpha$  (Figure 3.16D), IL-6 (Figure 3.16E) and leptin (Figure 3.16F) were measured. No noteworthy changes were observed in any of the parameters measured except for IL-6. In this case, a significant difference was observed between group H+T ( $64.95 \pm 11.62$  pg/ml,  $p < 0.01$ ) when compared to HFD group alone ( $24.17 \pm 5.59$  pg/ml). The over expression of this cytokine thus signifies the role that inflammation plays in promoting tumour progression by potentially regulating all hallmarks of cancer and multiple signalling pathways.

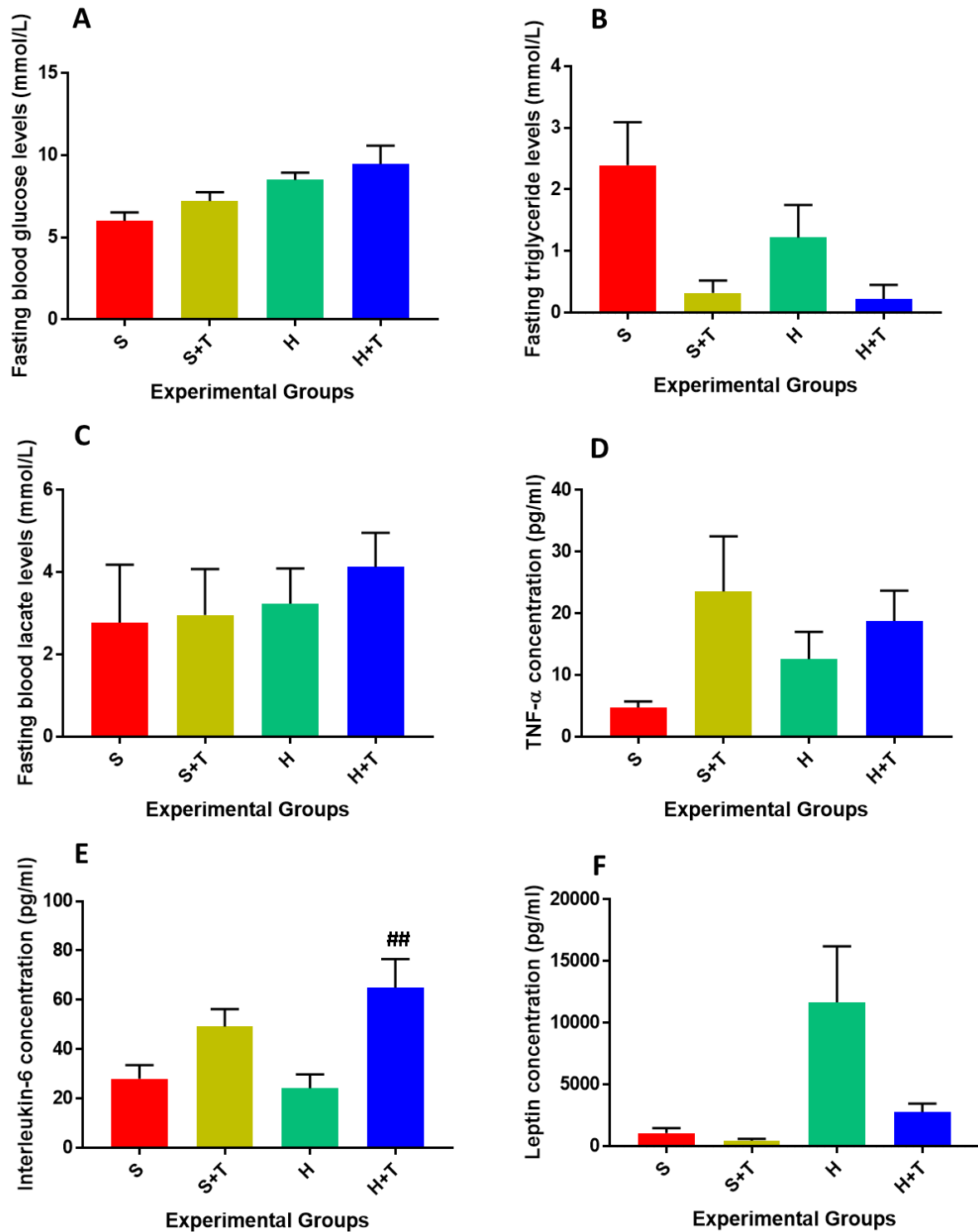


**Figure 3.16: Fasting blood parameters of mice fed a standard (S) or high fat diet (H) for  $\pm 12$  weeks, and/or inoculated with cancer cells from eight weeks.** Mice were starved for 12 hours prior to euthanasia to determine (A) glucose, (B) triglycerides, (C) lactate, (D) TNF- $\alpha$ , (E) interleukin-6 and (F) leptin levels. Data is represented as mean  $\pm$  SEM (n=5-6). <sup>##</sup>p<0.01 (versus H).

### 3.4 Effect of obesity and cancer on the heart

Our next objective for this study was to evaluate the impact of diet-induced obesity and cancer on myocardial health. Considering that both these conditions have an inflammatory component, it is likely that the secreted cytokines can also influence the function of the heart.

#### 3.4.1 The impact of diet-induced obesity and cancer on the cardiac hypertrophy index

According to the results obtained (Figure 3.17A), the overall heart weight was significantly reduced in both groups that had tumours (S+T:  $0.09 \pm 0.004$  g,  $p < 0.05$ ; H+T:  $0.10 \pm 0.005$  g,  $p < 0.05$ ) when compared to their control counterparts alone (S:  $0.11 \pm 0.005$  g; H:  $0.13 \pm 0.005$  g). However, taking into consideration the final body weight of all experimental animals, the heart-to-body weight ratio did not show any significant changes in any of the groups, and thus indicates that no hypertrophy took place in this scenario.

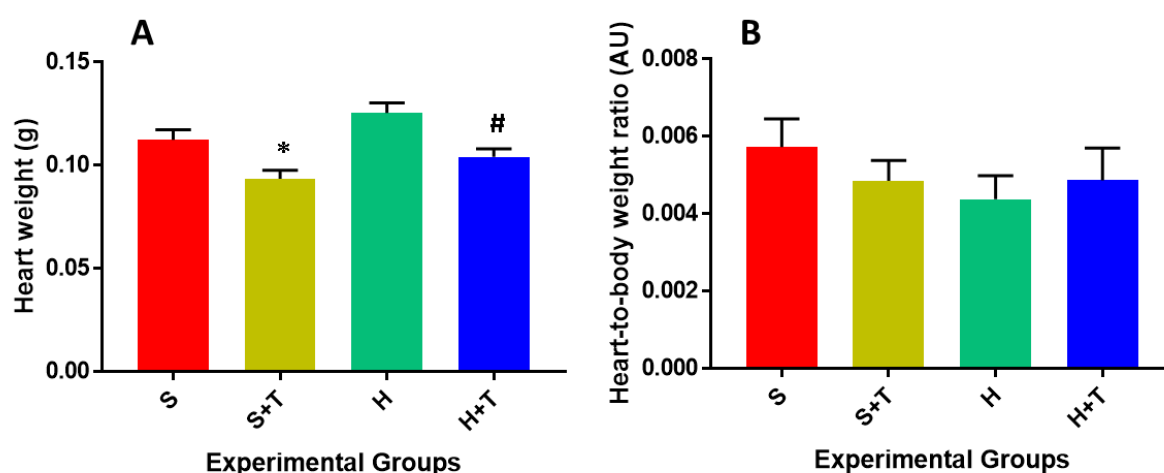


**Figure 3.17: Cardiac hypertrophy index of mice fed a standard (S) or High fat diet (H) for  $\pm 12$  weeks, and/or inoculated with cancer cells from eight weeks. (A) Heart weight and (B) heart-to-body weight ratio of experimental groups. Data is represented as mean  $\pm$  SEM (n=8-10). \* $p < 0.05$  (versus S), # $p < 0.05$  (versus H). Abbreviations: g – grams, AU-arbitrary units.**

#### 3.4.2 The effect of a high fat diet and cancer on myocardial ultrastructure and collagen deposition

Although the physical measurement of the heart-to-body weight ratio is important to evaluate potential cardiac hypertrophy, histological analysis of the tissue specimens often provides a

better visual representation of potential damage within the heart that may have occurred with the different experimental groups. The same scoring system that was used in Section 3.2.2 was also utilised in the current section. While neither diet had a major impact on structural defects of the myocardium, the presence of a tumour in the SD group (S+T) induced interstitial congestion (indicated by asterisk) which may in the end impact on cardiovascular function. No other alterations were observed (Figure 3.18). As shown on Figures 3.19 and 3.20, experimental animals fed the HFD indicated no changes in collagen deposition (fibrosis). However it was interesting to note that the animals fed the SD in the presence of a tumour (S+T) had significantly less ( $1.23 \pm 0.20$ ,  $p < 0.001$ ) fibrosis than those fed the SD alone ( $2.40 \pm 0.23$ ). This was an unexpected result considering that the cytokines and adipokines measured for this group did not significantly change.

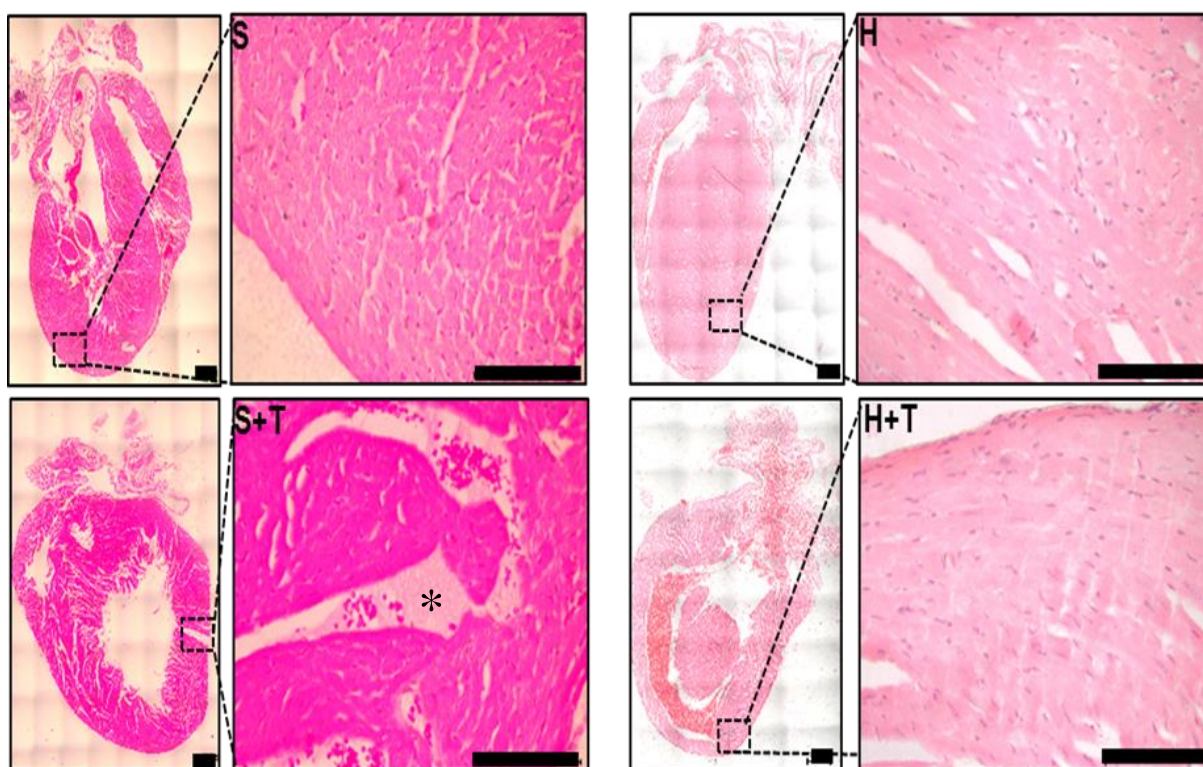


**Figure 3.18: H&E histological stains of heart tissue sections from mice fed a standard (S) or high fat diet (H) for  $\pm 12$  weeks, and/or inoculated with cancer cells from eight weeks.** Representative images of 5  $\mu$ m thick heart sections picked at random and stained for structural defects. 4-5 images from three different mice per group were assessed. Interstitial congestion is indicated by the asterisk. Magnification and scale bar: 10x and 100  $\mu$ m (entire section) and 40x and 500  $\mu$ m (enlargement). Purple colour- nucleus and pink colour – cytoplasm.

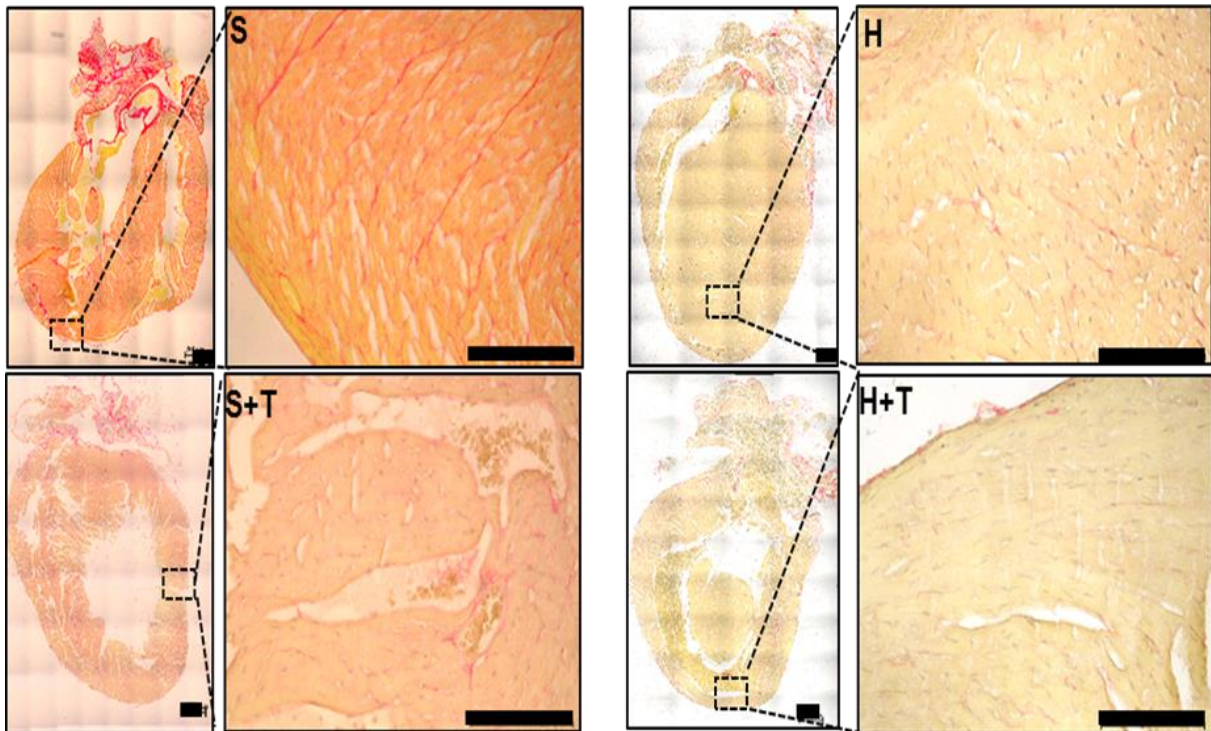


**Figure 3.19: Picosirius red histological stain of heart tissue sections from mice fed a standard (S) or high fat diet (H) for  $\pm 12$  weeks, and/or inoculated with cancer cells from eight weeks.** Representative images of 5  $\mu\text{m}$  thick heart sections picked at random and stained for collagen deposition (fibrosis). 4-5 images from three different mice per group were assessed. Magnification and scale bar: 10x and 100  $\mu\text{m}$  (entire section) and 40x and 500  $\mu\text{m}$  (enlargement) Red colour – fibrosis (collagen I and II), yellow colour - cytoplasm, brown, grey or black colour- nucleus.

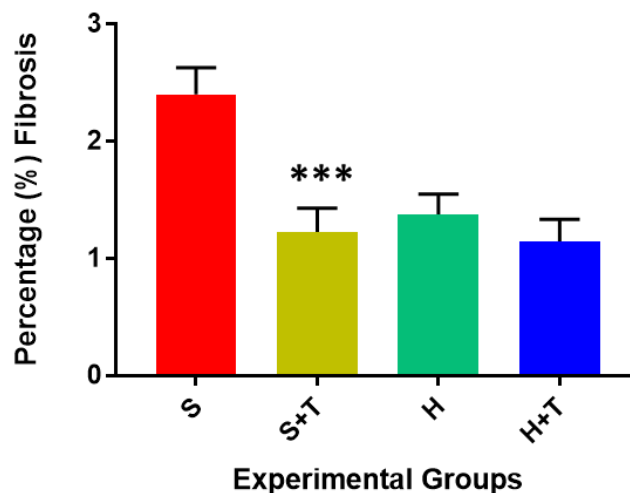


**Figure 3.20: Percentage fibrosis in the myocardium of mice fed a standard (S) or high fat diet (H) for  $\pm 12$  weeks, and/or inoculated with cancer cells from eight weeks.** 4-5 images from three different mice per group were quantified for fibrosis using the colour threshold of Image J analysis software. Data is represented as median  $\pm$  SEM (n=3). \*\*\*p<0.001 (versus S).

### 3.4.3 The effect of a high fat diet and cancer on apoptotic protein expression

To evaluate apoptotic cell death within the experimental groups, caspase-3 and PARP protein expression was semi-quantitatively measured by Western blotting. As indicated in Figure 3.21 below, no meaningful changes in the expression pattern of these proteins was evident. Since TNF- $\alpha$  is a pro-inflammatory cytokine that has previously been associated with apoptosis in different contexts, the insignificant results obtained may explain why no apoptosis was present.

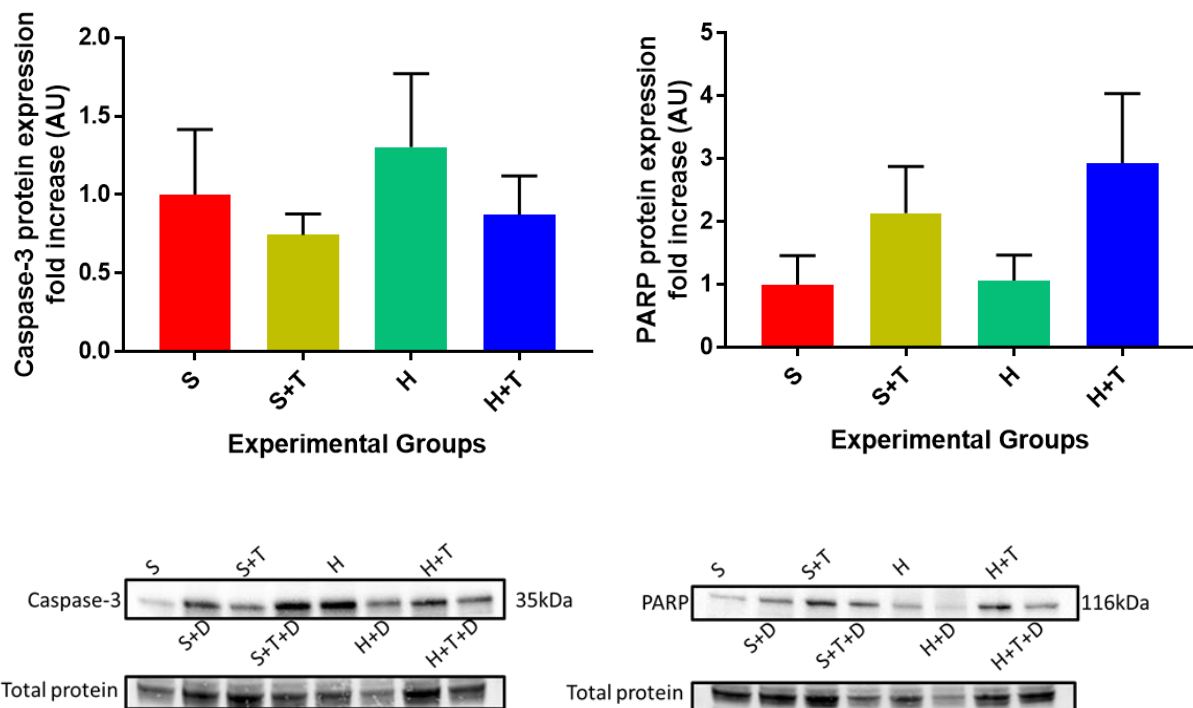


**Figure 3.21: Relative apoptotic protein expression of mice fed a standard (S) or high fat diet (H) for  $\pm$ 12 weeks, and/or inoculated with cancer cells from eight weeks.** Representative graphs and western blot images of full-length caspase-3 and PARP are illustrated. Protein expression was normalized to total protein and presented as a fold change relative to controls (S or H). All values are presented as mean  $\pm$  SEM (n=4). Abbreviations: AU - arbitrary units.

### 3.4.4 The effect of a high fat diet and cancer on oxidative stress parameters

Similarly to the results obtained above, no changes were observed for CDs and MDA in any of the experimental groups (Figure 3.22). It is therefore possible that the different experimental

approaches induced in the animals was not severe enough to induce molecular changes that were expected.

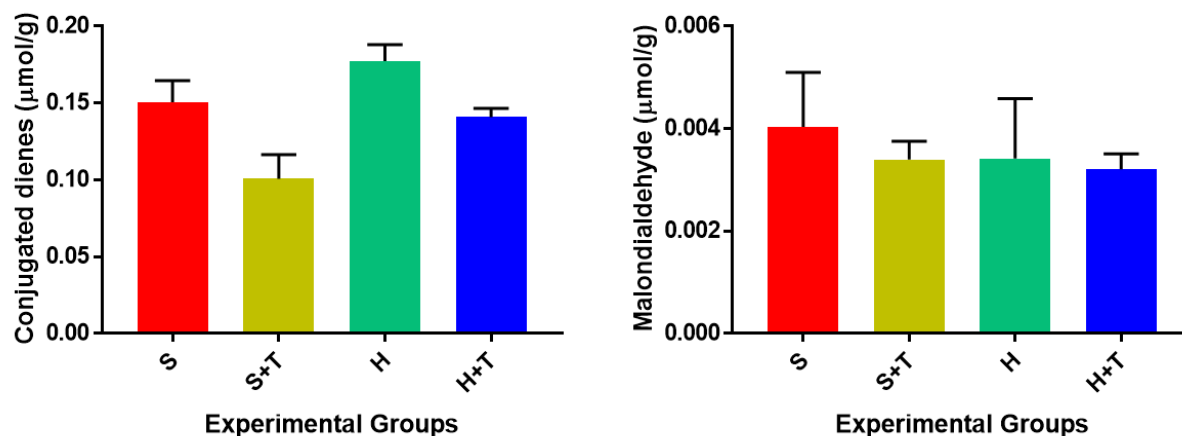


**Figure 3.22: Oxidative stress parameters from mice fed a standard (S) or high fat diet (H) for  $\pm 12$  weeks, and/or inoculated with cancer cells from eight weeks.** Heart tissue lysates were used to evaluate the expression of early (conjugate dienes) and late (malondialdehydes) markers of lipid peroxidation. Data is represented as mean  $\pm$  SEM (n=5-6).

### 3.5 Establishing a condition of obesity, cancer and acute cardiotoxicity

Now that a model of co-morbidity (obesity and cancer) has already been established, this study then introduced an additional factor being chemotherapy. Since this study induced breast cancer in this model, DOX treatment was utilized to initiate acute cardiotoxicity. Thus, each of the above four groups were further divided into two, to create eight different treatment groups. Our object in this final section was to determine whether these three inflammatory conditions (obesity, cancer and cardiotoxicity) influence one another, whether they make each other worse and what impact do they have on body weight and the heart.

#### 3.5.1 Body weight

As demonstrated in the figure below, major differences were found between groups S+D when compared to H+D, as well as groups H+D when compared to H+T+D (Figure 3.23). When looking at groups S+D versus H+D, the common factor is DOX treatment while the difference is the diet. Therefore, in this instance, the SD ( $19.05 \pm 0.23$  g,  $p < 0.001$ ) fed experimental

animals lost more weight than those fed a HFD in the presence of DOX ( $25.02 \pm 0.84$  g) during this period (Figure 3.24B). Not only did the animals in group H+D have a greater weight, they're percentage body weight increase was maintained (Figure 3.24C), as well as the percentage adiposity (Figure 3.24D). Similarly, when looking at groups H+D versus H+T+D, the common factor is the HFD and DOX treatment while the difference is the presence of a tumour. In this case, the H+T+D group lost significantly more weight than group H+D (Figure 3.23). However, the final body weight data as well as the percentage gonadal adiposity reveals that in the presence of a tumour and/or DOX treatment, animals fed the HFD significantly lost weight and adiposity when compared to the HFD fed animals alone. These results thus suggest that cancer and DOX treatment influences body weight negatively.

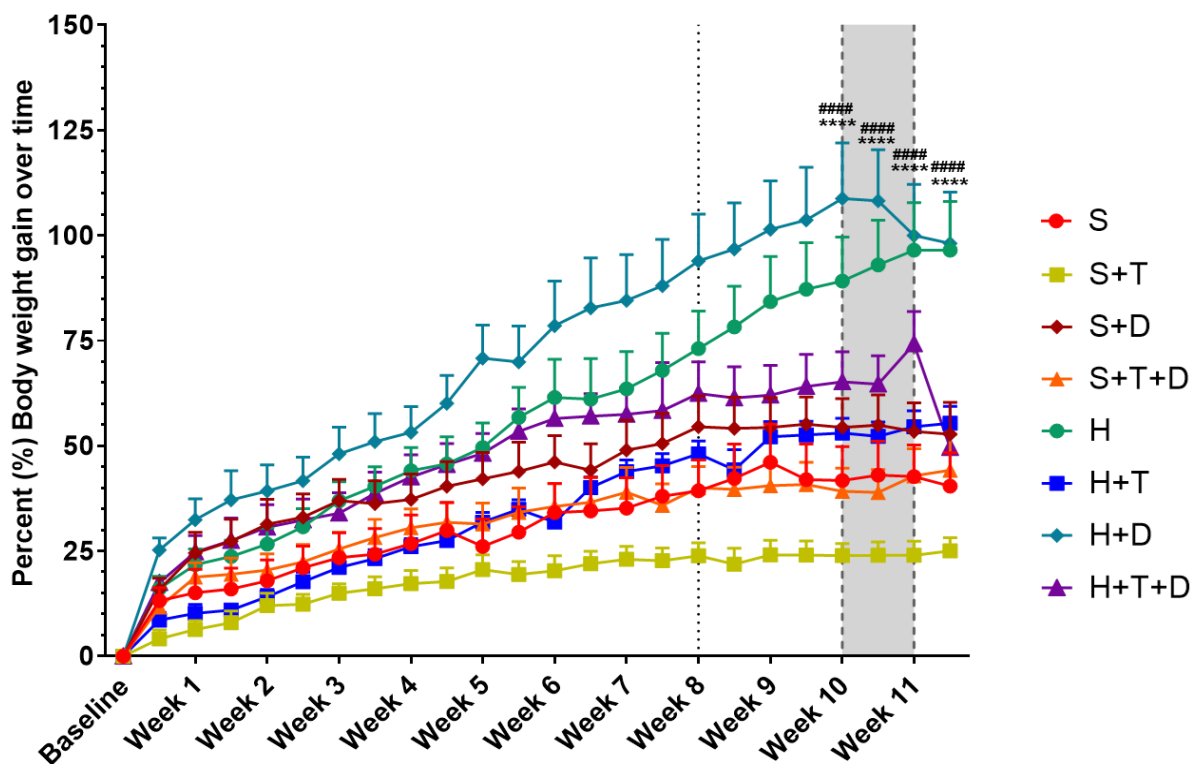


**Figure 3.23: Percent body weight gain overtime of mice fed a standard diet (S) or high fat diet (H) for  $\pm 12$  weeks, and/or inoculated with cancer cells from eight weeks (represented by the vertical dotted line), and /or treated with DOX (represented by the grey shaded area). Body weight data was recorded twice a week from the start of the respective diets and the inoculation of tumours until the end of the treatment protocol with DOX. Data is represented as mean + SEM (n=8-10). \*\*\*\*p<0.0001 (versus S+D), #####p<0.0001 (versus H+D).**

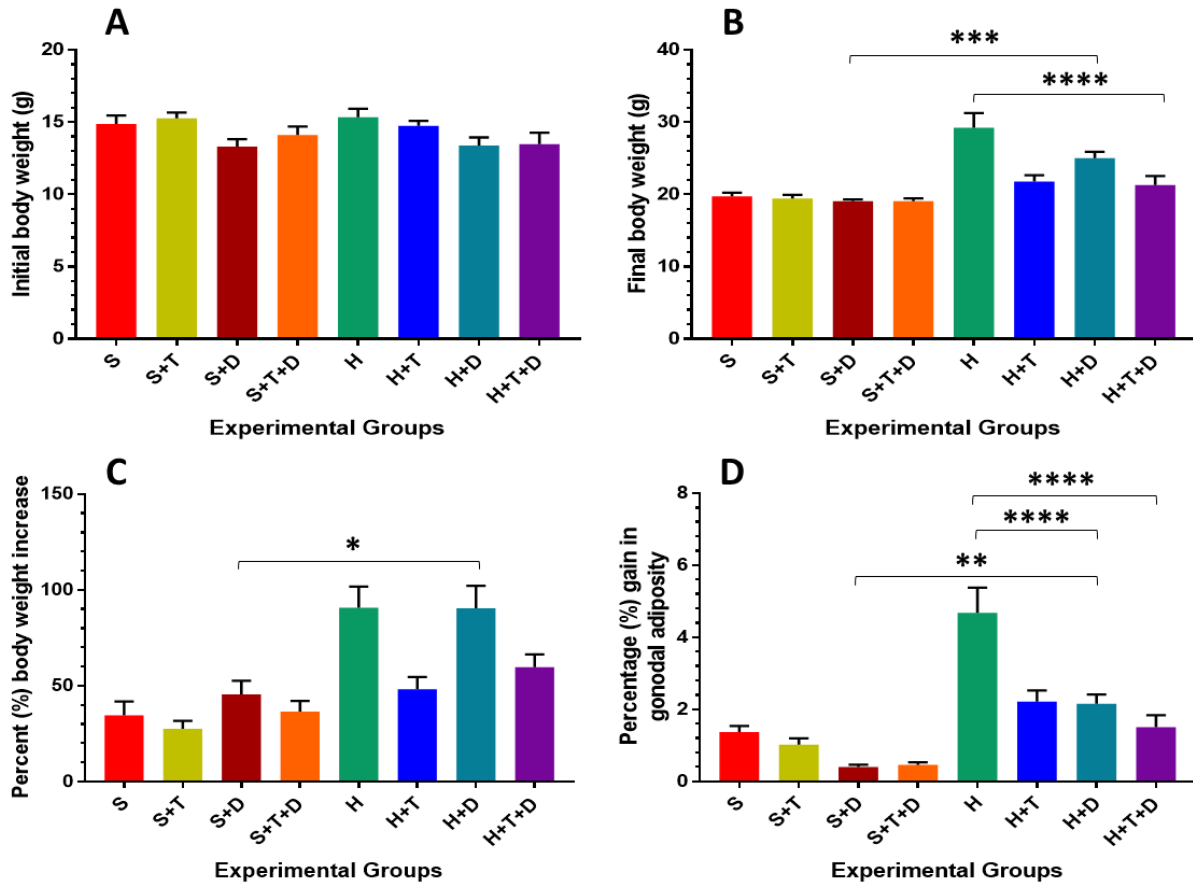


**Figure 3.24: Biometric parameters of mice fed a standard (S) or high fat diet (H) for  $\pm 12$  weeks, and/or inoculated with cancer cells from eight weeks, and/or treated with DOX. (A) Initial body weight, (B) final body weight before euthanasia, (C) percentage (%) body weight gain and (D) percentage (%) gonadal adiposity of experimental groups. Data is represented as mean  $\pm$  SEM (n=8-10). \* $p < 0.05$ , \*\* $p < 0.01$ , \*\*\* $p < 0.001$ , \*\*\*\* $p < 0.0001$ . Abbreviations: g – grams.**

### 3.5.2 Food consumption and water intake

To complement the data obtained above, food (Figure 3.25) and water (Figure 3.26) consumption was evaluated. Here we demonstrate that group S+T+D ( $53.50 \pm 2.47$  kcal,  $p < 0.01$ ) consumed significantly less food when compared to group S+D ( $59.69 \pm 0.94$  kcal). This was an interesting observation considering that the final body weight did not change between these two groups. Water consumption was elevated between group H+T+D ( $30.01 \pm 1.19$  ml,  $p < 0.05$ ) when compared to group H+D ( $20.95 \pm 0.54$  ml).

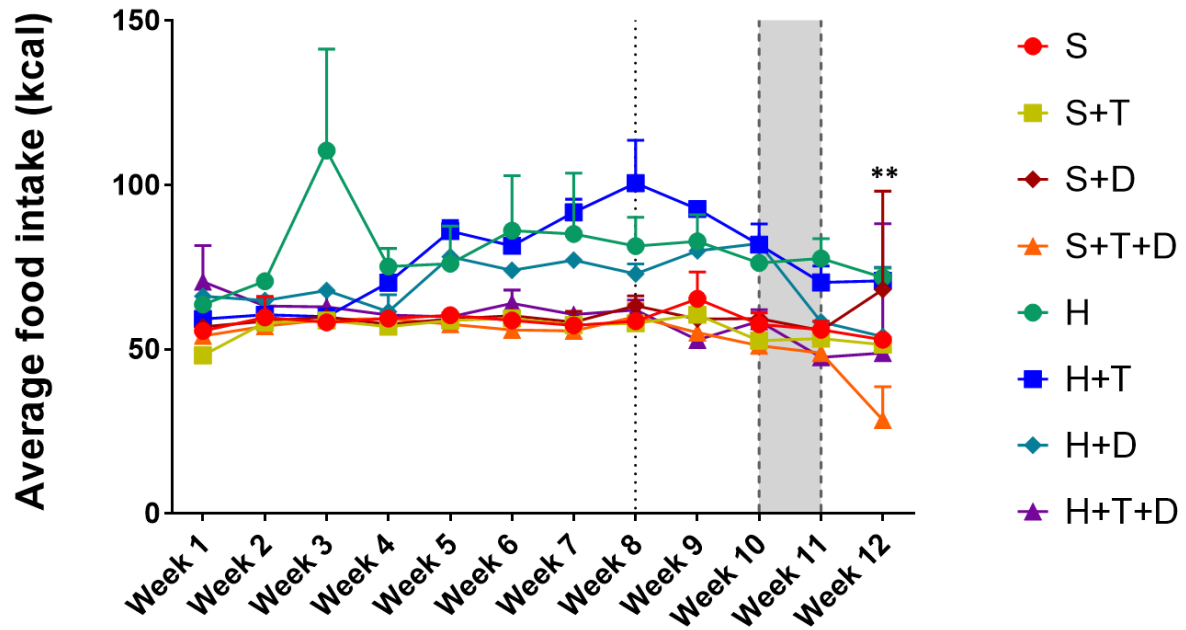


**Figure 3.25: Weekly food consumption in mice fed a standard (S) or high fat diet (H) for  $\pm 12$  weeks, and/or inoculated with cancer cells from eight weeks (represented by the vertical dotted line), and/or treated with DOX (represented by the grey shaded area). Food intake was measured weekly for each group to determine the average kilocalories (kcal) consumed. Data is represented as mean + SEM (n=8-10). \*\*p<0.01 (versus S+T+D). Abbreviations: kcal – kilocalories.**

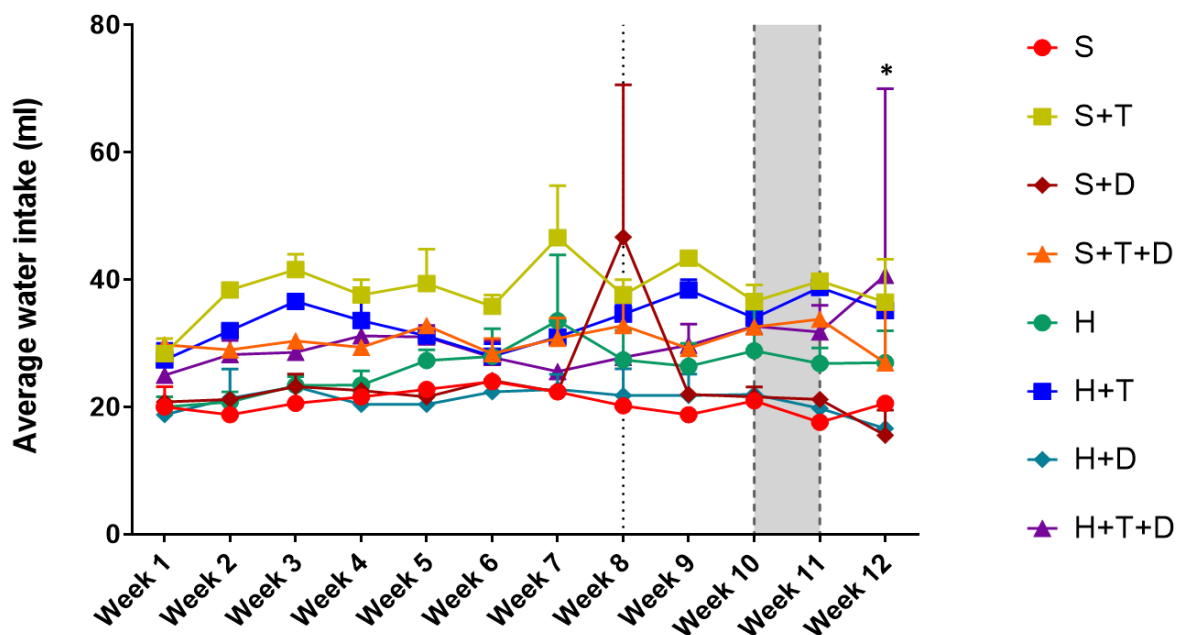


**Figure 3.26: Weekly water consumption in mice fed a standard (S) or high fat diet (H) for 12 weeks, and/or inoculated with cancer cells from eight weeks (represented by the vertical dotted line), and/or treated with DOX (represented by the grey shaded area). Water intake was measured daily but evaluated weekly for each group to determine the average amount of water consumed. Data is represented as mean + SEM (n=8-10). \*p<0.05 (versus H+T). Abbreviations: ml – millilitres.**

### 3.5.3 Fasting blood parameters

This study found no major changes in fasting blood glucose (Figure 3.27A), triglycerides (Figure 3.27B), lactate (Figure 3.27C) and TNF- $\alpha$  (Figure 3.27D) in any of the groups compared. However, significant changes were however observed with IL-6 (Figure 3.27E) and leptin (Figure 3.27F) concentrations between groups H and H+T+D. While IL-6 levels increased ( $126.90 \pm 34.92$  pg/ml,  $p < 0.05$ ), leptin levels declined ( $3277.00 \pm 1541.00$  pg/ml) in the HFD group with cancer and DOX when compared to animals fed a HFD alone (IL-6:  $24.17 \pm 5.59$  pg/ml; leptin:  $11671.00 \pm 4538.00$  pg/ml,  $p < 0.05$ ). These results therefore suggest that being obese with the complication of cancer with chemotherapy greatly increases inflammation. However due to the significant weight loss experienced by these animals, it is understandable why the levels of leptin declined.

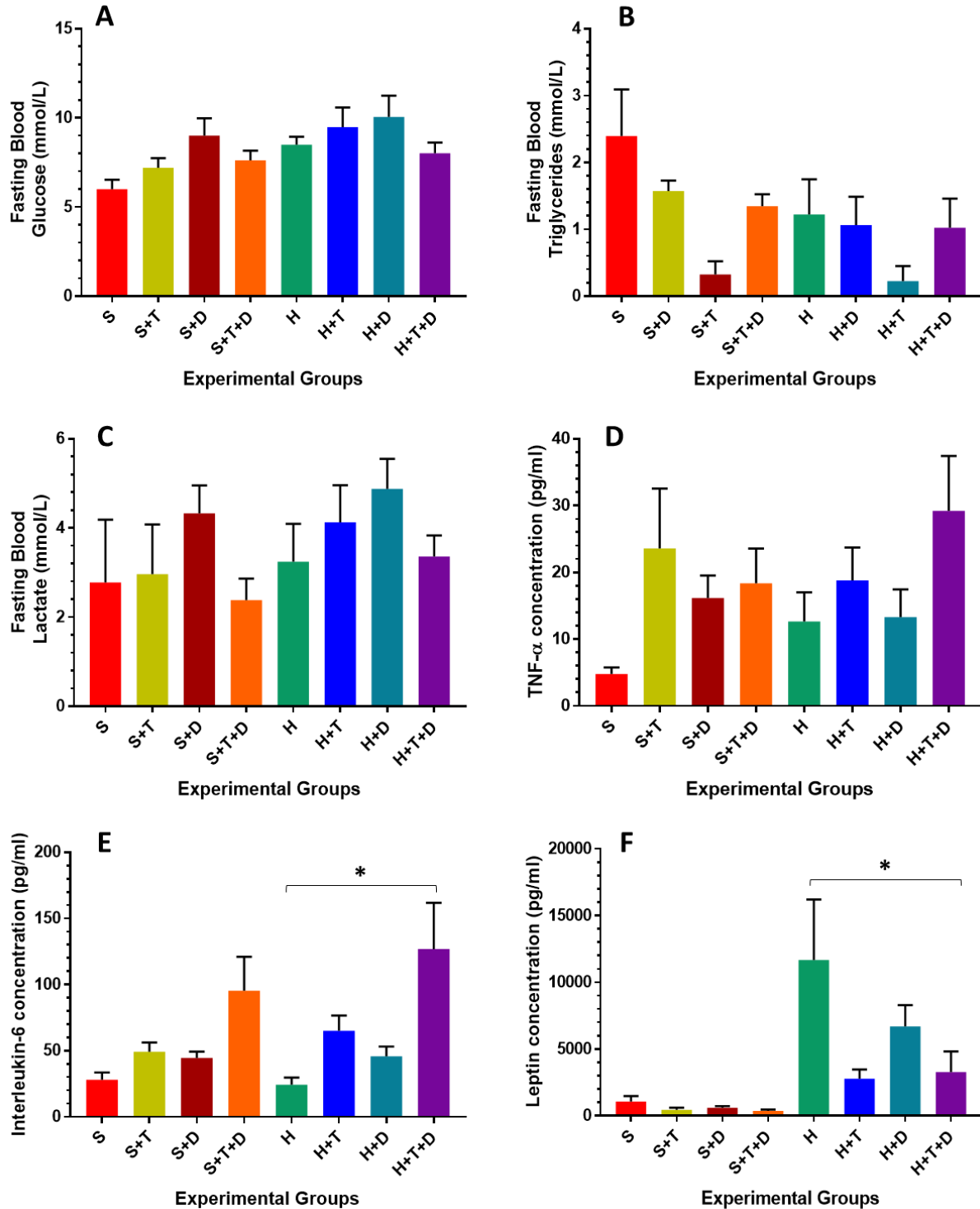


**Figure 3.27: Fasting blood parameters of mice fed a standard (S) or high fat diet (H) for  $\pm 12$  weeks, and/or inoculated with cancer cells from eight weeks, and/or treated with DOX. Mice were starved for 12 hours prior to euthanasia to determine (A) glucose, (B) triglycerides, (C) lactate, (D) TNF- $\alpha$ , (E) interleukin-6 and (F) leptin levels. Data is represented as mean  $\pm$  SEM (n=5-6). \*p<0.05.**

### 3.6 Effect of obesity, cancer and doxorubicin therapy on the heart

#### 3.6.1 The impact of diet-induced obesity, cancer and doxorubicin therapy on the cardiac hypertrophy index

DOX-induced cardiotoxicity has previously been associated with left ventricular hypertrophy which entails the enlargement of the heart and the death of cardiomyocytes. This study shows that the heart weight of group H+T+D was significantly reduced ( $0.10 \pm 0.007$  g,  $p < 0.05$ ) when compared to group H ( $0.13 \pm 0.005$  g) (Figure 3.28A). The heart-to-body weight ratio was used to examine potential hypertrophy in these experimental groups however, no changes of this aspect were observed (Figure 3.28B). According to these results, pathological hypertrophy was not present but possibly cardiac atrophy took place considering that DOX-induced hypertrophy is better associated with the chronic form of cardiotoxicity rather than the acute form.

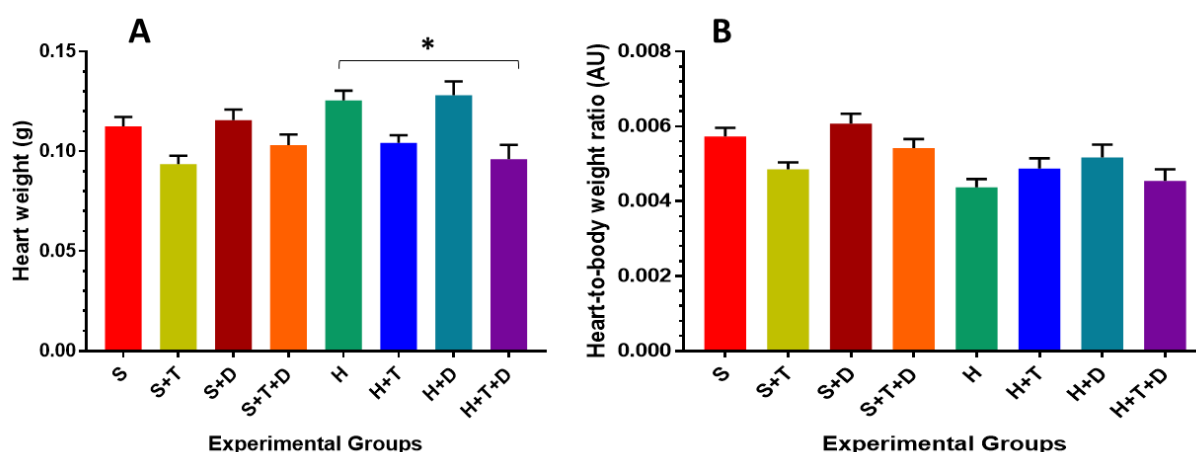


**Figure 3.28: Cardiac hypertrophy index of mice fed a standard (S) or high fat diet (H) for  $\pm 12$  weeks, and/or inoculated with cancer cells from eight weeks, and/or treated with DOX. (A) Heart weight and (B) heart-to-body weight ratio of experimental groups. Data is represented as mean  $\pm$  SEM ( $n=8-10$ ). \* $p < 0.05$ . Abbreviations: g – grams, AU-arbitrary units.**

### 3.6.2 The effect of a high fat diet, cancer and doxorubicin therapy on myocardial ultrastructure and collagen deposition

Although the hypertrophy index revealed no changes in any of the groups, microscopic changes within the tissue was further analysed for potential changes in myocardial ultrastructure (Figure 3.29) and the presence of fibrosis (Figures 3.30 and 3.31). It was only in group H+T+D did this study observe potential infiltration and distortion of the heart tissue (displacement of intracytoplasmic vacuoles) however, this observation was mild. Additionally no fibrosis was observed.

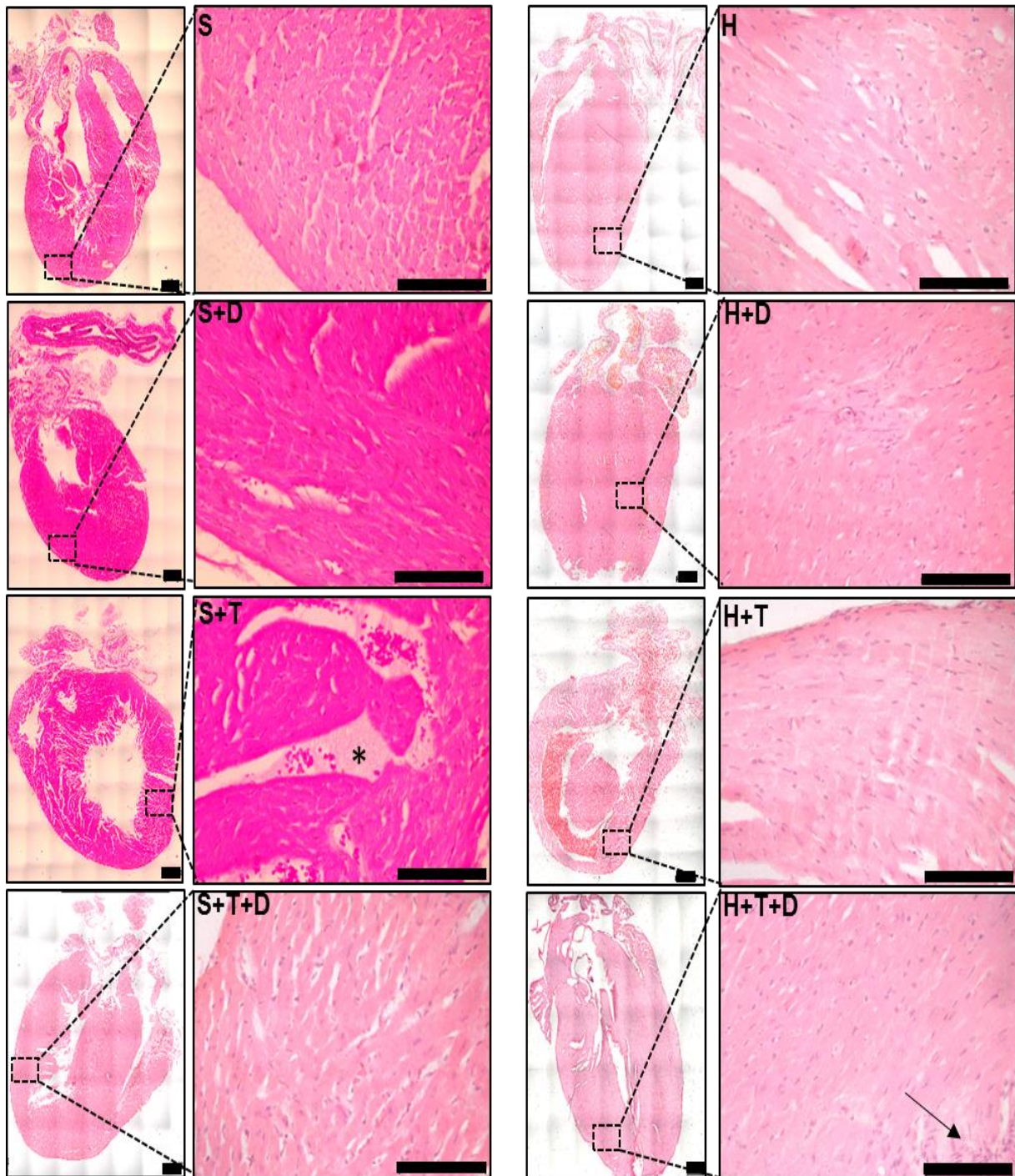


**Figure 3.29: H&E histological stains of heart tissue sections from mice fed a standard (S) or high fat diet (H) for  $\pm 12$  weeks, and/or inoculated with cancer cells from eight weeks, and/or treated with DOX.** Representative images of 5  $\mu\text{m}$  thick heart sections picked at random and stained for structural defects. 4-5 images from three different mice per group were assessed. Interstitial congestion is indicated by the asterisk. Inflammation infiltration is indicated by arrowhead. Magnification and scale bar: 10x and 100  $\mu\text{m}$  (entire section) and 40x and 500  $\mu\text{m}$  (enlargement). Purple colour- nucleus and pink colour – cytoplasm.

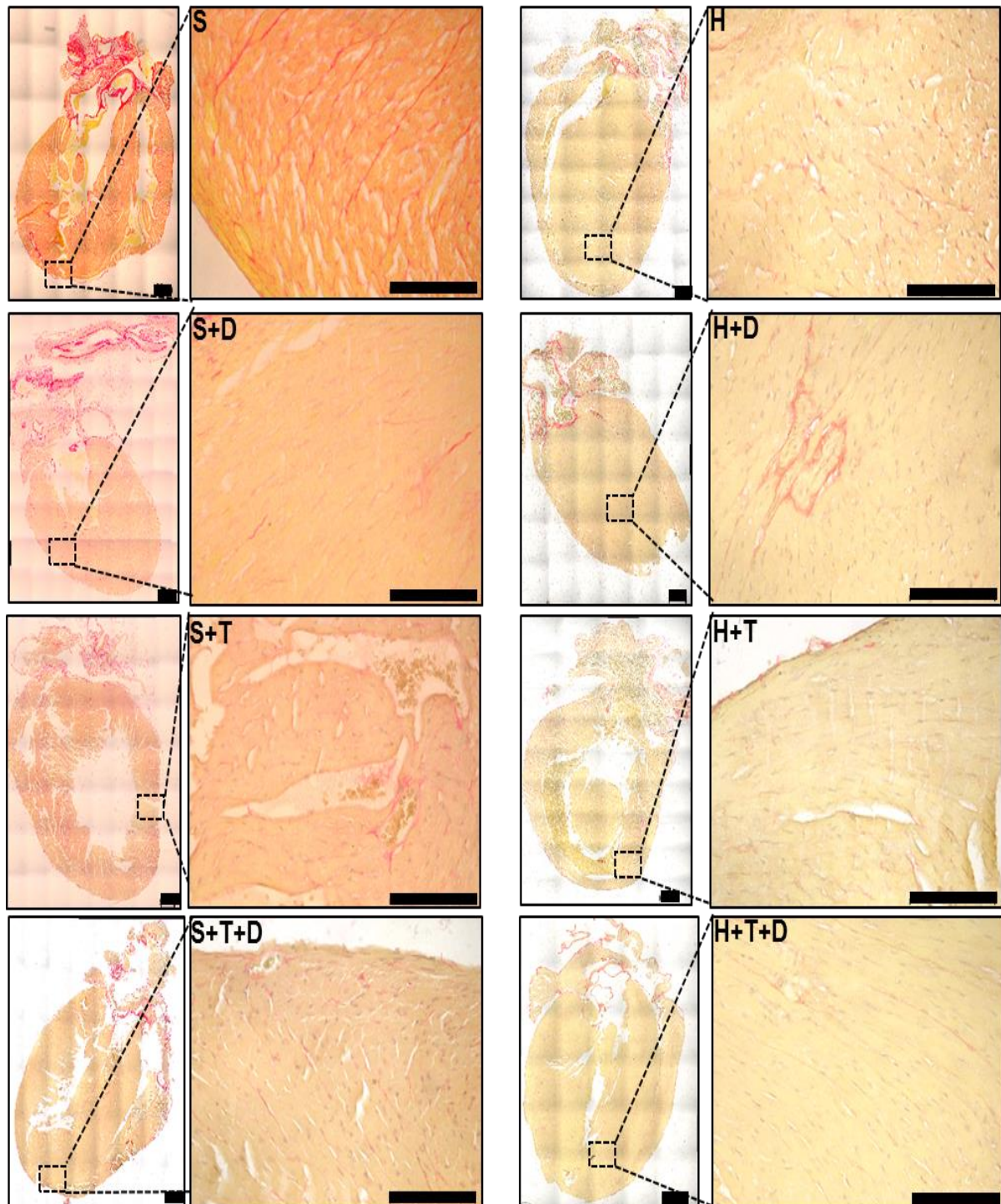


**Figure 3.30: Picosirius red histological stain of heart tissue sections from mice fed a standard (S) or high fat diet (H) for  $\pm 12$  weeks, and/or inoculated with cancer cells from eight weeks, and/or treated with DOX. Representative images of 5  $\mu$ m thick heart sections picked at random and stained for collagen deposition (fibrosis). 4-5 images from three different mice per group were assessed. Magnification and scale bar: 10x and 100  $\mu$ m (entire section) and 40x and 500  $\mu$ m (enlargement) Red colour – fibrosis (collagen I and II), yellow colour - cytoplasm, brown, grey or black colour- nucleus.**

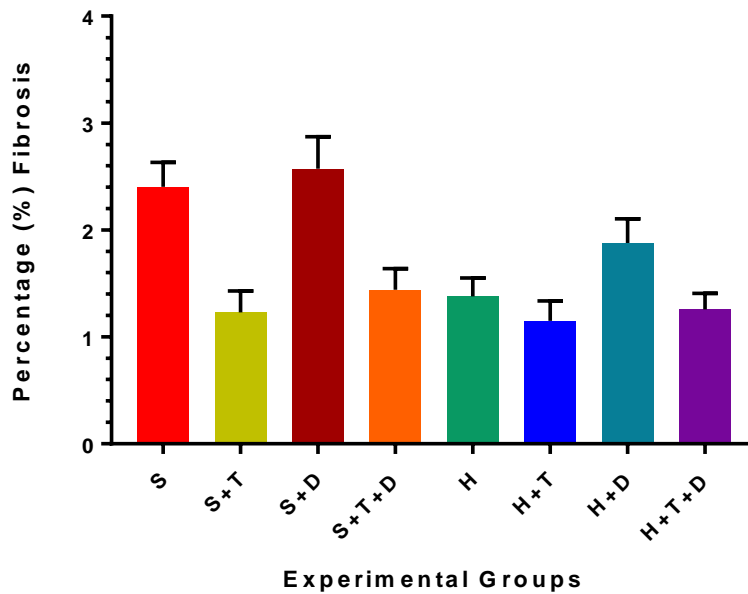


**Figure 3.31: Percentage fibrosis in the myocardium of mice fed a standard (S) or high fat diet (H) for  $\pm 12$  weeks, and/or inoculated with cancer cell from eight weeks, and/or treated with DOX. 4-5 images from three different mice per group were quantified for fibrosis using the colour threshold of Image J analysis software. Data is represented as mean  $\pm$  SEM (n=3).**

### 3.6.3 The effect of a high fat diet, cancer and doxorubicin therapy on apoptotic protein expression

Considering that DOX is known to induce apoptotic cell death as a mechanism of action, this study analysed this form of cell death in all experimental groups. As demonstrated in Figure 3.32 below, the markers for apoptosis did not significantly change suggesting that the dose and/or duration of treatment was not sufficient to trigger apoptosis since acute cardiotoxicity is more often associated with myocardial dysfunction rather than myocardial death.

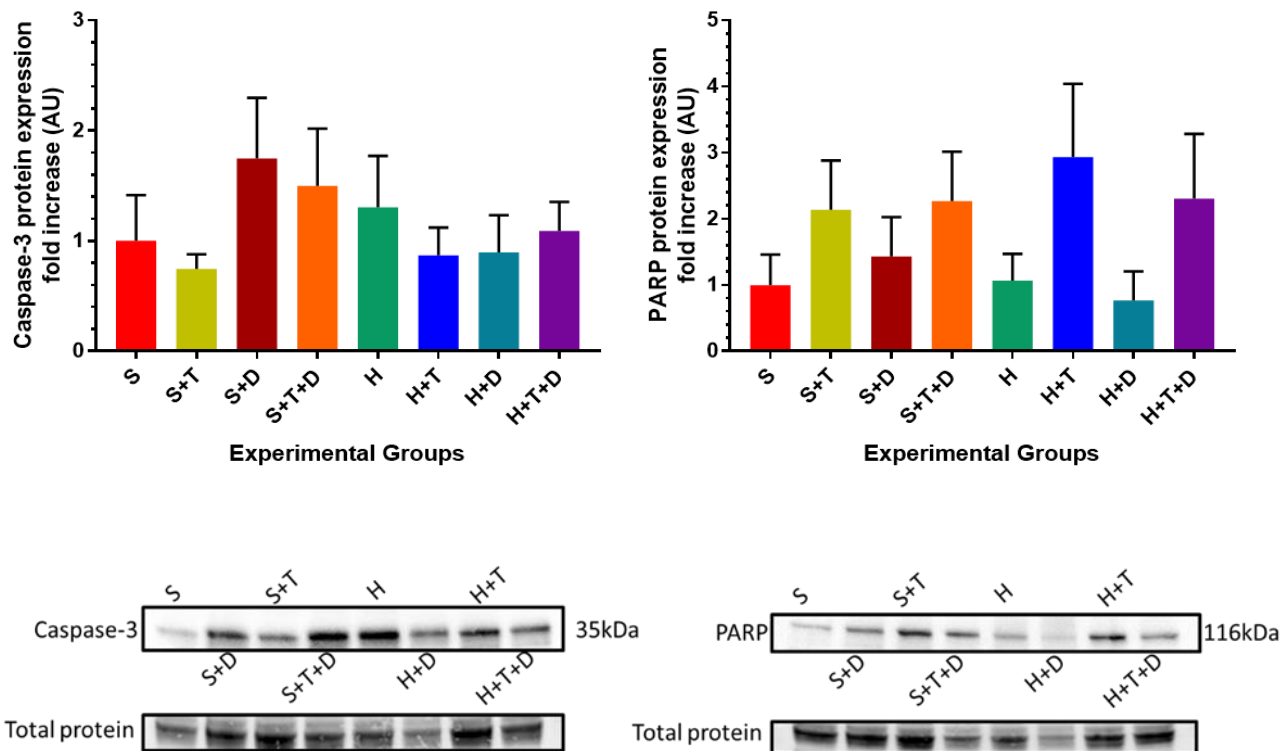


**Figure 3.32: Relative apoptotic protein expression of mice fed a standard (S) or high fat diet (H) for  $\pm 12$  weeks, and/or inoculated with cancer cells from eight weeks, and/or treated with DOX.** Representative graphs and western blot images of full-length caspase-3 and PARP are illustrated. Protein expression was normalized to total protein and presented as a fold change relative to controls (S or H). All values are presented as mean  $\pm$  SEM (n=4). Abbreviations: AU - arbitrary units.

### 3.6.4 The effect of a high fat diet, cancer and doxorubicin therapy on oxidative stress parameters

Similarly, to the results obtained above, no changes were observed for the early marker of oxidative stress (conjugated dienes) in any of the experimental groups (Figure 3.33). However, significant differences in malondialdehyde accumulation was observed between group H+T+D ( $0.009 \pm 0.003 \mu\text{mol/g}$ ,  $p < 0.05$ ) when compared to group H+T ( $0.003 \pm 0.002 \mu\text{mol/g}$ ). This increase in malondialdehydes indicates that DOX had an impact on oxidative stress levels.

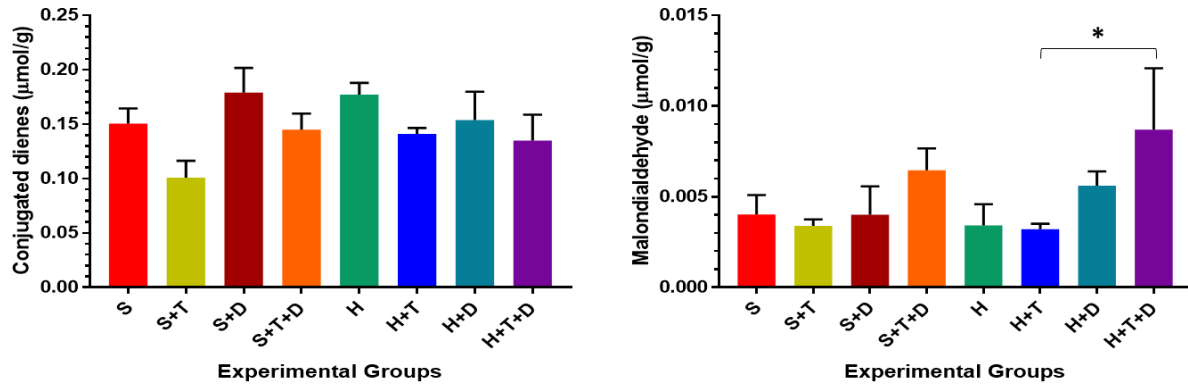


**Figure 3.33: Oxidative stress parameters from mice fed a standard (S) or high fat diet (H) for ±12 weeks, and/or inoculated with cancer cells from eight weeks, and/or treated with DOX.** Heart tissue lysates were used to evaluate the expression of early (conjugate dienes) and late (malondialdehydes) markers of lipid peroxidation. Data is represented as mean ± SEM (n=5-6). \*p<0.05.

## 4. DISCUSSION

Obesity forms part of the development of various pathologies including metabolic disorders (Aggoun, 2007), cardiovascular diseases (Poirier *et al.*, 2006), and the development of cancer (Basen-Engquist & Chang, 2011). In this context, obese women are often the leading group at risk for developing breast cancer (Yung & Ligibel, 2016). Obesity is a pro-inflammatory disease that is believed to assist in the angiogenesis and metastasis of cancer cells. This further results in the dysregulation of cytokines in the system (Matthews & Thompson, 2016) where these cytokines often serve as the modulators for cancer proliferation (Gilbert & Slingerland, 2013). Moreover, lipotoxicity, insulin resistance and excessive fatty acid production are indirectly or directly associated with obese patients' prognosis for breast cancer outcomes (Azrad & Demark-Wahnefried, 2014). Clinically, breast cancer is often treated with the potent chemotherapeutic agent DOX; however due to its dose-dependent cardiotoxicity, its use is limited. Since DOX administration is based on body surface area (BSA), obese patients are thus likely to receive higher dosages of DOX. In an effort to reduce the risk of developing cardiotoxicity within obese cancer patients, an arbitrary dose-capping for DOX has been implemented to prevent the adverse effects associated with DOX therapy in the heart (Lyman, 2011; Hall *et al.*, 2013). Furthermore, considering that obesity, cancer and cardiotoxicity are associated with inflammation and oxidative stress, the risk of cardiovascular complications increases. As cancer needs to be treated aggressively, clinicians are faced with the dilemma of treating cancer knowing the risks for cardiotoxicity. This leads to a reduced efficacy of treatment and a cancer-free survival in the obese-cancer population due to dose-capping (Lopes- Serrao *et al.*, 2011). The rationale for obesity being a risk factor for developing DOX-induced cardiotoxicity is under speculation due to limited research on the relationship between DOX and the state of obesity. Being overweight or obese greatly impacts on the pharmacokinetics of DOX since it has been shown that DOX within the plasma of obese patients is retained for extended periods (Ritzmo *et al.*, 2007). Since obese patients are already at increased risk of cardiovascular damage, the treatment of cancer with DOX can potentially accelerate the development of cardiotoxicity. As a result, obesity has not only become a risk factor for cardiovascular disease and cancer development, it is now a risk factor for the development of cardiotoxicity due to cancer treatment regimens (Puma *et al.*, 2008). In the experimental design of the current model, it was observed that the above stated diseases are either studied in isolation or in the context of DOX therapy, *in vivo* models often do not

have tumours, and therefore the effect of the cancer is not taken into account (Zhu *et al.*, 2010). In the current study, we aimed to establish a model of cancer in an obese state to not only determine how these diseases together impact on one another but most importantly, how they affect the myocardium. It was thus hypothesised that diet-induced obesity increases the risk for developing acute DOX-induced cardiotoxicity.

#### 4.1 Increased fat in the diet induced obesity

The major difference between the two diets used in this study was the fat content which accounted for 60% of calories in the high fat diet (HFD) versus a mere 10% contained in the standard diet (SD). The increase in food intake in the HFD group (Figure 3.3) resulted in a gain in body weight (Figure 3.2B) by the end of the study. The fat content in this diet consisted largely of soybean oil and lard which accounted for the higher calorie intake per day (Ulman, 2011). As it happens in humans, an increase in calorie intake without physical activity results in a gain in body weight and an increase in fat accumulation (adiposity) as observed in this study. Adipose tissue in this context thus becomes important because it is an essential and highly metabolic organ that secretes factors such as cytokines and adipokines with key endocrine functions (Kershaw & Flier., 2004). Under obese conditions, it is known that adipocytes undergo hyperplasia to store the excess fat accumulated and as a result causes dysregulated adipokine expression (Manna & Jain., 2015). Similarly to our observations, the increase in adiposity (Figure 3.2D) in the HFD group is related to increased fat accumulation. This was further exemplified by the abnormally high levels of glucose (Figure 3.5A) and leptin concentrations (Figure 3.5F). Hyperleptinemia is a direct consequence of obesity (Leopoldo *et al.*, 2016; O'Donnell *et al.*, 2000), and may play a role in mediating type 2 diabetes mellitus (T2DM) in obesity. While leptin in adipocytes prevents the uptake of glucose, inhibits lipolysis and impairs lipogenesis; in hepatocytes, leptin induces insulin-like effects by regulating the insulin-signaling pathway. It is therefore possible that there is cross-talk between leptin and insulin signaling, potentially making hepatocytes more sensitive to insulin in this context. Considering that obesity is an inflammatory disease, it was expected that the pro-inflammatory cytokine levels of TNF- $\alpha$  and IL-6 would be elevated, however this was not the case. Similar results were obtained in a study conducted by Pettersson and colleagues (2012) who showed

that female C57BL6 mice fed the same HFD as in the current study displayed reduced plasma IL-6 concentrations when compared to their male counterparts. It was concluded that estrogen may have played a significant role in this scenario as this hormone is known to offer protection and reduce inflammation.

#### 4.2 Effect of obesity on the heart

Obesity is a known independent risk factor for the development of CVD because excess weight may cause changes within the heart that requires it work harder to send blood to all the cells in the body. Although the HFD used in this study produced phenotypically obese experimental animals, no overt changes occurred within the heart weight (Figure 3.6A). Since body weight serves as the standardising value to evaluate the change in heart weight, the reduced heart-to-body weight ratio (cardiac hypertrophy index) (Figure 3.6B) in this study, was due to the higher final body weight rather than the actual heart weight in the HFD group. Considering the events that have to occur for cardiac remodeling to take place during obesity, it was unlikely to have occurred within the 12 week period of the study. These sentiments are echoed by Rennison and colleagues (2007) who illustrated an increase in body weight without detrimental changes to the myocardium. This suggests that it is difficult to distinguish between the adaptation and maladaptation phase of obesity's effect on the heart (Harmancey *et al.*, 2008).

Histological analysis (Figure 3.7) also revealed no signs of pathological hypertrophy between the two groups although this can be attributed to other factors since this study only assessed the whole heart to determine the ratio. Others (Lin *et al.*, 2000; Laflamme *et al.*, 2012; Kumar *et al.*, 2014) have suggested the use of tibia length or brain weight which are better parameters to determine the cardiac hypertrophy index since the body weight changed throughout the study. Moreover, obesity is associated with the onset of fibrosis in the heart and forms part of the structural changes that occur due to obesity (Abel *et al.*, 2008). Although the link between obesity and cardiac fibrosis has already been well-established, the pathophysiologic basis for fibrotic interstitial remodeling in the hearts of obese subjects remains poorly understood. The activation of fibroblasts has previously been shown to play a major role in obesity-associated fibrosis; however, inflammatory cells, cardiomyocytes and vascular cells may also trigger

fibrogenic signaling (Cavalera *et al.*, 2014). Molecular processes including the renin-angiotensin-aldosterone system, induction of transforming growth factor- $\beta$ , oxidative stress, advanced glycation end-products, endothelin-1, Rho-kinase signaling, leptin-mediated action and upregulation of matricellular proteins, have all been implicated in regulation of the fibrotic response in obesity and may play a role in the development of fibrosis in models of obesity and metabolic dysfunction. Based on the above cited studies, it still remains unclear whether the observed myocardial changes are as a direct effect of increased adiposity, or are reflective of the consequences of the many pathophysiologic associates of obesity. As we did not observe increased fibrosis in the HFD group (Figures 3.8 & 3.9), this can be explained by the fact that the development of cardiac fibrosis occurs late and requires prolonged feeding of a high-fat, or a high-fat/high-sugar diet for 6–16 months (Zibadi *et al.*, 2009; Qin *et al.*, 2012). High-fat diets may be even less effective in inducing cardiac fibrotic changes as Calligaris and co-workers (2013) found that male C57/BL6J mice required feeding with a HFD for 16 months to develop significant cardiac hypertrophy and myocardial fibrosis.

Numerous studies have demonstrated apoptosis of cardiomyocytes in experimental models of obesity (Barouch *et al.*, 2006). This mechanism of cell death is one of three that may be stimulated when cardiomyocytes become damaged (Cook & Poole-Wilson, 1999). The accumulation of fatty acids and triglycerides in the myocardium may induce toxic effects on cardiomyocytes that eventually leads to their dysfunction and death (Alpert *et al.*, 2014). It is therefore likely that since our model failed to demonstrate inflammation (Figure 3.5 D & E), fibrosis (Figures 3.8 & 3.9) and oxidative stress (Figure 3.11), all of which have been shown to induce apoptotic activity, this model was unlikely to demonstrate evidence of apoptosis (Figure 3.10). In summary, while the HFD used in this study was effective in inducing obesity which was accompanied by some metabolic changes, the duration of the study was inadequate to induce many of the obesity-related pathophysiological perturbations particularly those that put the myocardium at risk.

### 4.3 Cancer in an obese state induces body weight loss and increased inflammation

There are many other diseases that have been linked to obesity including various cancers (Ceschi *et al.*, 2007); and the novelty in the current model was the induction of breast cancer which was critical in understanding the biological interaction of two diseases in one experimental model. A person's risk of cancer depends on various factors, including those you cannot change such as age and genetics. Other factors that can cause cancer, whether that's obesity, smoking or the sun, increases a person's risk of cancer, however that does not mean that a person will definitely develop cancer. The majority of all the evidence that links obesity to cancer risk comes from large observational studies, however there is difficulty in interpreting such studies due to the fact that obese or overweight people may differ from lean people in ways other than their body fat and it is therefore difficult to establish that the cause of cancer was due to obesity. Regardless of this limitation there is consistent evidence that indicates that higher amounts of body fat are associated with increased risk of a number of cancers. There are several mechanisms that have been implicated to explain how obesity may increase the risk of different cancers. Obese people are known to have chronic low-grade inflammation, which can over time, cause DNA damage that leads to cancer development. Furthermore, overweight and obese individuals are more likely than normal-weight individuals to have disorders that are associated with or that cause chronic inflammation that are risk factors for certain cancers. For example, obese individuals have been shown to have elevated insulin and IGF-1 levels which can promote the development of colon, kidney, prostate, and endometrial cancers (Hsieh, 2011) possibly through cell growth regulators that include mTOR and AMPK. Adipose tissue during obesity produces excessive amounts of estrogen which has been linked with increased risks of breast, endometrial and ovarian cancers (Hsieh, 2011; Suzuki *et al.*, 2012). Adipocytes also secrete adipokines such as leptin which promotes cell proliferation during obesity, and adiponectin, which is less abundant in obese individuals and has anti-proliferative effects.

In the present experimental model, the presence of a tumour negatively affected body weight gain over time (Figure 3.12). The most significant weight loss was observed in the HFD group (Figure 3.13B) despite maintaining increased food intake (Figure 3.14), suggesting

that the presence of a tumour may have accounted for the body weight loss. In oncology, cancer cells are known to utilize glucose as their preferred source of energy while generating lactate. This is known as the Warburg effect, and why cancer cells choose to use a less efficient system (compared to oxidative phosphorylation) even in the presence of oxygen remains debatable. Since our model did not display considerable changes in fasting glucose (Figure 3.16A), triglyceride (Figure 3.16B) and lactate (Figure 3.16C) levels, it is difficult to interpret our findings against the currently available literature. What was interesting to note from our observations was that the significant decrease in adiposity (Figure 3.13D) coincided with a trend towards a decline in triglyceride levels, albeit insignificant. Considering that most cancer researchers focus on glycolysis, it is reasonable to speculate that the decrease in adiposity may have been attributed to the reduction of leptin levels (Figure 3.16F) which inhibits lipolysis in obesity. The relevance of fatty acid oxidation for cancer cell function has thus not been carefully examined, and its relevance in this context remains to be elucidated. In accordance with the literature (Kumari *et al.*, 2016), this study also observed significantly elevated levels of IL-6 in the HFD group with a tumour (Figure 3.16E). IL-6 is one of the main cytokines secreted by tumour cells within the microenvironment that is overexpressed in virtually all types of cancers. In this context, IL-6 promotes tumour development by regulating various signaling pathways and hallmarks of cancer. In addition, IL-6 provides protection for cancer cells against therapy-induced DNA damage, apoptosis and oxidative stress by initiating repair processes and/or anti-apoptotic and anti-oxidant mechanisms. Since cancer, like obesity is an inflammatory disease, the inhibition of IL-6 or its regulatory signaling pathways may potentially be an effective treatment strategy for cancers associated with increased IL-6 concentrations. Considering that inflammation is closely related to oxidative stress, which can stimulate apoptotic cell death; this was not the case in this study. The myocardial ultrastructure was similar to the control (Figure 3.18) and no oxidative stress (Figure 3.22) nor apoptosis (Figure 3.21) was observed. Although numerous studies have demonstrated myocardial damage in other inflammatory models (Sishi *et al.*, 2013; Eijsvogels *et al.*, 2012), it is likely that in this scenario, the duration of the study was too short for these adverse effects to be seen.

#### 4.4 DOX treatment and tumour presence decrease body weight

DOX treatment is linked to the secondary effect of development of cardiotoxicity and its proposed that obesity is a contributing risk factor to this state (Blaes *et al.*, 2017). Obesity is a known risk factor for the development of DOX-induced cardiotoxicity (Pai & Nahata., 2000). In a meta-analysis by Guenancia *et al.*, (2016) being overweight and obesity have showed to have a predisposing effect on the development of cardiotoxicity due to anthracyclines of which DOX is a part of. It was suggested that the findings were to be taken with close observation as it included various studies and the methodology was questioned with obesity being linked to various co-morbidities (Cheraghi *et al.*, 2017).

Firstly, DOX's effect on body weight was evaluated from week 10 (Figure 3.23). From the results the HFD induced-obesity and DOX effect on the mice final body weight showed a significant decrease in body weight, indicating that DOX treatment in the high fat group showed a slight reduction (Figure 3.24B). In a study by Biondo and colleagues (2016), using rats that were treated with DOX showed a decrease in body weight and adiposity, confirming this similar observation, the diet is one of the main factors to a reduced body weight increase (Figure 3.24C). This show-cases that DOX has the ability to affect the metabolic state of the animals since adipose tissue is an endocrine organ, which is involved in the regulation of energy balance. Throughout week 11 and week 12, when mice approximately received DOX treatment, DOX did not affect the food intake (Figure 3.25) or the water intake (Figure 3.26) amongst the experimental groups. DOX increased glucose (Figure 3.27A) but decreased plasma leptin (Figure 3.27F). The elevated fasting plasma IL-6 levels (Figure 3.27E) in the DOX treated groups is a possible indication of the DOX effect on the onset of the inflammatory state. DOX has the ability activate the production of cytokines and activate cytotoxic T lymphocyte and this activate the natural killer (NK) (Haskill, 1981). TNF- $\alpha$  is another pro-inflammatory cytokine upregulated in the obese condition (Van Kruijsdijk *et al.*, 2009). Plasma TNF- $\alpha$  like plasma IL-6 showed that the DOX treated mice irrespective of diet showed a trending increase in the experimental groups (Figure 3.27 D). This shows that DOX has the ability to activate the immune system (Tacar *et al.*, 2013), whether it is due to a natural response due to DOX being foreign or whether it is due to the mechanism by which DOX

affects both cancer and non- cancerous cells is unknown. Although only two inflammatory markers were evaluated this shows promising results that indeed supports the theory that the chronic inflammatory state is upregulated in the presence of obesity, cancer and DOX. This could be seen as the linkage mechanism by which early-stage cardiotoxicity can occur. However, in the study no special inflammatory stain was used to quantify this observation within the heart tissue and only the structural changes and semi-quantified inflammation infiltration was evaluated (Figure 3.29). The increase in circulating inflammation markers in the presence of DOX can however be related to the contribution that the innate immune system which is upregulated by DOX (Gambardella *et al.*, 2017). From the results, there is a plausible interlinked relationship between cancer and obesity with its overlapping observation of upregulated inflammation but whether it has a direct link with the heart is not clear in the outcomes of the study. However, the relation of the decrease in plasma leptin with DOX is not well understood, and whether it is beneficial or detrimental requires further analysis. Exogenous administered leptin has been shown to be cardioprotective after Ischemia-reperfusion (I/R) injury by the activations of RISK pathway activating PI3K-AKT and MAPK pathway which is involved in the protection of the heart (Smith *et al.*, 2006). This observation is due to exogenous leptin. For this study we evaluated leptin that is produced internally by adipose tissue and therefore could deflect different outcomes due to excessive production by adipose tissue.

#### 4.5 Effect of chemotherapeutic treatment during cancer in an obese context

DOX is a common therapeutic agent for the treatment of various cancers. As potent as it is, it is also associated with many side effects, particularly toxicity of the heart. Not only is DOX known for its ability to produce free radicals, cardiomyocyte apoptosis has also been demonstrated leading to structural disorganization ultimately resulting in the enlargement of the heart in the long term (Tacar *et al.*, 2013). Considering that cancer can cause significant body weight loss, DOX can exacerbate this condition as it has been shown to activate protein degradation pathways (Sishi *et al.*, 2013) that contributes to overall body or organ weight loss. While DOX treatment alone did not have an impact on body weight loss irrespective of diet,

the presence of a tumour greatly impacted the final body weight in the HFD group that received DOX treatment (Figure 3.24B). This group also displayed reduced adiposity (Figure 3.24D) and leptin concentrations (Figure 3.27F) but elevated IL-6 levels (Figure 3.27E). Although it may appear that the loss of weight in the obese context may be beneficial, the sustained systemic inflammation may have adverse effects in the long term if not reduced or regulated. In support of our observations, Fujita and colleagues (1996) elegantly demonstrated the role that chronic IL-6 exposure plays in stimulating protein breakdown, whereas van Hall and colleagues (2003) showed IL-6's role in inducing lipolysis. Similarly to the body weight loss observed in the HFD fed group inoculated with cancer cells and treated with DOX, the final heart weight mass was also reduced (Figure 3.28A). While this observation at face value may indicate cardiac atrophy, various factors have to be considered such as the study duration and the duration of DOX treatment. Since there was no functional evaluation of the heart it is difficult to ascertain whether DOX had any effect on the heart during DOX administration or immediately after. Moreover, we observed no severe structural adaptations other than mild displacement of intra- cytoplasmic vacuoles and infiltration (Figure 3.29). With regards to fibrosis, there are two different types: replacement fibrosis that occurs when cell death of tissue occurs; and reactive fibrosis, which is when an increase in work load is required (de Jong *et al.*, 2012), both of which can induce irregular cardiovascular function. In the current study we were unable to distinguish between the two since neither fibrosis (Figures 3.30 & 3.31) nor apoptosis was evident (Figure 3.32). Apoptotic activity can be triggered by elevated oxidative stress which can be triggered by increased inflammation. Although inflammation may have attributed to the oxidative stress shown in our model (Figure 3.33), the oxidative stress observed may not have been sufficient to stimulate apoptotic cell death as expected. In summary, the aim of the study was to establish the relationship between cancer in an obese context, and what impact these inflammatory diseases have in contributing to the development of acute DOX-induced cardiotoxicity. While we were able to provide evidence as to how a diet high in fat induces obesity and its impact on some metabolic parameters, it was difficult to provide conclusions about the diets effect on the heart. The complication of cancer in this context produced contrasting effects. A considerable amount of body weight and adiposity was lost, and consequently resulting in a decline in adipokine but elevated

cytokine expression. Despite these changes, no impacted on any of the cardiovascular parameters evaluated in this study. When DOX treatment was introduced, similar effects were observed with the exception of increased oxidative stress damage (Figure 3.34). Therefore in conclusion, future research is warranted to better understand the complexities involved during the initiation and progression of cancer in an obese environment, and what impact chemotherapy in this scenario would have on cardiovascular structure and function.

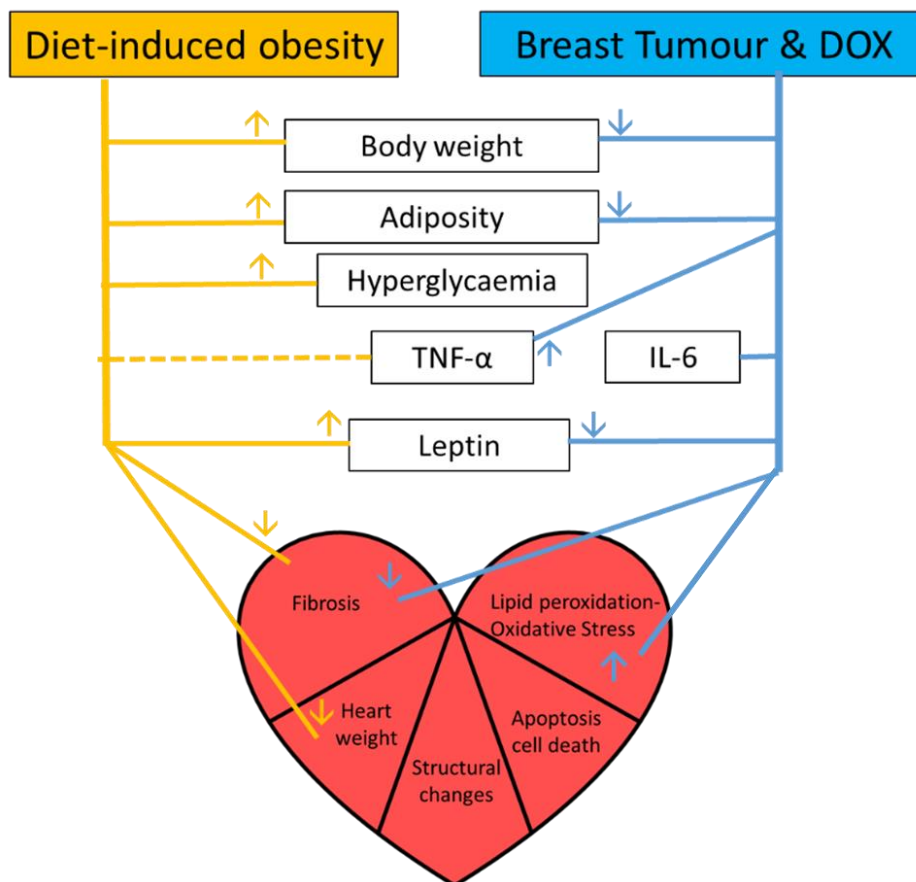


**Figure 3.34: Summary of the main findings from the study:** demonstrating the effects of a high fat diet, breast cancer and DOX treatment on the heart and the various pathways affected. Solid lines are confirmed observation and dashed lines are proposed outcomes. Up arrowheads indicate increase/activation and down arrowheads indicate a decrease/inhibition. Abbreviations: DOX - Doxorubicin, TNF- $\alpha$  - Tumour Necrosis Factor-alpha, IL-6 - interleukin- 6.

## **5. Limitations and future directions**

One of the main limitations in this study was the fact that we did not evaluate cardiovascular function which would have provided additional information with regards to how the heart is performing under the different experimental conditions. To further explore myocardial damage to supplement the histological stains performed, markers of damage such as cardiac troponins or brain natriuretic peptide could have been included to add value to this study. The presence of adiponectin and its relationship with leptin in the context of obesity-induced cancer would assist in the improved understanding of the molecular events take place. Due to financial constraints and logistical issues, the addition of the above was thus not possible.

## 6. REFERENCE LIST

- Abel, E.D., Litwin, S.E. & Sweeney, G. 2008. Cardiac remodeling in obesity. *Physiology Review*. 88: 389–419.
- Aggoun, Y. 2007. Obesity, metabolic syndrome, and cardiovascular disease. *Pediatric Research*. 61(6):653–659.
- Albuquerque, D., Stice, E., Rodríguez-López, R., Manco, L. & Nóbrega, C. 2015. Current review of genetics of human obesity: from molecular mechanisms to an evolutionary perspective. *Molecular Genetics and Genomics*. 290(4):1191–1221.
- Alpert, M.A., Lavie, C.J., Agrawal, H., Aggarwal, K.B. & Kumar, S.A. 2014. Obesity and heart failure: epidemiology, pathophysiology, clinical manifestations, and management. *Translational Research: The Journal of Laboratory & Clinical Medicine*. 164(4):345–356.
- Arola, O.J., Saraste, A., Pulkki, K., Kallajoki, M., Parvinen, M. & Voipio-Pulkki, L.M. 2000. Acute doxorubicin cardiotoxicity involves cardiomyocyte apoptosis. *Cancer Research*. 60(7):1789–1792.
- Azrad, M. & Demark-Wahnefried, W. 2014. The Association between Adiposity and Breast Cancer Recurrence and Survival: A Review of the Recent Literature. *NIH Public Access, Curr Nutr Rep*. 3(1):9–15.
- Barouch, L.A., Gao, D., Chen, L., Miller, K.L., Xu, W., Phan, A.C., Kittleson, M.M., Minhas, K.M., Berkowitz, D.E., Wei, C. & Hare, J.M. 2006. Cardiac myocyte apoptosis is associated with increased DNA damage and decreased survival in murine models of obesity. *Circulation Research*. 98:119–124.
- Barrett-Lee, P.J., Dixon, J.M., Farrell, C., Jones, a, Leonard, R., Murray, N., Palmieri, C., Plummer, C.J., Stanley, A. & Verrill, M.W. 2009. Expert opinion on the use of anthracyclines

in patients with advanced breast cancer at cardiac risk. *Annals of oncology : official journal of the European Society for Medical Oncology / ESMO*. 20(5):816–827.

Basen-Engquist, K. & Chang, M. 2011. Obesity and Cancer Risk: Recent Review and Evidence. *NIH Public Access, Curr Oncol Rep*. 13(1):71–76.

Basu, A., Johnson, D.E. & Woolard, M.D. 2002. Potentiation of tumor necrosis factor- $\alpha$ -induced cell death by rottlerin through a cytochrome-c-independent pathway. *Experimental Cell Research*. 278(2):209–214.

Bilić, I. 2014. Obesity and cancer. *Periodicum Biologorum*. 116(4):355–359.

Biondo, L.A., Junior, E.A.L., Souza, C.O., Cruz, M.M., Cunha, R.D.C., Alons-Vale, M.I., Oyama, L.M., Nascimento, C.M.O., Pimentel, G.D., dos Santos, R.V.T., Lira, F.S. & Neto, J.C.R. 2016. Impact of doxorubicin treatment on the physiological functions of white adipose tissue. *PLoS ONE*. 11(3):1–14.

Blaes, A., Prizment, A., Koene, R.J. & Konety, S. 2017. Cardio-oncology Related to Heart Failure: Common Risk Factors Between Cancer and Cardiovascular Disease. *Heart Failure Clinics*. 13(2):367–380.

Boden, G. 2011. Obesity , insulin resistance and free fatty acids. *Current Opinion in Endocrinology, Diabetes & Obesity*. 18:139–143.

Bromberg J. & Wang T.C. 2008. Inflammation and cancer: IL-6 and STAT3 complete the link. *Accounts of Chemical Research*. 45(6):788–802.

Brown, K.A. & Simpson, E.R. 2014. Obesity and breast cancer: The role of dysregulated estrogen metabolism. *Obesity and Breast Cancer: The Role of Dysregulated Estrogen Metabolism*. 1–56.

Calle, E.E. & Kaaks, R. 2004. Overweight, obesity and cancer: epidemiological evidence and proposed mechanisms. *Nature Reviews Cancer*. 4:579–591.

Calligaris, S.D., Lecanda, M., Solis, F., Ezquer, M., Gutiérrez, J., Brandan, E., Leiva, A., Sobrevia & Conget, P. 2013. Mice Long-Term High-Fat Diet Feeding Recapitulates Human Cardiovascular Alterations: An Animal Model to Study the Early Phases of Diabetic Cardiomyopathy. *PLoS ONE*. 8(4):1–10.

Carvalho, F.S., Burgeiro, A., Garcia, R., Moreno, A.J., Carvalho, R.A. & Oliveira, P.J. 2013. Doxorubicin-Induced Cardiotoxicity: From Bioenergetic Failure and Cell Death to Cardiomyopathy. *Medicinal Research Reviews, Wiley Online Library (wileyonlinelibrary.com)*. 1–30.

Cavalera, M., Wang, J. & Frangogiannis, N.G. 2014. Obesity, metabolic dysfunction, and cardiac fibrosis: pathophysiological pathways, molecular mechanisms, and therapeutic opportunities. *Translational Research*. 164(4):323-335.

Ceschi, M., Gutzwiller, F., Moch, H., Eichholzer, M. & Probst-Hensch, N.M. 2007. Epidemiology and pathophysiology of obesity as a cause of cancer. *Swiss Medical Weekly*. 137(3–4):50–56.

Chen, B., Peng, X., Pentassuglia, L., Lim, C.C. & Sawyer, D.B. 2007. Molecular and cellular mechanisms of anthracycline cardiotoxicity. *Cardiovascular Toxicology*. 7(2):114–121.

Cheraghi, Z., Ayubi, E. & Doosti-Irani, A. 2017. Obesity as a risk factor for anthracyclines and trastuzumab cardiotoxicity in breast cancer: Methodologic issues to avoid misinterpretation in the meta-analysis. *Journal of Clinical Oncology*. 35(8):923.

Cook, S.A. & Poole-Wilson, P.A. 1999. Cardiac myocyte apoptosis. *European Heart Journal*. 20(22):1619–1629. Cove-Smith, L., Woodhouse, N., Hargreaves, A., Kirk, J., Smith, S., Price, S.A., Galvin, M., Betts, C.J., Brocklehurst, S., Backen, A., Radford, J., Linton, K., Roberts, R.A., Schmitt, M., Dive, C., Tugwood, J.D., Hockings, P.D. & Mellor H.R. 2014. An integrated characterization of serological, pathological, and functional events in doxorubicin-induced cardiotoxicity. *Toxicological Sciences*. 140(1):3–15.

- Deswal, A. 2011. Obesity, leptin, and incident heart failure. *Journal of the American College of Cardiology*. 58(18):1878–1880.
- Deurenberg, P. 1999. The assessment of obesity: methods for measuring body fat and global prevalence of obesity. *Baillière's Clinical Endocrinology and Metabolism*. 13(1):1–11.
- Devasagayam, T.P.A., Tilak, J., Bloor, K.K., Sane, K.S., Ghaskadbi, S.S. & Lele, R.D. 2004. Free radicals and antioxidants in human health: current status and future prospects. *J Assoc Physicians India*. 52(October):794–804.
- Eijsvogels, T.H.M., Veltmeijer, M.T.W., George, K., Maria T. E. Hopman, M.T.E. & Thijssen, D.H.J. 2012. The impact of obesity on cardiac troponin levels after prolonged exercise in humans. *European Journal of Applied Physiology*. 112(5):1725-1732.
- Fernández-Sánchez, A., Madrigal-Santillán, E., Bautista, M., Esquivel-Soto, J., Morales-González, Á., Esquivel-Chirino, C., Durante-Montiel, I., Sánchez-Rivera, G., Valadez-Vega, C., & Morales-González, J.A. 2011. Inflammation, oxidative stress, and obesity. *International Journal of Molecular Sciences*. 12(5):3117–3132.
- Ferreira, A.L.A., Matsubara, L.S. & Matsubara, B.B. 2008. Anthracycline-Induced Cardiotoxicity. *Cardiovascular & Hematological Agents in Medicinal Chemistry*. 6(4):278–281.
- Finkelstein, E.A., Ruhm, C.J. & Kosa, K.M. 2005. Economic Causes and Consequences of Obesity. *Annual Review of Public Health*. 26(1):239–257.
- Folkerd, E.J. & Dowsett, M. 2010. Influence of sex hormones on cancer progression. *Journal of Clinical Oncology*. 28(26):4038–4044.
- Ford, E.S., Li, C., Zhao, G. & Tsai, J. 2011. Trends in obesity and abdominal obesity among adults in the United States from 1999-2008. *International Journal of Obesity*. 35(5):736–743.
- Fuemmeler, B.F., Lovelady, C.A., Zucker, N.L. & Østbye, T. 2013. Parental obesity moderates the relationship between childhood appetitive traits and weight. *HHS Public Access, Obesity*

(*Silver Spring*). 21(4):815–823.

Fujita, J., Tsujinaka, T., Ebisui, C., Yano, M., Shiozaki, H., Katsume, A., Ohsugi, Y. & Monden, M. 1996. Role of interleukin-6 in skeletal muscle protein breakdown and cathepsin activity in vivo. *European Surgical Research*. 28(5):361-366.

Gambardella, J., Trimarco, B., Iaccarino, G. & Sorriento, D. 2017. Review Article Cardiac Nonmyocyte Cell Functions and Crosstalks in Response to Cardiotoxic Drugs. *Oxidative Medicine and Cellular Longevity*. 2017:1–12.

Gammella, E., Maccarinelli, F., Buratti, P., Recalcati, S. & Cairo, G. 2014. The role of iron in anthracycline cardiotoxicity. *Frontiers in Pharmacology*. 5(25):1–6.

Gianni, L., Herman, E.H., Lipshultz, S.E., Minotti, G., Sarvazyan, N. & Sawyer, D.B. 2008. Anthracycline Cardiotoxicity: From Bench to Bedside. *J Clin Oncol*. 26(22):3777–3784.

Gilbert, C.A. & Slingerland, J.M. 2013. Cytokines, Obesity, and Cancer: New Insights on Mechanisms Linking Obesity to Cancer Risk and Progression. *Annual Review of Medicine*. 64(1):45–57.

Guenancia, C., Lefebvre, A., Cardinale, D., Yu, A.F., Ladoire, S., Ghiringhelli, F., Zeller, M., Rochette, L., Cottin, Y. & Vergely, C. 2016. Obesity As a Risk Factor for Anthracyclines and Trastuzumab Cardiotoxicity in Breast Cancer : A Systematic Review and Meta-Analysis. 34(26): 3157-3165

Guerre-Millo, M. 2008. Adiponectin: An update. *Diabetes and Metabolism*. 34(1):12–18.

Güngör, N.K. 2014. Overweight and obesity in children and adolescents. *Journal of Clinical Research in Pediatric Endocrinology*. 6(3):129–143.

- Gustafsson, A.B. & Gottlieb, R.A. 2006. Bcl-2 family members and apoptosis, taken to heart. *AJP: Cell Physiology*. 292(1):C45–C51.
- Hall, R.G., Jean, G.W., Sigler, M. & Shah, S. 2013. Dosing Considerations for Obese Patients Receiving Cancer Chemotherapeutic Agents. *Annals of Pharmacotherapy*. 47(12):1666–1674.
- Hanahan, D. & Weinberg, R.A. 2000. The hallmarks of cancer. *Cell*. 100(1):57–70.
- Hariri, N. & Thibault, L. 2010. High-fat diet-induced obesity in animal models. *Nutrition Research Reviews*. 23(2):270–299.
- Harmancey, R., Wilson, C.R. & Taegtmeier, H. 2008. Adaptation and maladaptation of the heart in obesity. *Hypertension*. 52(2):181–187.
- Haskill, J.S. 1981. Adriamycin-activated Macrophages as Tumor Growth Inhibitors. *Cancer Research*. 41:3852–3856.
- Hom, J. & Sheu, S.S. 2009. Morphological dynamics of mitochondria- A special emphasis on cardiac muscle cells. *Journal of Molecular and Cellular Cardiology*. 46(6):811–820.
- Hopkins, T.A., Ouchi, N., Shibata, R. & Walsh, K. 2007. Adiponectin actions in the cardiovascular system. *Cardiovascular Research*. 74(1):11–18.
- Horobin, R.W., Kiernan, J.A. & Conn, H.J. 2002. *Conn's biological stains : a handbook of dyes, stains and fluorochromes for use in biology and medicine*. 10th ed. J.A. Horobin, R.W., Kiernan (ed.). Oxford, UK: Biological Stain Commission by BIOS Scientific Publishers.
- Housman, G., Byler, S., Heerboth, S., Lapinska, K., Longacre, M., Snyder, N. & Sarkar, S. 2014. Drug resistance in cancer: An overview. *Cancers*. 6(3):1769–1792.
- Hruby, A. & Hu, F.B. 2015. The Epidemiology of Obesity: A Big Picture. *Pharmacoeconomics*. 33(7):673–689.

- Hsieh, P. 2011. Review Article Obesity and Carcinogenesis. *Journal of Cancer Research and Practice*. 27(6):242–256.
- Hui, X., Lam, K.S., Vanhoutte, P.M. & Xu, A. 2012. Adiponectin and cardiovascular health: An update. *British Journal of Pharmacology*. 165(3):574–590.
- Ishihara, K. & Hirano, T. 2002. IL-6 in autoimmune disease and chronic inflammatory proliferative disease. *Cytokine and Growth Factor Reviews*. 13(4–5):357–368.
- de Jong, S., van Veen, T.A.B., de Bakker, J.M.T. & van Rijen, H.V.M. 2012. Monitoring cardiac fibrosis: A technical challenge. *Netherlands Heart Journal*. 20(1):44–48.
- Kahn, B.B. & Flier, J.S. 2000. Obesity and insulin resistance. *The Journal of Clinical Investigation*. 106(4):473–481.
- Kavazis, A.N. 2015. Pathological vs. physiological cardiac hypertrophy. *Journal of Physiology*. 593(17):3767.
- Kershaw, E.E. & Flier, J.S. 2004. Adipose tissue as an endocrine organ. *Journal of Clinical Endocrinology and Metabolism*. 89(6):2548–2556.
- Kikuchi, K. & Poss, K.D. 2012. Cardiac regenerative capacity and mechanisms. *Annual review of cell and developmental biology*. 28(1):719–41.
- Kirilova, I., Chaisson, M. & Fausto, N. 1999. Tumor necrosis factor induces DNA replication in hepatic cells through nuclear factor kappaB activation. *Cell Growth Differentiation*. 10:819–28.
- Kolwicz, S.C., Purohit, S. & Tian, R. 2013. Cardiac metabolism and its interactions with contraction, growth, and survival of cardiomyocytes. *Circulation Research*. 113(5):603–616.
- Kubli, D.A. & Gustafsson, A. 2012. Mitochondria and mitophagy: the yin and yang of cell death control. *Circ Res*. 2012;111(9):1208-21. 111(9):1208–21.
- Kumar, N.T., Liestøl, K., Løberg, E.M., Reims, H.M. & Mæhlen, J. 2014. Postmortem heart

weight: Relation to body size and effects of cardiovascular disease and cancer. *Cardiovascular Pathology*. 23(1):5–11.

Kumari, N., Dwarakanath, B.S., Das, A. & Bhatt, N.A. 2016. Role of interleukin-6 in cancer progression and therapeutic resistance. *Tumor Biology*. 37(9): 11553–11572.

Kwon, H. & Pessin, J.E. 2013. Adipokines mediate inflammation and insulin resistance. *Frontiers in Endocrinology*. 4(JUN):1–13.

Laflamme, M.A., Sebastian, M.M. & Buetow, B.S. 2012. Cardiovascular. In *Comparative Anatomy and Histology*. 135–153.

Lau, D.C.W., Dhillon, B., Hongyum, Y., Szmilko, P.E. & Verma, S. 2005. Adipokines: molecular links between obesity and atherosclerosis. *AJP: Heart and Circulatory Physiology*. 288(5):H2031–H2041.

Lawrence, T. & Gilroy, D.W. 2007. Chronic inflammation : a failure of resolution ? 85–94.

Leopoldo, A.S., Lima-Leopoldo, A.P., Nascimento, A.F., Luvizotto, R.A.M., Sugizaki, M.M., Campos, D.H.S., Da Silva, D.C.T., Padovani, C.R. & Cicogna, A.C. 2016. Classification of different degrees of adiposity in sedentary rats. *Brazilian Journal of Medical and Biological Research*. 49(4):1–9.

Li, J., Romestaing, C., Han, X., Li, Y., Hao, X., Wu, Y., Sun, C., Liu, X., Jefferson, L.S., Xiong, J., LaNoue, K.F., Chang, Z., Lynch, C.J., Wang, H. & Shi, Y. 2010. Cardiolipin remodeling by ALCAT1 links oxidative stress and mitochondrial dysfunction to obesity. *Cell Metabolism*. 12(2):154–165.

Lin, S., Thomas, T.C., Storlien, L.H. & Huang, X.F. 2000. Development of high fat diet-induced obesity and leptin resistance in C57Bl/6J mice. *International Journal of Obesity*. 24(5):639–646.

Lopes-Serrao, M.D., Gresett Ussery, S.M. & Hall, R.G. 2011. Evaluation of Chemotherapy-

Induced Severe Myelosuppression Incidence in Obese Patients With Capped Dosing. *American Society of Clinical Oncology*. 7(1):13–17.

Lyman, G.H. 2011. Commentary: Chemotherapy Dosing in Obese Patients With Cancer—The Need for Evidence-Based Clinical Practice Guidelines. *Journal of Oncology Practice*. 7(1):17– 18.

Mahajan, R., Lau, D.H. & Sanders, P. 2015. Impact of obesity on cardiac metabolism, fibrosis, and function. *Trends in Cardiovascular Medicine*. 25(2):119–126.

Malhotra, V. & Perry, M.C. 2003. Classical Chemotherapy. *Cancer Biology & Therapy*. 2(4):S1–S4.

Manna, P. & Jain, S.K. 2015. Obesity, Oxidative Stress, Adipose Tissue Dysfunction, and the Associated Health Risks: Causes and Therapeutic Strategies. *Metabolic Syndrome and Related Disorders*. 13(10):423–444.

Marieb, E. N., & Hoehn, K. 2013. Cardiovascular System: The Heart. In Boston, Pearson. *Human anatomy & physiology*.

Maskari, M.Y. Al & Alnaqdy, A.A. 2006. Correlation between Serum Leptin Levels, Body Mass Index and Obesity in Omanis. *Sultan Quabos University Medical Journal*. 6(2):27–31.

Matthews, S.B. & Thompson, H.J. 2016. The obesity-breast cancer conundrum: An analysis of the issues. *International Journal of Molecular Sciences*. 17(6):1–19.

McGowan, J. V., Chung, R., Maulik, A., Piotrowska, I., Walker, J.M. & Yellon, D.M. 2017. Anthracycline Chemotherapy and Cardiotoxicity. *Cardiovascular Drugs and Therapy*. 31(1):63–75.

Minotti, G., Cairo, G. & Monti, E. 1999. Role of iron in anthracycline cardiotoxicity: new tunes for an old song? *The FADEB journal: official publication of the Federation of American Societies for Experimental Biology*. 13(2):199–212.

Minotti, G., Menna, P., Salvatorelli, E., Cairo, G. & Gianni, L. 2004. Anthracyclines: molecular advances and pharmacologic developments in antitumor activity and cardiotoxicity. *Pharmacological reviews*. 56(2):185–229.

Montaigne, D., Hurt, C. & Nevriere, R. 2012. Mitochondria death/survival signaling pathways in cardiotoxicity induced by anthracyclines and anticancer-targeted therapies. *Biochemistry Research International*. 306(11): R861–R867

Moulin, M., Piquereau, J., Mateo, P., Fortin, D., Rucker-Martin, C., Gressette, M., Lefebvre, F., Gresikova, M., Solgadi, A., Veksler, V., Garnier, A. & Ventura-Clapier, R. 2015. Sexual dimorphism of doxorubicin-mediated cardiotoxicity potential role of energy metabolism remodeling. *Circulation: Heart Failure*. 8(1):98–108.

Mraz, M. & Haluzik, M. 2014. The role of adipose tissue immune cells in obesity and low-grade inflammation. *Journal of Endocrinology*. 222(3):113–127.

Nalabolu, M., Palasamudram, K. & Jamil, K. 2014. Adiponectin and Leptin Molecular Actions and Clinical Significance in Breast Cancer. *International Journal of Hematology Oncology and Stem Cell Reserch*. 8(1):31–40.

Nam, S.Y., Lee, E.J., Kim, K.R., Cha, B.S., Song, Y.D., Lim, S.K., Lee, H.C. & Huh, K.B.

1997. IGF-1 and IGFBNs in Obesity. *International Journal of Obesity*. 21:355–359.

National Cancer Institute. 2017. Obesity and Cancer. [Online], Available: <https://www.cancer.gov/about-cancer/causes-prevention/risk/obesity/obesity-fact-sheet> [2017, October 06].

Noeman, S.A., Hamooda, H.E. & Baalash, A.A. 2011. Biochemical Study of Oxidative Stress Markers in the Liver, Kidney and Heart of High Fat Diet Induced Obesity in Rats. *Diabetology & Metabolic Syndrome*. 3(1):17.

NYHA .2019. *The New York Heart Association (NYHA) functional classification in a patient with heart disease*. Available at: [http://palliscience.com/sites/default/files/PDF/classification\\_nyha\\_new\\_york\\_heart\\_association.pdf](http://palliscience.com/sites/default/files/PDF/classification_nyha_new_york_heart_association.pdf).

O'Donnell, C.P., Tankersley, C.G., Polotsky, V.Y., Schwartz, A.R. & Smith, P.L. 2000. Leptin, obesity, and respiratory function. *Respiration physiology*. 119(2–3):163–70.

O'Neill, S. & O'Driscoll, L. 2015. Metabolic syndrome: A closer look at the growing epidemic and its associated pathologies. *Obesity Reviews*. 16(1):1–12.

Octavia, Y., Tocchetti, C.G., Gabrielson, K.L., Janssens, S., Crijns, H.J. & Moens, A.L. 2012. Doxorubicin-induced cardiomyopathy: From molecular mechanisms to therapeutic strategies. *Journal of Molecular and Cellular Cardiology*. 52(6):1213–1225.

Otto, A.M. 2016. Warburg effect(s)—a biographical sketch of Otto Warburg and his impacts on tumor metabolism. *Cancer & Metabolism*. 4(1):5.

Ouchi, N., Shibata, R. & Walsh, K. 2006. Cardioprotection by Adiponectin. *Trends in Cardiovascular Medicine*. 16(5):141–146.

Pai, V.B. & Nahata, M.C. 2000. Cardiotoxicity of chemotherapeutic agents: incidence, treatment and prevention. *Drug safety : an international journal of medical toxicology and drug experience*. 22(4):263–302.

Petersen, K.F. & Shulman, G.I. 2006. Etiology of insulin resistance. *American Journal of Medicine*. 119(5):S10–S16.

Pettersson, U.S., Walden, T.B., Carlsson, P., Jansson, L. & Phillipson, M. 2012. Female Mice are Protected against High-Fat Diet Induced Metabolic Syndrome and Increase the Regulatory T Cell Population in Adipose Tissue. *PLoS ONE*. 7(9):1–10.

Poirier, P., Giles, T.D., Bray, G.A., Hong, Y., Stern, J.S., Pi-Sunyer, F.X. & Eckel, R.H. 2006. Obesity and cardiovascular disease: Pathophysiology, evaluation, and effect of weight loss: An update of the 1997 American Heart Association Scientific Statement on obesity and heart disease from the Obesity Committee of the Council on Nutrition, Physical. *Circulation*. 113(6):898–918.

Puma, N., Ruggiero, A., Ridola, V., Maurizi, P., Lazzareschi, I., Attina, G., Mastrangelo, S., De Rosa, G. & Riccardi, R. 2008. Anthracycline-related cardiotoxicity : risk factors and therapeutic options in childhood cancers. *Signa Vitae*. 3(1):30–34.

Qin, F., Siwik, D.A., Luptak, I., Hou, X., Wang, L., Higuchi, A., Weisbrod, R.M., Ouchi, N., Tu, V.H., Calamaras, T.D., Miller, E.J., Verbeuren, T.J., Walsh, K., Cohen, R.A., & Colucci, W.S. 2012. The polyphenols resveratrol and S17834 prevent the structural and functional sequelae of diet-induced metabolic heart disease in mice. *Circulation*. 125(14):1757–1764.

Rabinowitz, J. D. and White, E. (2010) ‘Autophagy and metabolism.’, *Science*, 330(6009), pp. 1344–1348. doi: 10.1126/science.1193497.

Regitz-Zagrosek, V., Lehmkühl, E. & Weickert, M.O. 2006. Gender differences in the metabolic syndrome and their role for cardiovascular disease. *Clinical Research in Cardiology*. 95(3):136–147.

- Reilly, J.J. 2005. Early life risk factors for obesity in childhood: cohort study. *Bmj*. 330(7504):1357–0.
- Rennison, J.H., McElfresh, T. a, Okere, I.C., Vazquez, E.J., Patel, H. V, Foster, A.B., Patel, K.K., Chen, Q., Hoit, B.D., Tserng, K-Y., Hassan, M.O., Hoppel, C.L. & Chandler, M.P. 2007. High-fat diet postinfarction enhances mitochondrial function and does not exacerbate left ventricular dysfunction. *American journal of physiology. Heart and circulatory physiology*. 292(3):H1498–H1506.
- Riehle, C. & Abel, E.D. 2016. Insulin Signaling and Heart Failure. *American Heart Association journal*. 118(7):1151–1170.
- Ritterhoff, J. & Tian, R. 2017. Metabolism cardiomyopathy: every substrate matters. *Cardiovascular Research*. 113(4):411–421.
- Ritzmo, C., Söderhäll, S., Karlén, J., Nygren, H. & Eksborg, S. 2007. Pharmacokinetics of doxorubicin and etoposide in a morbidly obese pediatric patient. *Pediatric Hematology and Oncology*. 24(6):437–445.
- Ronti, T., Lupattelli, G. & Mannarino, E. 2006. The endocrine function of adipose tissue: An update. *Clinical Endocrinology*. 64(4):355–365.
- Russo, I. & Frangogiannis, N.G. 2016. Diabetes-associated cardiac fibrosis: Cellular effectors, molecular mechanisms and therapeutic opportunities. *Journal of Molecular and Cellular Cardiology*. 90:84–93.
- Saeidnia, S. & Abdollahi, M. 2013. Toxicological and pharmacological concerns on oxidative stress and related diseases. *Toxicology and Applied Pharmacology*. 273(3):442–455.
- Sawyer, D.B., Peng, X., Chen, B., Pentassuglia, L. & Lim, C.C. 2010. Mechanisms of anthracycline cardiac injury: Can we identify strategies for cardioprotection? *Progress in Cardiovascular Diseases*. 53(2):105–113.

- Schäffler, A. & Schölmerich, J. 2010. Innate immunity and adipose tissue biology. *Trends in Immunology*. 31(6):228–235.
- Schimmel, K.J.M., Richel, D.J., van den Brink, R.B.A. & Guchelaar, H.-J. 2004. Cardiotoxicity of cytotoxic drugs. *Cancer Treatment Reviews*. 30(2):181–191.
- Schulze, P.C. 2009. Myocardial lipid accumulation and lipotoxicity in heart failure . 50:2137–2138.
- Schutz, S., Machleidt, T. & Kronke, M. 1992. Mechanisms of tumour necrosis factor action. *Semin Oncol*. 2:16–24.
- Scolletta, S. & Biagioli, B. 2010. Energetic myocardial metabolism and oxidative stress: Let's make them our friends in the fight against heart failure. *Biomedicine and Pharmacotherapy*. 64(3):203–207.
- Segal, L.M., Rayburn, J. & Beck, S.E. 2017. *The State of Obesity: Better policies for a healthier America 2017*. [Online], Available: <https://stateofobesity.org/files/stateofobesity2017.pdf>.
- Selçuk, E. B., Sungu, M., Parlakpınar, H., Ermiş, N., Taslıdere, E., Vardı, N., Yalçınsoy, M., Sagır, M., Polat, A., Karatas, M., Kayhan-Tetik, B. 2015. Evaluation of the cardiovascular effects of varenicline in rats. *Drug design, development and therapy*. 9:5705–5717.
- Shanmugalingam, T., Bosco, C., Ridley, A.J. & Hemelrijck, M. Van. 2016. Is there a role for IGF-1 in the development of secondprimary cancers ? *Cancer Medicine*. 5(11):3353–3367.
- Shibata, R., Ouchi, N. & Murohara, T. 2009. Adiponectin and Cardiovascular Disease. *Circulation Journal*. 73(4):608–614.
- Šimůnek, T., Štěrba, M., Popelová, O., Adamcová, M., Hrdina, R. & Gerši, V. 2009. Anthracycline-induced cardiotoxicity: Overview of studies examining the roles of oxidative stress and free cellular iron. *Pharmacological Reports*. 61(1):154–171.
- Singla, Parul; Bardoloi, Animesh; Parkash, A.A. 2010. Metabolic effects of obesity: A review.

*World Journal of Diabetes*. 1(3):76–88.

Sishi, B.J.N., Loos, B., Van Rooyen, J. & Engelbrecht, A.M. 2013a. Autophagy upregulation promotes survival and attenuates doxorubicin-induced cardiotoxicity. *Biochemical Pharmacology*. 85: 124-134

Smith, C.C.T., Mocanu, M.M., Davidson, S.M., Wynne, a M., Simpkin, J.C. & Yellon, D.M. 2006. Leptin, the obesity-associated hormone, exhibits direct cardioprotective effects. *British journal of pharmacology*. 149(1):5–13.

Stanley, W.C. & Chandler, M.P. 2002. Energy metabolism in the normal and failing heart: potential for therapeutic interventions. *Heart Fail Rev*. 7:115–130.

Stehling, O. & Lill, R. 2013. The Role of Mitochondria in Cellular Iron – Sulfur Processes , and Diseases. *Cold Spring Harbor Laboratory Press*. 1–17.

Suckow, M., Danneman, P. & Brayton, C. 2001. *The Laboratory Mouse, A volume in the laboratory animal pocket reference series*.

Swinburn, B.A., Sacks, G., Hall, K.D., Mcpherson, K., Finegood, D.T., Moodie, M.L. & Gortmaker, S.L. 2011. Series Obesity 1 The global obesity pandemic : shaped by global drivers and local environments. 378:804–814.

Tacar, O., Sriamornsak, P. & Dass, C.R. 2013. Doxorubicin : an update on anticancer molecular action ,. *Journal of Pharmacology and Pharmacology*. 65:157–170.

Takemura, G. & Fujiwara, H. 2007. Doxorubicin-Induced Cardiomyopathy. From the Cardiotoxic Mechanisms to Management. *Progress in Cardiovascular Diseases*. 49(5):330–352.

Tanaka, T., Narazaki, M. & Kishimoto, T. 2014. IL-6 in Inflammation, Immunity, and Disease. *Cold Spring Harbor Perspectives in Biology*. 6:1–16.

Thorn, C., Oshiro, C., Marsh, S., Hernandez-Boussard, T., McLeod, H., Klein, T.E. & Altman, R.B. 2012. Doxorubicin pathways: pharmacodynamics and adverse effects. *Pharmacogenet Genomics*. 21(7):440–446.

Ulman, E.A. 2011. The “Original” High-Fat Diets for Diet Induced Obesity. *Product Dat - DIO series diets*. 1–3.

Vázquez-Vela, M.E.F., Torres, N. & Tovar, A.R. 2008. White Adipose Tissue as Endocrine Organ and Its Role in Obesity. *Archives of Medical Research*. 39(8):715–728.

van Hall, G., Steensberg, A., Sacchetti, M., Fischer, C., Keller, C., Schjerling, P., Hiscock, N., Møller, K., Saltin, B., Febbraio, M.A. & Pedersen., B.K. 2003. Interleukin-6 stimulates lipolysis and fat oxidation in humans. *The Journal of Clinical Endocrinology & Metabolism*. 88(7):3005–3010.

van Kruijsdijk, R.C.M., van der Wall, E. & Visseren, F.L.J. 2009. Obesity and cancer: The role of dysfunctional adipose tissue. *Cancer Epidemiology Biomarkers and Prevention*. 18(10):2569–2578.

Vincent, D.T., Ibrahim, Y.F., Espey, M.G. & Suzuki, Y.J. 2013. The role of antioxidants in the era of cardio-oncology. *Cancer Chemotherapy and Pharmacology*. 72(6):1157–1168.

Vonn Hoff, D.D., Layard, M.W., Basa, P., Davis, H.L., Von Hoff, A.L., Rozenzweig, M. & Muggia, F.M. 1979. Risk factors for doxorubicin-induced congestive heart failure. *Annal of Internal Medicine*. 710–717.

Webster, K.A. 2012. Mitochondrial membrane permeabilization and cell death during myocardial infarction: Roles of calcium and reactive oxygen species. *Future Cardiology*.

8(6):863–884.

Wende, A.R. & Abel, E.D. 2011. Lipotoxicity in the heart. *NIH Public Access, Biochim Biophys Acta*. 1801(3):311–319.

Westermann, B. 2010. Mitochondrial fusion and fission in cell life and death. *Nature reviews. Molecular cell biology*. 11(12):872–884.

WHO. 2018. Obesity and overweight. *World Health Organisation*. [Online], Available: <https://www.who.int/en/news-room/fact-sheets/detail/obesity-and-overweight>

Wueest, S., Item, F., Boyle, C.N., Jirkof, P., Cesarovic, N., Ellingsgaard, H., Boni-Schnetzler, M., Timper, K., Arras, M., Donath, M.Y., Schoenle, E.J. & Konrad, D. 2014. Interleukin-6 contributes to early fasting-induced free fatty acid mobilization in mice. *AJP: Regulatory, Integrative and Comparative Physiology*. 306(11):R861–R867.

Yung, R.L. & Ligibel, J.A. 2016. Obesity and breast cancer: Risk, outcomes, and future considerations. *Clinical Advances in Hematology and Oncology*. 14(10):790–797.

Zhang, S., Liu, X., Bawa-Khalfe, T., Lu, L.-S., Lyu, Y.L., Liu, L.F. & Yeh, E.T.H. 2012. Identification of the molecular basis of doxorubicin-induced cardiotoxicity. *Nature Medicine*. 18(11):1639–1642.

Zhang, Y.W., Shi, J., Li, Y.J. & Wei, L. 2009. Cardiomyocyte death in doxorubicin-induced cardiotoxicity. *Archivum Immunologiae et Therapiae Experimentalis*. 57(6):435–445.

Zhu, W., Shou, W., Payne, R.M., Caldwell, R., Field, L.J. & Heart, R. 2010. A mouse model for juvenile doxorubicin-induced cardiac dysfunction. *Medicine*. 64(5):488–494.

Zibadi, S., Vazquez, R., Moore, D., Larson, D.F. & Watson, R.R. 2009. Myocardial lysyl oxidase regulation of cardiac remodeling in a murine model of diet-induced metabolic syndrome. *American Journal of Physiology: Heart & Circulatory Physiology*. 297:H976–H982.

## 7. APPENDICES

### 7.1 Appendix A: Supplementary Results

#### 7.1.1 Tumour volume

The second disease state to establish in the co-morbid model was to introduce E0771 murine breast cancer cell in the tumour bearing mice after eight weeks on the diet. The interest for the study was not the tumour but it was important to establish that the mice had grown a tumour and that the chemotherapeutic treatment with Doxorubicin (DOX) was effective in mimicking the clinical setting. In the results (Figure 7.1), we were able to show that the accumulative 12mg/kg DOX was able to reduce the growth rate in both the SD mice compared to the HFD mice compared to vehicle control. Specifically looking at 27 Days after the inoculation of the tumour (Figure 7.2A) S+T+V vs S+T+D ( $1379.73 \pm 301.54 \text{ mm}^3$  vs  $677.12 \pm 159.97 \text{ mm}^3$   $p < 0.001$ ) and (Figure 7.2D) H+T+V vs H+T+D ( $2043.52 \pm 446.62 \text{ mm}^3$  vs  $1569.28 \pm 190.05 \text{ mm}^3$   $p < 0.001$ ) show that DOX treated mice had a reduced tumour volume.

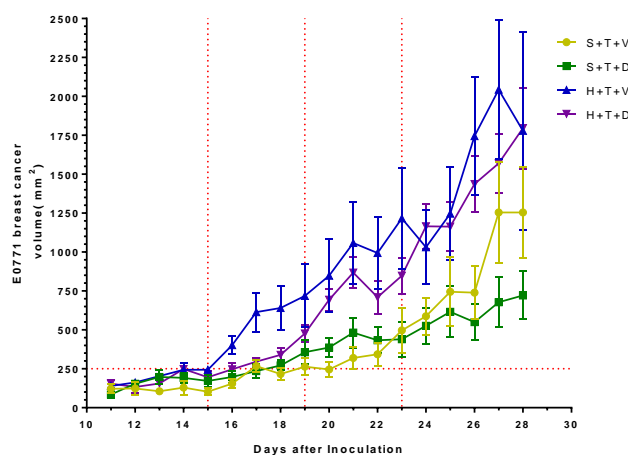


**Figure 7.1: E0771 breast cancer (Tumour) Volume of mice fed a standard (S) or high fat diet (H) and that were inoculated with a tumour and received doxorubicin treatment**

All tumour bearing female C57Bl6 mice at eight week on diet were injected with  $1.2 \times 10^5$  E0771 breast cancer cells into the 4<sup>th</sup> mammary pads, growing volume per day is shown. Vertical lines (red dotted lines) projects the average day on which mice receive the first ( $\pm$ Day 15), second ( $\pm$ Day 19) and third ( $\pm$ Day 23) treatment injection of Hank's balanced salt solution (HBSS= vehicle control) or DOX. The horizontal red dotted line represent the approximate average tumour volume ( $200\text{-}300\text{mm}^3$ ) before first treatment injection occurred. . Abbreviations: S- Standard diet, H- High Fat diet, T- Tumour, D-Doxorubicin

DOX used in the study was effective in reducing the rate at which the tumour was growing however, the HFD mice showed a larger tumour volume for both DOX and vehicle treatment (**Figure 7.2B & C**). The tumour volume and growth analyses was not part of the scope of the study and was additional to show that DOX was effective in its primary function in treating the tumour and that the tumour was present in the tumour bearing groups.

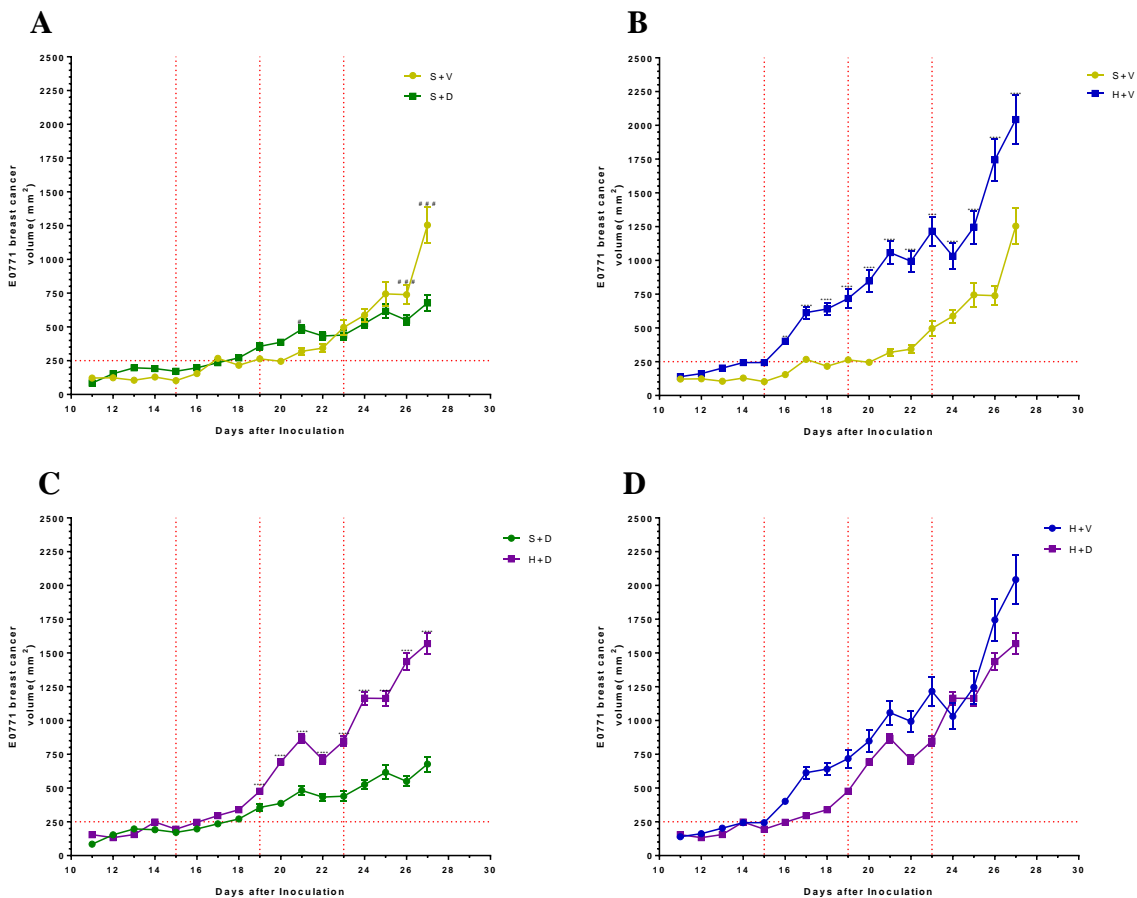


**Figure 7.2: E0771 breast cancer (Tumour) Volume of mice fed a standard (S) or high fat diet (H) and that were inoculated with a tumour and received doxorubicin treatment.**

Representing A) Standard diet fed mice B) vehicle control mice C) DOX treated mice and D) High fat fed mice. Female C57Bl6 mice at eight week on their respective diets (Standard or high fat) were injected with murine E0771 breast cancer cells into the mammary pads and served as the tumour groups. Ventricle lines (red dotted lines) projects the average day on which mice receive the first (Day 15), second (Day 19) and third (Day 23) treatment injection of Hank's balanced salt solution or DOX. The horizontal red dotted line represent the

approximate minimum tumour volume before first treatment injection (200-300mm<sup>3</sup>). Data represented as mean  $\pm$  SEM, (n=8-10). Abbreviations: S- Standard diet, H- High Fat diet, T- Tumour, D-Doxorubicin

Mice tumour volumes were compared due to the effect of the specific diet by comparing S+T+V vs H+T+V (Figure 7.2A) tumour volume due to diet irrespective of treatment with Hank's balanced salt solution (HBSS= vehicle control). As well as comparing the effect of the diet Comparing S+T+D vs H+T+D (Figure 7.2C) tumour volume due to treatment irrespective of treatment with DOX.

#### Total Protein stain free membrane

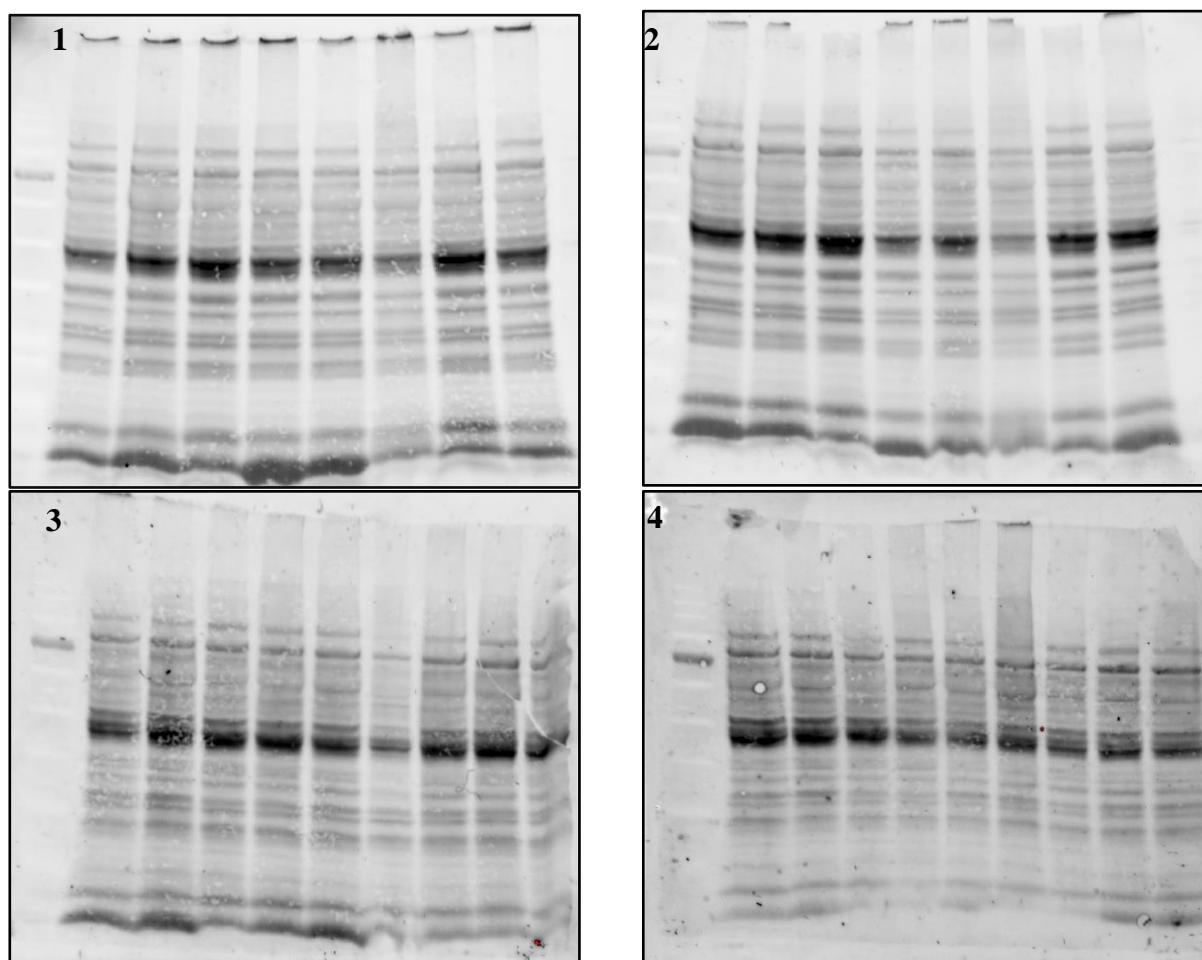


**Figure 7.3: Showing membrane 1, 2, 3 and 4 total protein image of mouse heart tissue used for apoptosis protein expression (CAS-3 & PARP) in western blot analysis**



**Figure 7.4: Positive staining Controls for fibrosis using Picrosirius Red stain, Skin and colon tissue stained with the same Sirius red as the heart tissue.**

## 7.2 Appendix B: Detailed Protocols

### Protocol 1: Cell Culture

#### Cell Culturing

- *Work aseptically by wearing a clean lab coat, washing hands, wearing gloves, lab coat cover selves and washing gloves.*
- *Spray gloves with 70% ethanol, spring laminar flow hood, as well as anything entering the hood with 70% ethanol.*

#### 1.1 Cracking a vile and Growth of Cells

- Thaw a vile of cells from liquid Nitrogen cascade at 37 °C
- Add 5 ml of growth medium (see Appendix C) to T25 flask
- Pipette 1 ml of cells into flask, close cap and shake (north, south, east, and west)
- Incubate, 37 °C with CO<sub>2</sub> at 5%
- Check cell growth and change growth media (see Appendix C), every 2-3 days, until cells are 80% confluent then cells are ready to be passaged or used for experimental purposes.

#### 1.2 Passing/ Splitting cells

- Put medium and trypsin in water bath at 37 °C, about 2 tubes each
- Check for confluence (80% saturation), and then move to the hood.
- Remove media using 5 ml pipettes, then add:
  - 4 ml trypsin to each T25
  - 8 ml trypsin to each T75
- Place on shaker for 5 minutes, check that cells are round and detached
- Add double the medium to neutralize the trypsin
  - 8 ml for T25

- 16 ml for T75
- Transfer all content of flask into 15 ml tube
- Centrifuge at 1500 rpm for 3 minutes
- Remove media from tube (supernant), dispose of the media leaving only pellet at the bottom.
- Use new pipette to add 2 ml of media and resuspend pellet gently without causing any bubbles.
- Count cells if seeding density is necessary or if amount of cells are needed to be known otherwise , Pipette 1 ml each into T75 equally and add additional media

### 1.3 Cell Counting

- Prepare haemocytometer and cover slip by wiping down with 70% ethanol
- Moisturize haemocytometer to make the surface adhesive for the cover slip to stick with out bubbles.
- Pipette 20  $\mu$ l of cell resuspension both sides of the haemocytometer undercover slip make sure no bubbles have form
- Count as follows:
  - Only count cells that fall on the Top and left of the counting grid square
  - The more blocks counted the more accurate.
- Using haemocytometer count as follow using **Figure 7.1** as a guide.

Total amount of cells block A + Total amount of cells block B + Total amount of cells block C  
+ Total amount of cells block D + Total amount of cells block E.

Divided by total blocks counted = Total cells per 1 mm by 1 mm (on average)

- Repeat the same for the other side of the haemocytometer average the two values.
  - Total cells (1 mm by 1 mm) x 1000  $\mu$ l /0.1  $\mu$ l= cells/ml
  - Once total amount of cells/ml is calculated multiply by the amount of cells suspend.

- Use the value to calculate how much volume of cell suspend is required to give a certain value of cells to seed in flasks for cell growth or used in experiment

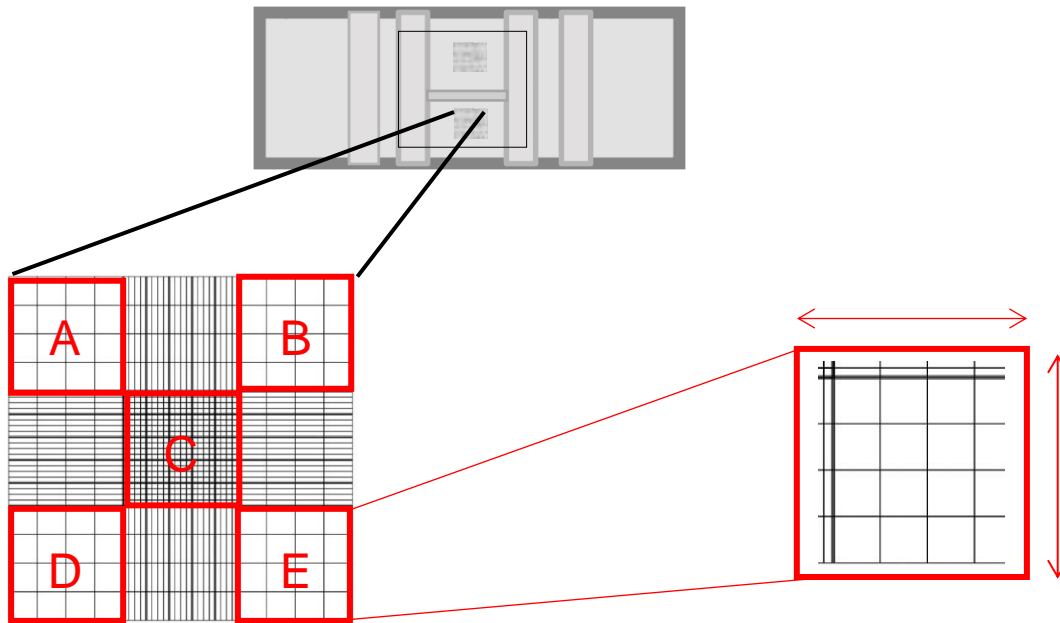


**Figure 7.1.** Haemocytometer grid of cell counting

## Protocol 2: Tumour preparation and injection

### 2.1 Tumour preparation

Follow cell growth procedure as mentioned in cell culture procedure. Once cells are counted use the required volume for 1 500 000 cells of E0711 cells for each mouse made in 250  $\mu$ l. Therefore when injected 1 200 000 cells are injected in 200 $\mu$ l.

- Centrifuge cell suspend
- After cell count has been completed centrifuge at 1500 rpm for 3 minutes
- Add the specific volume of Hank's balance salt solution to give 6 000 000 cells/ml

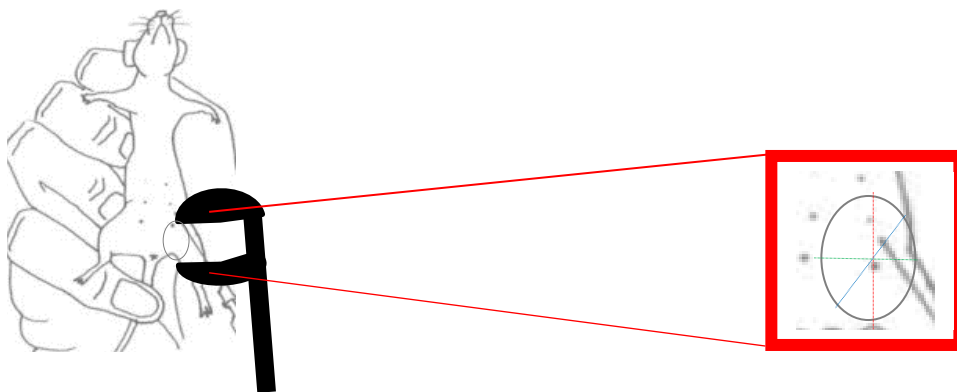
- Add 250  $\mu$ l Aliquot suspends into 1 ml Eppendorf tubes and use immediately for injections.

## 2.2 Tumour Injections

- Place mice under 3% isoflurane in aesthetic chamber.
- Spray area of injection with 70% ethanol and wipe down.
- Prepare tumour inject using 1 ml 28 gauge sterile needle and remove any air bubbles.
- Make suspension to 200  $\mu$ l ( 1 200 000 cells)
- Inject into 4<sup>th</sup> mammary pad of mice until skin bulge.
- Allow mice to wake up and monitor movement and cognitive response.

## 2.3 Tumour growth

- Every day after injection monitored mice daily for tumour growth by restraining mice.
- If bulge/ pimple was felt was listed as palpable but not measurable.
- Once tumour were able to be measured daily tumour measurement were carried out by using a digital calliper.
- Volume of tumour was measure as following: three reading were taken, the largest volume served as length (longitudinal) and the smallest volume the width (transverse), the third measurement was not used for the calculation.



$$\text{Tumour Volume}(\text{mm}^3) = 0.5 \times (\text{length}) \times (\text{width}^2)$$

**Figure 7.2:** Tumour measurement

### Protocol 3: Making up Doxorubicin ((DOX) treatment

100  $\mu\text{l}$  Doxorubicin (4 mg/kg) treatment was given once tumour's reached volume of 200-300  $\text{mm}^3$  of which they receive 3 intraperitoneal injections every 4<sup>th</sup> day. Vehicle groups received 100  $\mu\text{l}$  Hank's balance salt solution. Mice skin cribbed at neck and held in a way that mice are restricted to movement. Using a 28 gauge needle filled with 100  $\mu\text{l}$  of DOX or HSSB injected in between nipples in the intraperitoneal cavity on the mouse's right. If pimples formed mice's left side was injected.

**Table 7.1: Treatment Injection**

Day 0	Day 1	Day 5	Day 9	Day 13
200-300 $\text{m}^3$	DOX(4 mg/kg) /Vehicle Injection 1	DOX(4 mg/kg) /Vehicle Injection 2	DOX(4 mg/kg) /Vehicle Injection 3	Euthanasia

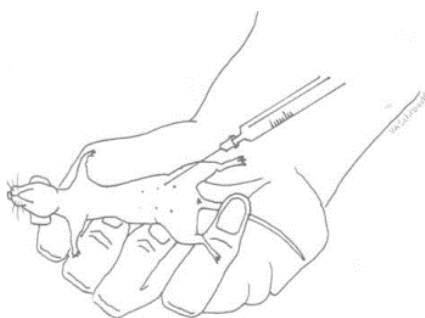


**Figure 7.3: Showing injection.** Picture Adapted from (Suckow, Danneman & Brayton, 2001)

### 3.1 Material

- DOX STOCK (5 mg/ml or 5 µg/µl)
- Hank's balance salt solution
- 1 ml insulin needle

### 3.2 Preparation

- Weigh mice the day before or the morning before injection
- Make injection to administer 4 mg/kg (4 µg/g) of DOX for each mouse
- Calculate:

$$4 \mu\text{g/g} \times \text{weight of mouse (g)} = \text{weight of DOX (}\mu\text{g)} \quad \dots \textcircled{1}$$

$$\text{weight of DOX (}\mu\text{g)} \div 5 \mu\text{g}/\mu\text{l} = \text{amount of } \mu\text{l from DOX stock} \quad \dots \textcircled{2}$$

$$\text{amount of } \mu\text{l from DOX stock} + \text{amount of HBSS} = 100 \mu\text{l for injection.} \quad \dots \textcircled{3}$$

- Injections are given as 100 µl but to compensate for loss of volume when placing in syringe and bubble that occur volume is made to 20% or 50% more = 120 µl or 150 µl respectively
- amount from DOX stock (µl) (×1.2) + amount of HBSS (µl) (×1.2) = 120 µl... $\textcircled{4}$ 
  - Example:
    - If mouse weight = 25.3 g
- Sub into  $\textcircled{1}$ 
  - $4 \mu\text{g/g} \times 25.3 \text{ g} = 101.2 \mu\text{g}$
- Sub into  $\textcircled{2}$ 
  - $101.2 \mu\text{g} \div 5 \mu\text{g}/\mu\text{l} = 20.24 \mu\text{l}$
- Sub into  $\textcircled{3}$

- $20.24 \mu\text{l} + 79.76 \mu\text{l} = 100 \mu\text{l}$
- Sub into ④
  - $40.5 \mu\text{l} + 159.5 \mu\text{l} = 200 \mu\text{l}$
  - Therefore  $40.5 \mu\text{l}$  from DOX STCOK plus  $159.5 \mu\text{l}$  HBSS in Eppendorf mix
- Collect  $100 \mu\text{l}$  of DOX suspension for Eppendorf tube into sterile syringe
- Place mice under 3% isoflurane sedation
- Clean mice with ethanol before injection
- Inject mice intraperitoneal, discard syringe after every use
- Allow mice to recover and check vitals

#### Protocol 4: ProcartaPlex Multiplex Immunoassay

##### 4.1 Sample Preparation

- At euthanasia after heart was excised
- Blood from the chest cavity was collected in EDTA tubes
- Kept on ice until euthanasia was complete
- Centrifuge at 2000 rpm at  $4^\circ\text{C}$  for 10 minutes
- $50 \mu\text{l}$  Aliquots were prepared and store at  $-80^\circ\text{C}$

Day before assay was performed plasma aliquots were thawed gradually from  $-80^\circ\text{C}$  to  $-20^\circ\text{C}$  to  $4^\circ\text{C}$  gradually

## 4.2 Assay Reagents Preparation

**Table 7.2 Regents supplied in ProcartaPlex Mix & Match Mouse 4-plex Luminex kit**

Quality	Reagents	Buffer preparations
2	Antigen standard	
1	Mouse Immune Monitoring Bead Mix	
1	Mouse Immune Monitoring Detection Antibody Mix	
1	Reading Buffer	
1	Wash Buffer Concentrate (10x)	Make 1x. Bring to room temperature, vortex for 15 secs. Add 20 ml wash buffer concentrate (10x) with 180ml dH <sub>2</sub> O. Store 2-8 C for 6 months
1	Streptavidin -PE	
1	Universal Assay Buffer	
	PCR 8-tube Strip	
1	96-well flat bottom plate	
2	Plate sealers	
	Controls High	
	Controls Low	

### 4.3 Reconstitution of standards and controls

- Centrifuge the antigen standard vials and controls at  $2000 \times g$  for 10 seconds.
- Add 250  $\mu\text{L}$  of 1x Universal Assay Buffer into each standard or control vial.
- Gently vortex the vial(s) for 10 seconds and centrifuge at  $2000 \times g$  for 10 seconds to collect contents at the bottom of the vial(s).
- Incubate on ice for 10 minutes to ensure complete reconstitution.
- Note: After reconstitution, standards and controls are ready to be used for the Assay Protocol

### 4.4 Prepare 4-fold serial dilution

- Prepare a 4-fold serial dilution of the reconstituted standard(s) using the PCR 8- tube strip provided.
- Label tubes Std1, Std2, Std3, Std4, Std5, Std6, and Std7.
- Follow Serial dilution depicted in Figure 4.1
- Add 200  $\mu\text{L}$  of the reconstituted antigen standard into the first tube of the strip and label as Standard 1 (Std1).
- Add 150  $\mu\text{L}$  of 1X Universal Assay Buffer into Std tubes 2–7.
- Transfer 50  $\mu\text{L}$  of the reconstituted antigen standard from Tube 1 into Tube 2
- Mix by pipetting up and down for a total of 10 times.
- Transfer 50  $\mu\text{L}$  of the mixed standards from Tube 2 into Tube 3.
- Mix by pipetting up and down for a total of 10 times.
- Repeat steps 4–7 for Std tubes 4–7.
- Add 200  $\mu\text{L}$  of Universal Assay Buffer into tube 8, which serves as a blank.
- Keep on ice until ready to use.

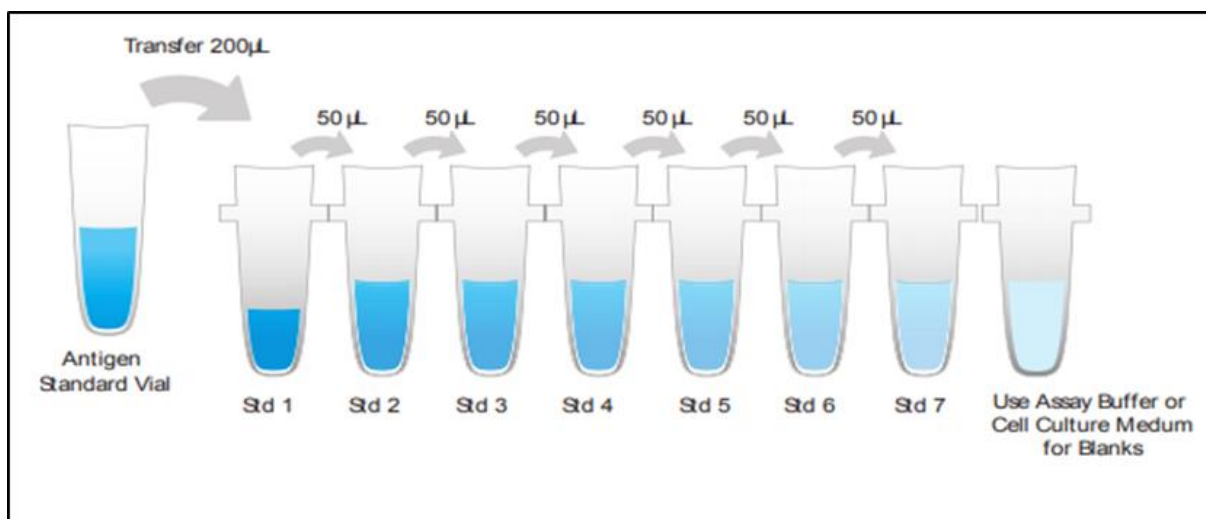


**Figure 7.4: Serial Dilution**

- Expected values of controls
  - Control High: S2-S3
  - Control Low: S5-S6
- Note: All control ranges were evaluated in Universal Assay Buffer and 2 hours incubation at room temperature.

#### 4.5 Assay protocol

- Prepare Antigen Standard
- Vortex magnetic capture beads for 30 seconds
- Add 50µl of the magnetic beads to each well, remove liquid
- Add 25 µl of Universal Assay Buffer to each well
- Add 25 µl of standards, control or plasma
- Seal plate incubate with shaking at room temperature for 60-120 minutes
- Wash beads(3x)
- Add 25 µl of Detection Antibody Mix(1x)
- Seal plate. Incubate with shaking at room temperature for 30 minutes
- Wash beads (3x)

- Add 50  $\mu$ l Streptavidin- Phycoerythrin to each well
- Seal Plate. Incubate with shaking at room temperature for 30 minutes
- Wash beads(3x)
- Add 120  $\mu$ l of reading buffer
- Seal Plate. Shake at room temperature for 5 minute
- Overnight incubation and Read on Magpix <sup>TM</sup> system the next day

**Table 7.3 Plasma markers analysed using Luminex assay**

Bead/Analyte Name	Luminex Magnetic Bead Region	Catalogue Number
Anti-IL-6 Beads	28	EX01A-20603-901
Anti-TNF $\alpha$ Beads	45	EX01-20607-901
Anti-IL-10 Beads	13	EPX01A-20614-901
Anti-Leptin Beads	65	EX01A-26036-901

#### Protocol 5: Tissue lysate preparation (Oxidative Stress)

*Conjugated dienes (CDs) and Thiobarbituric acid reactive substances (TBARs) assay sample preparation used the sample tissue sample preparation step.*

- Thaw  $\pm$  20mg of frozen tissue sample in a labelled Eppendorf on ice.
- Add cold phosphate buffer to each Eppendorf in a 1: 10 ratio of tissue sample (e.g. 20mg tissue to 200 $\mu$ l p-buffer).
- Homogenize tissue and sonicate at 10A, 5-10 seconds or water sonicate for 10 minutes.
- Allow froth to settle ( $\pm$ 30 minutes). Once settled Centrifuge for 10 minutes at 12000 rpm. Take off the supernant and transfer to chilled labelled Eppendorf, discard the pellet. Freeze at -80 $^{\circ}$ C or use directly for assay.

## Protocol 6: Conjugated Dienes (CD) assay

Work on ice

- Added 50  $\mu$ l of cell lysate (prepared in Protocol 5) to centrifuge tubes in a 1:5 ratio chloroform + methanol buffer (1:2)
  - 100  $\mu$ l chloroform + 200  $\mu$ l methanol
- Centrifuged at 10 000 rpm for 10 minutes = 2 layers form, transferred 200  $\mu$ l bottom chloroform layer to new centrifuge tube.
- Leave overnight with Eppendorf lid open in 4°C fridge to allow the nitrogen to evaporate.
- Added 1 ml cyclohexane to centrifuge tube and vortex for  $\pm$  20 seconds
- Loaded 300  $\mu$ l Blank (cyclohexane) and samples into UV clear 96 wells (performed in triplicate).
- Read plate at 234 nm absorbance with Multiskan® Spectrum microplate and Spectrophotometer (51119200, Thermo Electron Corporation, Massachusetts, USA).

## Protocol 7: Thiobarbituric acid reactive substances (TBARS) assay

### 7.1 Preparation

- Add 250  $\mu$ l of Sodium hydroxide (NaOH) in 10 ml of distilled water (0.1M)
- Weighed 0.125 g 2-Thiobarbituric acid (TBA) and dissolved in 10 ml of NaOH
- Weight 0.008 g of Butylated hydroxytoluene (BHT) dissolved in 10 ml of 96% ethanol
- Added 684.93  $\mu$ l O-phosphoric acid OPA to 50 ml distilled water (14.6 M)

### 7.2 Procedure

- Set the water bath to 90 °C (fill it to 80%) and used 2 ml Eppendorf tubes open and punch holes in their lids.
- Add 50  $\mu$ l of sample lysate (prepared in protocol 5) into an Eppendorf tube

- Add 6.25  $\mu\text{L}$  of Butylated hydroxytoluene (BHT).
- Add 50  $\mu\text{L}$  o-phosphoric acids (0.2M) to each sample, Vortex.
- Add 6.25  $\mu\text{L}$  TBA reagents to each sample, Vortex.
- Heat at 90  $^{\circ}\text{C}$  for 45 minutes (be strict with time and degrees for each repeat).
- Place samples in an ice bath for 2 minutes (or until needed)
- Transfer to 96 wells, use butanol as the blank and read  $A_{532} - A_{572}$

### 7.3 Analysis of results

Makes use of the Beer lambert Law

#### **EQUATIONS:**

- $\epsilon = 1.54 \times 10^5$
- Inter-assay CV = <8%
- $C = A / \epsilon$
- Use the absorbance value obtained and divide by  $\epsilon$  to obtain the concentration for each sample

### Protocol 8: Tissue lysate preparation and Electrophoresis (Western Blot)

#### 8.1 Protein extraction

*Work on ice*

- Thaw tissue on ice
- Using scissors manually homogenized tissue on ice ( $\pm 20$  mg)
- Add 200  $\mu\text{l}$  (1:10 ratio) of RIPA buffer to tissue sample and use tissue homogenizer to homogenize tissue working on ice.
- Once homogenize sonicate tissue for 15 seconds at 10Amps.
- Allow foam to settle on ice for  $\pm 30$  minutes.
- Centrifuge tissue lysates at 12 00 rpm for 15 minutes ( $4^{\circ}\text{C}$ ).

- Transfer supernatant to chilled Eppendorf tubes and discard pellet
- Use directly or freeze at -80°C

## 8.2 Protein determination

- Switch on Direct Detect™ Spectrometer (Merck) to allow machine to warm up and calibrate humidity.
- Run direct Detect program under operator
- Click proteins and buffer for standard –RIPA buffer
- Add 2 µl of each sample, vortex and it is placed on Direct Detect card and measured, RIPA buffer served as blank.
- Select pre drying of transparent membrane
- Vertically insert card into slot, card is dried and each sample is measured
- Protein is determined in mg/ml concentration, which is used in accordance to loading 40 mg tissue lysate.

## 8.3 Preparation of tissue lysates

- Appropriate amount of tissue lysate is determined using protein determination of which 40 mg of tissue is used as mentioned above.
- Add the correct volume and additional RIPA buffer used to make equal volume (15 µl) as well as 15µl Laemlli's sample buffer added in 1:1 ratio total volume should be 30 µl.
- Once added Eppendorf tubes were punctuated with needle
- Proteins are denatured by boiling for 5 minutes at 95°C.
- Samples Centrifuged at 10 000 rpm quickly
- Use immediately for gel electrophoresis or freezer at -80°C.

## 8.4 Assembly of Gel for electrophoresis

- Clean glass plates and rubber with 70% alcohol

- Place frames into the caskets and align glass frames clip into place( make sure the smaller plate faces forward)
- Make a 1.00 mm mini Gel (10 wells) using BIO-RAD TGX stain free™ Fastcast™ Gels add the required components to make the stacker and resolver according to table 7.4.

**Table 7.4: Component to make 12% Stain free™ Fastcast™ Gel**

1.0mm Bio-Rad Glass plates(n=gels)		
	Stacker	Resolver
Resolver A	-	3 ml x n
Resolver B	-	3 ml x n
Stacker A	1 ml x n	-
Stacker B	1 ml x n	-
Total Volume	2 ml x n	6 ml x n
TEMED	2 µl x n	3 µl x n
10% APS	10 µl x n	30 µl x n

- First add Resolver using a Pasteur pipette to the top of the green line
- Add the stacker using a Pasteur pipette and gently place the comb to avoid air bubbles
- Allow gel to set ( ± 1 hour)
- Boiled samples for 5 minutes at 95°C
- Centrifuge quickly
- Remove gel from casket and place into Bio-rad chamber
- Place gels facing towards buffer dam and clamp in, add Running buffer in middle compartment and the outside well
- Carefully remove the comb from the gel

### 8.5 Loading samples

- Pipette using special loading tips 5 µl BLUeye Prestained ladder into the first well of the gel
- Pipette samples in the rest of the wells see Figure 7.5
- Add more running buffer to the outside compartment

- Place lid onto the tank and ensure the electrodes are oriented accordingly red with red and black with black.
- Set machine to 100 V, and current of 300 mA for approximately 60-90 minutes

## 8.6 Membrane transfer

- Once gels have run they are transferred using transfer blot to nitrocellulose membrane.
- Using Trans-Blot® Turbo™ RTA Mini PVDF Transfer Kit
- Immerse nitrocellulose membrane in 30 ml 1x transfer buffer for 3 minutes
- Immerse PVDF in 100% methanol until translucent, then equilibrate membrane in 1x transfer buffer for 3 minutes
- Immerse 2 stacks of transfer stacks in 50 ml transfer buffer for 3 minutes
- Assemble as follows
  - Place one transfer stack at the bottom of cassette
  - Place wetted membrane on the stack
  - Remove gel from glass casket and remove staking gel section, gently place gel on membrane ( remove air bubbles using blot roller)
  - Place second wetted transfer stacker on top
- Roll the assembled sandwich with blot roller
- Remove excessive transfer buffer
- Close and lock cassette lid, Insert cassette in to Trans-Blot® Turbo™ transfer system
- Setting: 30 minutes at 25 V ,1.0 A
- After transferred membrane were soak in 100% methanol and dried
- Gels and wetted Membrane were checked using the ChemiDoc™ XRS+ System
- Membrane washed in 1x TBS-T (5 minutes ,3x)
- Blocked in blocking buffer (5% milk) for a 2 hour.
- Membrane was placed in 1x TBS-T containing specific primary antibody probing for 48 hours at 4 °C.
- Membrane was washed again in 1x TBS-T (3x for 5 minutes)
- Placed in secondary antibody for 1 hour at room temperature.

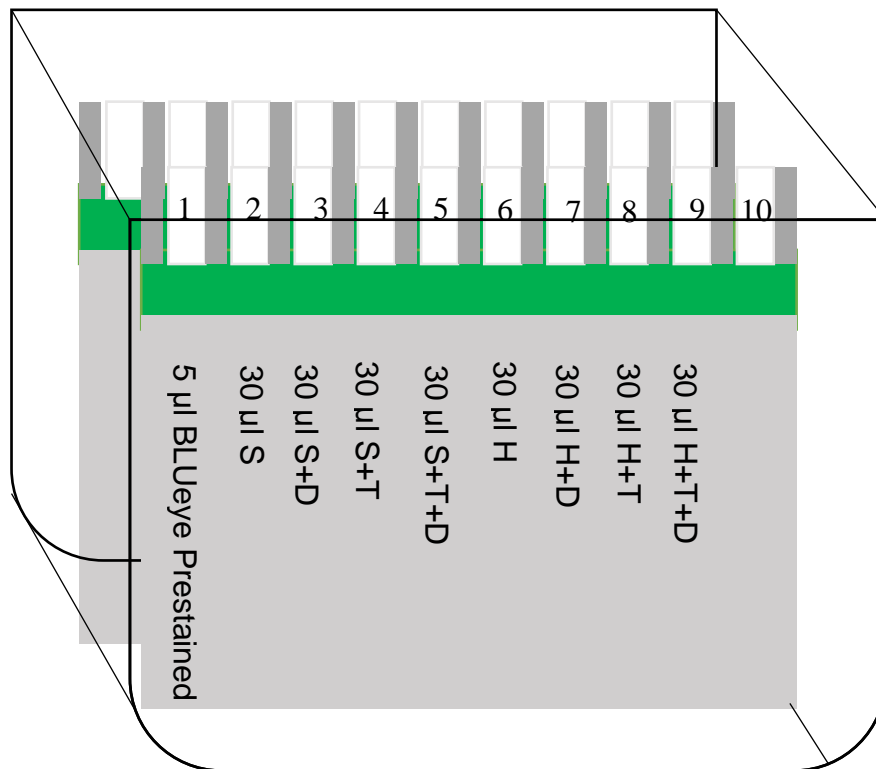


Figure 7.5 Loading samples into gel for electrophoresis

Table 7.5: Primary and secondary antibodies used for western blot analysis

Primary Antibody	Molecular weight (kDa)	Secondary Antibody	Dilution factor	Company and Catalogue #
Caspase-3	Total: 35 kDa Cleaved: 17 and 19 kDa	Anti-Rabbit	1:1000	Cell Signalling Technology #9662S
PARP1	Total: 116 kDa Cleaved: 89 kDa	Anti-Rabbit	1:1000	Cell Signalling Technology #9532S
<b>Secondary Antibody</b>				
Anti-Rabbit Secondary HRP-Linked			1:10000	Cell Signalling Technology #7074S

## 8.7 Image analysis

- Using Chemi-Doc (Bio-Rad) image membrane by addition of ECL (1:1 ratio) reagent, 200  $\mu$ l should be sufficient for membrane if protein of interest molecular weight is known.
- Run specific protocol set image frame at 9.1 x 7.5:
- Membrane (band of interest):
  - Application → Blot → Chemi

(With the addition of ECL)

- Total protein:
  - Application → Blot → Stain free
- Image of Ladder:
  - Application → Blot → Colometric
- And images and run protocol report will display. Save images.

## Protocol 9: Histological preparation of tissue

### 9.1: Tissue processing

For histological analysis, the 10% neutral formalin-fixed heart tissue was placed in a pre-labelled embedding cassette. The tissue was then processed using the Shandon Elliott Suplex processor (Biotech lab, SCE 0540, UK) using a 20-hour processing protocol outlined as follows:

**Table 7.6: 20-hour Automated Tissue processing procedure**

Step	Solution	Time (Hours)
Dehydration	70% alcohol	1.5
	70% alcohol	1.5
	90% alcohol	1.5
	95% alcohol	1.5
	95% alcohol	1.5
	100% alcohol	1.5
	100% alcohol	1.5
Clearing	100% alcohol	2
	Xylene	1.5
	Xylene	2
Impregnation	Paraplast <sup>®</sup> wax	2
	Paraplast <sup>®</sup> wax	2

### 9.2: Embedding tissue

- Processed tissue is placed into the appropriate mould size from cassette add a small amount of molten paraffin wax and place tissue in correct orientation for sectioning.
- Cool so that tissue can remain in correct orientation and fill the rest of the mould with moulded paraffin wax followed by the labelled cassette to hold mould down.
- Place on cold plate and allow wax to solidify ( $\pm 30$  minutes)
- Once complete mould can be removed from moulding block.

### 9.3: Sectioning using microtome

- Before actual section/ ribbons of tissue can be made the blocks require trimming to get to the tissue.
- Place tissue in freezer for 30 minutes.
- Set up water bath as well as glass slides to collect tissue.
- Trim until ribbon of tissue form.
- Pick up ribbon of tissue with glass slide at 90° angle.
- Place 2 times ribbon of each tissue on to different slides
- Place slides in oven (70°C).
- Once wax has melted, slides are ready for staining.

## Protocol 10: H and E staining

### 10.1 Staining procedure (using automated system)

- De-wax and hydrate paraffin sections.
- Cleared in xylol
- Dehydrate in three changes of 100% ethanol (100%, 95% and 70%).
- Rinse in distilled water
- Stain Harris hematoxylin
- Rinse in distilled water
- Add 10% acid alcohol
- Scott's tap water
- Distilled water
- Eosin
- Distilled water
- Dehydrate in three changes of ethanol (70%, 95% and 100%).
- Clear in xylene and mount in resinous media.

## Protocol 11: Picro-sirius red solution staining for collagen

### 11.1 Staining procedure

- De-wax and hydrate paraffin sections.
- Stain nuclei with haematoxylin for 8 minutes
- Rinse the slides for 10 minutes in running water.
- Stain in picro-sirius red for 1 hour.
- Wash in acidified water (see Appendix C).
- Vigorously shake water from slide.
- Dehydrate in three changes of 100% ethanol.
- Clear in xylene and mount in resinous media.

## Protocol 12: Quantification of fibrotic tissue

- Protocol obtained online: [Quantifying Stained Liver Tissue <https://imagej.nih.gov/ij/docs/examples/stained-sections/index.html> 5/5 | Examples]
- Using Image J software

### 12.1 Change the scale to micrometres

- Measure the length of the scale bar and using the Analyze >Set Scale command to set the scale to micrometres.
- Measure the scale bar, use the straight line selection tool (fifth tool from the left on the Image J tool bar) to create a line selection along the length of the scale bar.
- Open the Analyze>Set Scale dialog box. Notice that the length of the line selection (317 pixels) is automatically entered as the "Distance in Pixels". Enter the scale bar length (200  $\mu\text{m}$ ) as the "Known Distance" and "um" as the "Unit of Length". Image J will automatically convert the "u" to the micrometre symbol ( $\mu$ ). Click "OK" and notice that the image size has changed to 858.95x646.74  $\mu\text{m}$ .

## 12.2 Convert the image to grayscale

- Use the Image>Type>RGB Stack command to split the image into red, green and blue channels. This is necessary because the Image>Adjust>Threshold tool only works with grayscale images.
- Move the slider to view each of the channels. Notice that the green channel has the best separation.
- Use the Image>Stacks>Make Montage command to view all three channels at the same time.
- Select the RGB stack (with the Green channel selected) and press shift-t (Image>Adjust>Threshold). The "Threshold" tool opens and the green channel is automatically threshold.
- Manually adjusted the threshold. Do this by moving the lower slider until the stained collagen is highlighted in red. Notice that the threshold level arrived at manually is about half the automatically set level of 175.
- Click on "Set" and set the upper level to  $175/2$ , or 87. Setting a threshold that is a fraction of the automatically determined threshold will allow us to later create a macro that does not require manual thresholding.

## 12.3 Segment (isolate) the red-stained collagen using thresholding

- Erase the scale bar to prevent it from being included in the calculated area. Select rectangular selection tool to select the scale bar, then press Backspace (Delete on the Mac).
  - If the current background is not white, use the color picker tool (Image>Color>Color Picker) to change it to white. Note that the current background color is indicated by the color of the border surrounding the eye dropper tool icon.

#### 12.4 Measure the threshold area

- Command Image J what to measure by opening the Analyze>Set Measurements dialog and checking "Area", "Area Fraction", "Limit to Threshold" and "Display Label".
- Press "m" (Analyze>Measure) and the area and percent area will be displayed in the "Results" window.
- Right click in the "Results" window and select "Save As" to save the results as a tab-delimited text file or select "Copy" to copy the results to the Clipboard transfer results to Excel Spreadsheet.

## 7.3 Appendix C-Reagents and solutions preparation

### Protocol 1: Growth Media (500ml)

#### 1.1 Materials:

- 500 ml Dulbecco's Modified Eagle Medium (DMEM)
- 50 ml 10% Fetal Bovin Serum (FBS)
- 5 ml Penicillin Streptomycin (PenStrep)

#### 1.2 Preparation:

- Work at a temperature of 37 °C
- Place 500 ml DMEM in shaking incubator to bring temperature to 37 °C remove 55 ml DMEM from stock bottle
- Add 50 ml filtered 10% FBS and 5 ml PenStrep and swirl mixture.
- Make aliquots of 50 ml in falcon tubes , cover with parafilm and store at 4 °C

### Protocol 2: Doxorubicin stock

- Under sterile conditions , make a stock of DOX
- Weigh out 0.002 g DOX and dissolve in 400 ml HBSS
- 5 mg/ml or 5 µg/µl STOCK
- Vortex, make aliquots in Eppendorf tubes
- Wrap in foil Store at -20 °C

### Protocol 3: Phosphate buffer 50 mM, pH 7.5 (100 ml)

- Dissolve 0.7098 g Na<sub>2</sub>HPO<sub>4</sub> in 100 ml dH<sub>2</sub>O and mix- solution 1
- Dissolve 0.029 g of EDTA in 100 ml dH<sub>2</sub>O and mix- solution 2
- Add 18 ml of solution 1 with 82 ml of solution 2, adjust pH to 7.4
- Store at 4°C

#### Protocol 4: Thiobuturic Acid (0.11M)

- Concentration of 0.11M in 0.11M NaOH
- $N(\text{mol}) = \frac{m(\text{grams})}{Mr(\text{grams/mol})}$
- Therefore  $m(\text{grams}) = Mr(\text{grams/mol}) \times N(\text{mol})$  Equation 1

$$**n = \frac{m}{MR} \dots\dots m = MR \times n \qquad C = \frac{n}{V} \dots\dots n = CV$$

- therefore  $m(\text{g}) =$
- $g = M_R \times C \times V$
- $= 144.15(\text{mol/g}) \times 0.11\text{M} \times 0.010\text{L}$
- $= 0.159\text{g TBA in } 10 \text{ mL of NaOH}$
- Add 0.159g TBA in 10 ml NaOH

#### Protocol 5: 10% Neutral Formalin Buffer (1 Litre)

- 100 ml 37% Formaldehyde
- 4 g Sodium phosphate monobasic
- 7.5 g Sodium phosphate dibasic ( $\text{Na}_2\text{HPO}_4$ )
- pH to 6.8 and top up with  $\text{dH}_2\text{O}$  to make 1 Liter

#### Protocol 6: Different ethanol preparations (1 Litre)

100% → use pure ethanol

95% → dilute 950 ml of 100% ethanol in 50 ml  $\text{dH}_2\text{O}$

90% → dilute 900 ml of 100% ethanol in 100 ml  $\text{dH}_2\text{O}$

70% → dilute 700 ml of 100% ethanol in 300 ml  $\text{dH}_2\text{O}$

#### Protocol 7: Radio immunoprecipitation (RIPA) assay buffer (STOCK)

- 50 mM Tris-HCL
  - Add 700 mg Tris to 75ml dH<sub>2</sub>O
- Add 900 mg NaCl and stir the adjust pH to 7.4
- Add 10% NP-40
  - Dissolve 1 ml NP-40 in 9ml dH<sub>2</sub>O
- Add 2.5 ml Sodium –deoxycholate
  - Dissolve 1g in 10ml
- Add 1 ml EDTA(1 mM)
  - 44.67 mg in 1.2 ml dH<sub>2</sub>O
- Aliquot and store 4°C

#### Protocol 8: RIPA assay buffer (working solution) 1ml

For 1 ml RIPA (STOCK) add:

- 42 µl Protease inhibitor cocktail(PI) [-20°C]
- 5 µl Sodium Fluoride (NaF) [room temperature]
- 5 µl Sodium orthovanadate (Na<sub>2</sub>VO<sub>4</sub>) [-20°C]
- 10 µl Pheylmethylsulphonyl Fluoride (PMSF) [ 4°C]

Preparation is kept on ice

#### Protocol 9: Laemmli's Sample buffer (STOCK)

- 16 ml dH<sub>2</sub>O
- 5 ml 0.5 M Tris- HCL , pH 6.8
- 4 ml glycerol
- 8 ml 10% (w/v) Sodium dodecyl sulphate (SDS)
  - Dissolve 1 g in 10 ml
- 2 ml 0.05% ( w/v) Bromophenol blue

STORE at room temperature covered with foil

#### Protocol 10: Laemmli's Sample buffer (Working STOCK)

- 850  $\mu$ l Laemmli's Sample buffer (STOCK)
- 150  $\mu$ l  $\beta$ -mercaptonol

Add together on the day of usage

#### Protocol 11: Running Buffer (1 litre)

- 100 ml Tris- glycine- SDS buffer (TGS) 10X [ready-made, BIO RAD]
- 900 ml dH<sub>2</sub>O
- Storage 4°C

#### Protocol 12: Transfer Buffer-BIORAD kit (1Litre)

- 200 ml 5x transfer buffer [part of kit]
- 600 ml dH<sub>2</sub>O
- 200 ml ethanol
- Mix reagents together keep at room temperature

#### Protocol 13: 10x TBS (1 Litre)

- 24.5 g Tris
- 80 g NaCl
- Dissolve in 600 ml distilled water, set pH to 7.6 and top up to 1 L with dH<sub>2</sub>O

#### Protocol 14: 1x TBS-T (1Litre)

- 100 ml 10X TBS-T
- 900 ml dH<sub>2</sub>O
- 1 ml Tween 20

#### Protocol 15: Blocking Buffer (100 ml)

- 95 ml 1 X TBS-T
- Add 5 ml Milk
- Mix well on magnetic stirrer

#### Protocol 16: 10% Ammonium persulphate

- Weight out 0.1 g APS into Eppendorf tube and add 1 ml dH<sub>2</sub>O

#### Protocol 17: Primary Antibody

- Add 5 ml 1x TBS-T into falcon tube
- Pipette 5 µl primary antibody into solution
- Keep on ice

#### Protocol 18: Secondary Antibody

- Add 5 ml 1x TBS-T into falcon tube
- Pipette 0.5 µl primary antibody into solution
- Keep on ice

#### Protocol 19: Paul's Stripping Buffer

Dissolve in 400ml dH<sub>2</sub>O:

- 7.5 g glycine
- 0.5 g SDS
- Add 5 ml Tween
- Adjust pH to 2.2
- Top up to 500 ml

Protocol 20: 10% acid alcohol-acidified water (1 litre)

- 10 ml 1% HCl
- Dissolved in 100% ethanol

Protocol 21: Scott tap water (1 Litre)

- 3.5 g NaHCO<sub>3</sub>
- 20 g MgSO<sub>4</sub>
- 1 ml 37% formalin
- 1 litre dH<sub>2</sub>O

## 7.4 Appendix D: Equipment and Reagents list

Table 7.7: Equipment used in experiments

EQUIPMENT	CATALOGUE NUMBER	COMPANY	CITY	COUNTRY
Accu-Chek <sup>®</sup> Performa Nano		Roche Diagnostics	Mannheim	Germany
Accutrend Plus <sup>®</sup>		Roche Diagnostics	Mannheim	Germany
Bio-Plex <sup>®</sup> MAGPIX <sup>™</sup> Multiplex reader	MAGPIX13046704	Bio-Rad Laboratories, Inc.	California	USA
ChemiDoc <sup>™</sup> XRS+ System	170-8265	Bio-Rad Laboratories, Inc.	California	USA
Direct Detect <sup>™</sup> Infrared Spectrometer	DDHW00010	Merck	Massachusetts	USA
Leica AutoStainer XL	ST5010	Leica Biosystems	Wetzlar	Germany
Leica microtome	RM 2125 RT	Leica Biosystems	Wetzlar	Germany
Leica Modular Tissue Embedder	EG1160	Leica Biosystems	Wetzlar	Germany
Mini - PROTEAN <sup>®</sup> II electrophoresis cell	165-2940	Bio-Rad Laboratories, Inc.	California	USA
Thermo Scientific Multiskan <sup>®</sup> Spectrum microplate and Spectrophotometer	51119200	Thermo Electron Corporation	Massachusetts	USA
Multiskan <sup>®</sup> Spectrum plate reader	51118600	Thermo Fisher Scientific	Massachusetts	USA
Nikon Eclipse E400 microscope		Nikon Instruments	Tokyo	Japan
POLYTRON <sup>®</sup> PT2100 Homogenizer		Thermo Fisher Scientific	Massachusetts	USA
SPOT RT Color Digital Camera ( Microscope)		Diagnostics Instruments, Inc.		USA
Shandon Elliot Suplex processor	SCE 0540	Biotech laboratories		UK
Trans-Blot <sup>®</sup> Turbo <sup>™</sup> transfer system	1704270	Bio-Rad Laboratories, Inc.	California	USA
Ultrasonic Liquid processor	630-0427	Sonics & Material, Inc.	Newtown	USA

**Table 7.8: Reagents and material used to perform experiments**

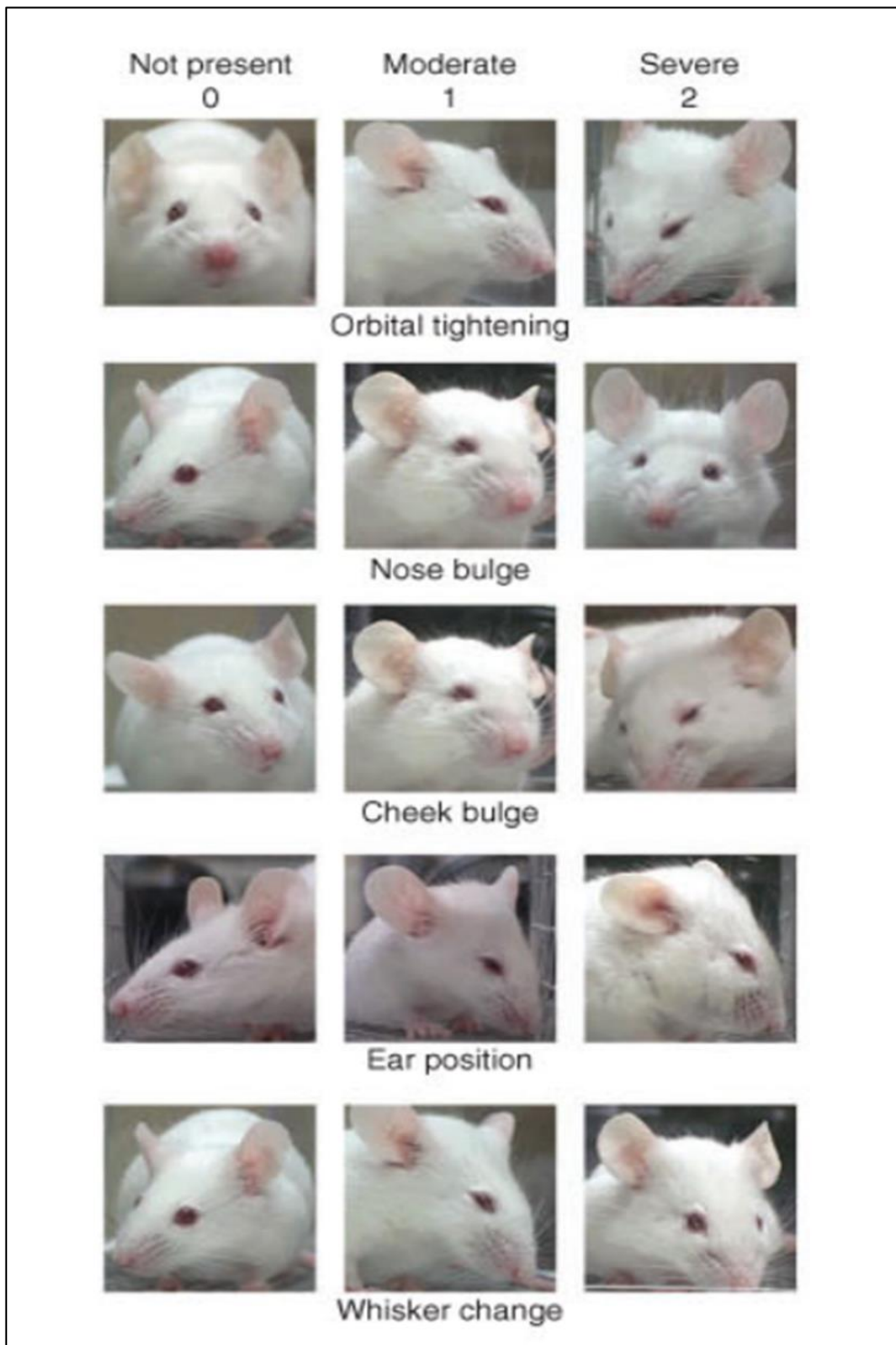
REAGENT/MATERIAL	ABBREVIATIONS	CATALOGUE NUMBER	COMPANY	CITY COUNTRY
1% Nondet P 40	NP40	74385-1L	Sigma-Aldrich	Missouri USA
2-Mercaptoethanol		M6250	Sigma-Aldrich	Missouri USA
Na-deoxycholate	Na	D6750	Sigma-Aldrich	Missouri USA
Acetic acid (glacial)		537020	Sigma-Aldrich	Missouri USA
Ammonium Persulphate	APS	A3678-25G	Sigma-Aldrich	Missouri USA
BluEye Prestained ladder	Protein Ladder	PM007-0500	Biocom Biotech	Centurion South Africa
Bromophenol blue		SAAR1437500CB	Merck	Massachusetts USA
Butylated hydroxytoluene	BHT	B1378	Sigma-Aldrich	Missouri USA
Chloroform		102444	Merck Millipore	Massachusetts USA
Clarity™ ECL Western Blotting Substrate		1705061	Bio-Rad Laboratories, Inc.	California USA
Container specimen jar 40ml		PTLC1468R1	Lasec	Cape Town South Africa
Cyclohexane		102822	Merck	Massachusetts USA
Doxorubicin Hydrochloride	DOX	D5794	LKT @laboratories	Minnesota USA
DPX mounting medium		06522	Sigma-Aldrich	Missouri USA
Dulbecco's Modified Eagle Medium	DMEM	41965-062	LifeTechnologies	California USA
DTNB		D21820	Sigma-Aldrich	Missouri USA
Ethylenediaminetetraacetic acid	EDTA	EDS-100G	Sigma Aldrich	St Louis USA
Embedding cassettes		Z672122	Sigma-Aldrich	Missouri USA
Ethanol 99.9%		32221	Reidel deHaen	Seelze Germany

REAGENT /MATERIAL	ABBREVIATIONS	CATOLOGUE NUMBER	COMPANY	CITY COUNTRY
Eosin solution	E	3801600E	Leica Biosystems	Wetzlar Germany
Fetal Bovin Serum	FBS	FBS-G1-12A	Biocom Biotech	Centurion South Africa
Formaldehyde sol min. 37%		K46046503441	Merck	Massachusetts USA
Glycine		357002-1KG	Merck	Massachusetts USA
Glycerol		SAAR2676520	Merck	Massachusetts USA
Hank's balanced salt solution(modified)	HBSS	H8264	Sigma-Aldrich	Missouri USA
Hydrochloric acid	HCL	SAAR3063040LP	Merck	Massachusetts USA
Isoflurane		Isofor	Safeline Pharmaceutical	Florida South Africa
Mayer's haematoxylin solution	H	SAAR2822001LC	Merck	Massachusetts USA
Minicollect <sup>®</sup> K3EDTA Blood collection tubes		VGRV450474R	Lasec	Cape Town South Africa
Malondialdehyde	MDA	820756 805797	Merck	Massachusetts USA
Methanol	MeOH	1.06007 UN1250	Merck	Massachusetts USA
Microscope coverslips		GLAS2C9M2250 REC	Lasec	Cape Town South Africa
Microscope slides		GLAS4S22M300 F	Lasec	Cape Town South Africa
Milk		Everfresh Fat Free long life	Spar	Stellenbosch South Africa
Ortho-phosphoric acid	OPA	100573 UN1805	Merck	Massachusetts USA

REAGENT/ MATERIAL	ABBREVIATIONS	CATALOGUE NUMBER	COMPANY	CITY COUNTRY
Paraplast® wax		A6330-4LB	Sigma- Aldrich	Missouri USA
Penicillin Streptomycin	PenStrep	15140-122	LifeTechnolo gies	California USA
Pheylmethylsulpon yl Fluoride	PMSF	93482-50ml-F	Sigma- Aldrich	Missouri USA
Picric acid		P6744-1GA	Sigma- Aldrich	Missouri USA
ProcartaPlex Mix & Match Mouse 4- plex Luminex kit		PPX-04- MXCE327	Biocom- Invitrogen	Massachuset ts USA
cOmpete™ Protease inhibitor cocktail	PI	11873580001	Roche	Basel Switzerland
Running Buffer Tris- glycine- SDS buffer(TGS) 10X		161-0772	Bio-Rad Laboratories, Inc.	California USA
Sirius Red	Direct Red 80	365548	Sigma –Alrich	Missouri USA
Sodium Cholride	NaCl	1.06404	Merck	Massachuset ts USA
Sodium dodecyl sulfate	SDS	L3771	Sigma- Aldrich	Missouri USA
Sodium fluoride	NaF	193270	Merck	Masschusett s USA
Sodium hydroxide	NaOH	S5881	Sigma- Aldrich	Missouri USA
Sodium phosphate monobasic	NaH <sub>2</sub> PO <sub>4</sub>	S8282	Sigma- Aldrich	Missouri USA
Sodium phosphate diabasic	Na <sub>2</sub> HPO <sub>4</sub>	S3264	Sigma- Aldrich	Missouri USA
Sodium orthovanadate	Na <sub>3</sub> VO <sub>4</sub>	S6508	Sigma- Aldrich	Missouri USA
Syringe 1ml with 29G Needle			Stelmed cc	Stellenbosch South Africa

REAGENT/ MATERIAL	ABBREVIATIONS	CATALOGUE NUMBER	COMPANY	CITY COUNTRY
Tetramethylethylenediamine	TEMED	1.10732.0100	Merck	Massachusetts USA
Thiobarbituric Acid	TBA	T5500	Sigma-Aldrich	Missouri USA
TGX Stain-Free™ Fast Cast™ Acrylamide Kit, 12%		1610185	Bio-Rad Laboratories, Inc.	California USA
Tris Basic		648310	Merck	Massachusetts USA
Tran-Blot® Turbo™ RTA Mini PVDF Transfer Kit		1704272	Bio-Rad Laboratories, Inc.	California USA
Tween ®20		P1379	Sigma-Aldrich	Missouri USA
Trypsin-EDTA		25200072	LifeTechnologies	California USA
Paraplast® wax		A6330-4LB	Sigma-Aldrich	Missouri USA
Phenylmethylsulfonyl fluoride	PMSF	93482	Sigma-Aldrich	Missouri USA
Picric acid		P6744-1GA	Sigma-Aldrich	Missouri USA
cOmplete™ Protease inhibitor	PI	11873580001	Sigma-Aldrich	Missouri USA
Running Buffer Tris- glycine- SDS buffer(TGS) 10X		161-0772	Bio-Rad Laboratories, Inc.	California USA
Xylene		1330-20-7	Sigma-Aldrich	Missouri USA

7.5 Appendix E: Grime scale



## 7.6 Appendix F: Ethics Letter



UNIVERSITEIT•STELLENBOSCH•UNIVERSITY  
jou kennisvenoot • your knowledge partner

**Protocol Approval**

Date: 10-Jul-2013

PI Name: Engelbrecht, Anna AM

Protocol #: SU-ACUM13-00015

Title: An investigation into the role of melatonin and punnic acid in the prevention of doxorubicin-induced toxicity and chemoresistance in a mouse xenograft model.

Dear Anna Engelbrecht, the Initial Application, was reviewed on 09-Jul-2013 by the Research Ethics Committee: Animal Care and Use via committee review procedures and was approved. Please note that this clearance is only valid for a period of twelve months. Ethics clearance of protocols spanning more than one year must be renewed annually through submission of a progress report, up to a maximum of three years.

**Applicants are reminded that they are expected to comply with accepted standards for the use of animals in research and teaching as reflected in the South African National Standards 10386: 2008. The SANS 10386: 2008 document is available on the Division for Research Developments website [www.sun.ac.za/research](http://www.sun.ac.za/research).**

Please remember to use your protocol number, SU-ACUM13-00015 on any documents or correspondence with the REC: ACU concerning your research protocol.

Please note that the REC: ACU has the prerogative and authority to ask further questions, seek additional information, require further modifications or monitor the conduct of your research.

We wish you the best as you conduct your research.

If you have any questions or need further help, please contact the REC: ACU secretariat at or .

Sincerely,

REC: ACU Secretariat  
Research Ethics Committee: Animal Care and Use